THE MECHANISM OF HIV-1 VIROLYTIC INACTIVATION BY ENV-TARGETING PEPTIDE TRIAZOLE THIOLS

A Thesis

Submitted to the Faculty of

Drexel University

by

Laurèn Danielle Bailey

in partial fulfillment

of the requirements for the degree

of

Doctor of Philosophy

November 2015

Dedications

To my family - Joanne and Claude Barnes and Christopher Bailey

Your encouragement and support has been the momentum propelling me
to accomplish my dreams

To my fiancé- John Michael Sweeney, Esquire

Your unconditional love and patience has been my cornerstone throughout my PhD

Acknowledgements

I would like to express my gratitude to my advisor Dr. Chaiken and my thesis committee members, Drs. Bradford Jameson, Patrick Loll, Joseph Salvino, and Amos Smith. I appreciate your constructive criticism and unwavering support throughout the turbulent times of my research project. Your continued guidance has challenged my intellectual curiosity thereby helping to develop my scientific skills.

I am thankful of the Speicher Lab at the Wistar Institute of the University of Pennsylvania for their expertise and guidance in mass spectroscopy and proteomics research.

I am appreciative of colleagues who I am fortunate enough to call friends, Dr. Kantharaju Kamanna, Dr. Rachna Arora, Dr. Rosemary Bastian, Dr. Ramalingam Venkat Kalyana Sundaram, Andrew Holmes, Caitlin Duffy, Charles Ang, Aakansha Nangarlia, Dr. Srivats Rajagopal, Dr. Ferit Tuzer, Dr. Bibek Parajuli, Kriti Acharya, Dr. Ali Emileh, Dr. Mark Contarino, and Dr. Diogo Moreira. Thank you all for patiently teaching a chemist the fundamentals of biology from maintaining cell cultures and performing transformations to producing virus, expressing protein, and analyzing SPR analysis data.

Table of Contents

Table of Contents

List of Tables

.

List of Figures

Abstract

The mechanism of HIV-1 virolytic inactivation by
Env-targeting peptide triazole thiols
Laurèn D. Bailey
Irwin Chaiken, Ph.D.

The HIV-1 entry process is mediated by the interaction of the trimeric envelope glycoprotein (Env) on the virus membrane surface with the host cell receptors, CD4 and co-receptors CCR5 or CXCR4. Each Env trimer consists of two non-covalently associated glycoproteins, a gp41 transmembrane protein, and an external gp120 surface protein. Because Env is the only virus-specific protein on the virion surface and is essential for cell receptor interactions and subsequent virus-cell fusion, it is an important therapeutic target for directly inhibiting and blocking the initial steps leading to host cell infection. Peptide triazoles (PTs) are a novel class of dual antagonistic entry inhibitors of HIV-1 Env, which function by blocking gp120 binding to CD4 and co-receptor on the host cell. We have determined that a subclass of PTs that contain a C-terminal cysteine, peptide triazole thiols (PTTs), cause irreversible viral inactivation and lysis. In this work, we demonstrated that PTT- induced lytic inactivation is triggered by a disulfide exchange reaction between the peptide sulfhydryl group and conserved gp120 disulfides. Interestingly, disulfide exchange is a process previously found to be necessary for fusion and entry of several viruses.

To understand the mechanism of action of virolytic PTT inhibitors, my research focused on structure activity relationship (SAR) studies of PTTs in concert with protein chemistry and virus/cells analysis. The studies were initiated by synthesizing and characterizing

truncated PTTs to define the distance relationship between the PT-SH groups and gp120 disulfides. Furthermore, understanding the lytic mechanism involved the use of gp120 protein ligands, sulfhydryl blocking, and reducing chemicals to determine their effects on PTT-induced p24 release. We determined that the PT thiol group is required for lytic activity and we observed a strong dependence of lysis activity on length of the linker between the IXW pharmacophore and SH group in PTT truncate SAR studies. Furthermore, we used a molecular dynamics (MD) simulation of a PTT-gp120 complex to identify the PT-SH point of contact region in gp120. The MD simulation displayed the trajectory of the peptide SH group and suggested that it could interfere with conserved disulfides clustered proximal to the CD4 binding site in gp120. We next performed mutational analysis of these conserved cysteine residues in this gp120 region as well as gp41 to identify a specific contact site. HIV-1 Env cysteine mutagenesis studies implicated the role of gp41 in virolytic mechanism, possibly by stabilizing six-helix bundle formation, due to PTTs inability to cause lysis in viral particles lacking the conserved gp41 disulfide.

In the last part of this work, we synthesized a biotinylated variant of PTT used to confirm the covalent binding of PTT to gp120. The biotinylated PTT was characterized and shown to exhibit functions comparable to that of its' parent PTT. When the biotin tagged PTT variant was incubated with gp120, the two were found to bind covalently, a feature which was also observed in BaL.01 virions. Furthermore, we defined that the thiol in PTTs is necessary to bind gp120 covalently to exert its mechanism of action, disulfide exchange. Our data suggest that PTTs hijack the native HIV entry process by triggering disulfide exchange leading to molecular transformations of the HIV-1 trimer, which normally occur

upon virus-cell entry and later membrane fusion. We infer that PTT's undergo disulfide exchange between gp120 and the peptide thiol group, a process that mimics native cell entry.

Chapter 1: HIV-1 Background

1. Introduction

It has been more than 30 years since the first cases of Human Immunodeficiency Virus (HIV) were reported in the United States and in this time we have found that HIV has much in common with other viruses[1]. We know that HIV weakens the immune system by creating a "deficient" immune response that cannot defend our bodies[2]. However, unlike most other viruses, which the body usually eradicates, the human body is incapable of clearing HIV due to the continued viral exploitation of T cells. Consequently, HIV- positive patients with extremely damaged immune systems progress from HIV to Acquired Immunodeficiency Syndrome (AIDS) [2,3]. Since its identification in 1981 more than 30 million people have died due to AIDS - related infections, more than 34 million people are currently living with HIV, and nearly 2.5 million individuals are newly infected each year, thereby making HIV transmission a global health concern[4,5]. Although these numbers may seem daunting it is important to recognize how far HIV/AIDS research has advanced over the past 30 years. A HIV-positive diagnosis was once thought to be a death sentence, but now patients can expect to live for several decades due to the introduction of a cocktail of inhibitors referred to as highly active antiretroviral therapy (HAART) in 1996. Promisingly, HAART has led to a 70% drop in mortality rates thereby making HIV a chronic yet manageable disease, but it is important to emphasize that HAART is not a cure [4,5]. Due to the ever-changing nature of viruses, HAART is not effective in HIV positive patients that may be infected with resistant viral strains. Additionally, continued administration of HAART can itself lead to resistance, making the once effective treatment futile [6,7]. There is still much research to be done and many advancements to be made.

Effort has been thrust into developing vaccines, but there are currently not any vaccines which are capable of neutralizing the virus [8,9]. Although the efforts mentioned above have displayed some

success in reducing HIV-1 transmission, there is still a pressing need for alternative therapies, prevention strategies, novel drugs, drug targets, and microbicide development. Understanding the structure and function of HIV-1 Env is essential for prophylactic development because Env-targeting drugs may have the ability to destroy virus particles before they engage target CD4 cells, which enhances their potential as a therapeutic.

1.1 HIV-1 Life Cycle

1.1.1 HIV-1 Structure and Entry:

HIV-1 is an enveloped retrovirus belonging to the lentivirus genus and has a spherical shape with a diameter of about 120 nm, making it a rather large virus. HIV particles are encapsulated by a lipid bilayer that encloses viral proteins and viral RNA (**Figure 1**)[10,11]. In the viral particle twelve of these proteins are present including four Gag proteins MA (matrix), CA/p24 (capsid), NC (nucleocapsid), and p6. Additionally, the two Env proteins, which are the structural components of the virus, are gp120 and gp41. Furthermore, HIV contains three Pol proteins PR (protease), RT (reverse transcriptase), and IN (integrase), all of which provide essential enzymatic functions. The accessory proteins Vpr, Nef, and Vif are also packaged into the virion. Tat, Rev, and Vpu are gene-regulatory accessory proteins that aid in HIV infection and life cycle[10].

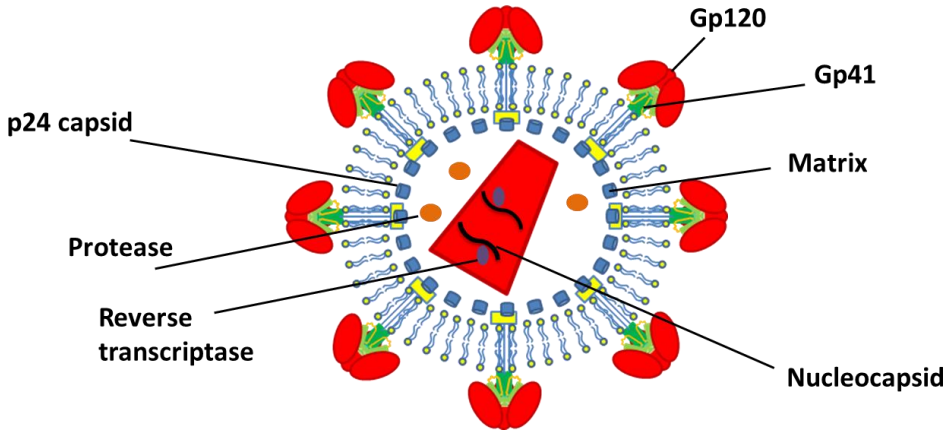

Figure 1. Schematic depiction of an HIV particle. HIV consists of two RNA strands with associated enzymes, which are protected by the conical shaped p24 capsid proteins. p24 is surrounded by the matrix protein and a phospholipid bilayer encloses the viral envelope from which the gp160 proteins are anchored to. Schematic adapted from Charles Ang.

The HIV viral membrane contains the trimeric envelope glycoprotein (Env). Each Env trimer consists of two non-covalently associated glycoproteins, a gp41 transmembrane protein, and an external gp120 surface protein [12-14]. HIV Env infects vital immune cells that display CD4 receptors on their surface along with a chemokine co-receptor CXCR4 or CCR5, such as T cells, macrophages, and dendritic cells[15]. Several conformational changes within Env are required to initiate co-receptor binding after CD4 engagement (**Figure 2**) [12,16]. Specifically, a bridging sheet conformation of gp120 is induced by the formation of two beta sheets brought together to form a four - stranded beta sheet. The CD4 binding also results in the exposure of the V1/V2 and V3 loop structures, which orients gp120 so that the bridging sheet and V3 loop are directed toward the host membrane [17-19].

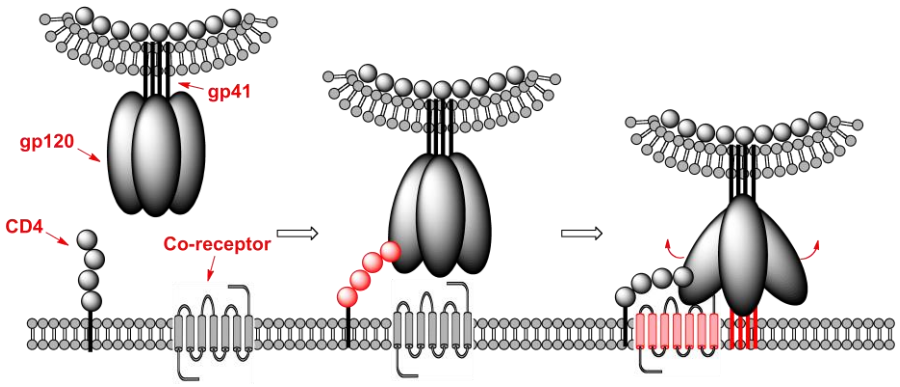

Figure 2. Schematic representation of the HIV entry process. Schematic by Andrew Holmes.

This series of Env conformational rearrangements causes the exposure of the hydrophobic fusion peptide of the N terminus sequence of the transmembrane protein, gp41, the host cell membrane. The extended conformation of gp41 forms a "prehairpin intermediate" (**Figure 3**), this takes place when the N- terminus of gp41 inserted in the cell membrane and its C- terminus in the viral membrane[15,20].

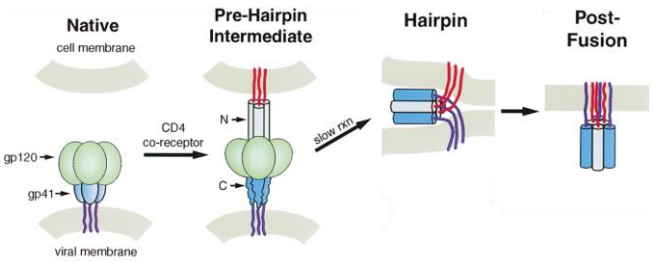

Figure 3. Model of HIV Membrane Fusion[15]. The model shows the conversion of the pre-hairpin intermediate into the hairpin "six helix bundle" formed with one spike and folded perpendicular to the viral membrane. The HR1 and HR2 regions are displayed in white and blue, respectively. Copyright permission granted.

The two heptad repeat regions of gp41 fold onto each other to form a stable and energetically favorable 6-helix bundle, thereby guiding the viral and host cell membranes adjacent to each other to allow membrane fusion[20]. The membrane fusion process is essential for infection because it ensures the transmission of the RNA viral genome into the host cell along with MA, RT, IN, and Vpr. This material is transported to the host cell nucleus where the viral RNA is transcribed to DNA by RT, next IN integrates the viral DNA into the host genome[10]. It is at this point that the host cell is now completely exploited by HIV to produce viral components. The integrated provirus DNA is transcribed into mRNA and then spliced and exported to the cytoplasm for translation into the regulatory protein, Tat. Gag and Env are produced from unspliced full-length mRNA and are packaged into new viral particles that bud off the cell surface membrane and go on to infect more

cellular targets to create new progeny. Upon budding, the capsid undergoes protease cleavage, which yields a mature fully infectious viral particle.

1.1.2. Structure of HIV Envelope:

The numerous intricate conformational changes that are needed for HIV entry demonstrates the crucial role of gp120. Env is the only virus-specific protein on the virion surface and is essential for cell - receptor interactions and subsequent virus-cell fusion. Therefore, HIV-1 Env is an important target to directly inhibit and thus block the initial steps leading to host cell infection. For this reason, Env-specific inhibitors that inactivate the virus and block receptor engagement would be useful for suppressing HIV-1 infection and the spread of AIDS.

Gp120 is a heavily glycosylated protein. It is extensively modified with high mannose and complex carbohydrates resulting in almost 50% of its molecular weight[21]. Its sequence consists of five conserved regions (C1-C5) intertwined with five highly variable loops (V1-V5)[21]. Extensive research has shown that the "core" gp120 is made of the conserved regions and the variable loops extend from the core[22]. The architecture of gp120 is thought to behave as a series of layers, which respond and move according to its association with receptor and co-receptor[23]. The "unliganded" state of gp120 is structurally metastable and its highly glycosylated domains are arranged in a manner that protects the virus from the immune system by forming a "glycan shield"[23]. Only after receptor engagement do the layers of the "liganded" gp120 move to reveal the binding sites. It is in the bound or active state of gp120 that the conformation can be divided into two separate

domains[24]. Both domains contribute two beta sheets which converge at the bridging sheet where the co-receptor binds (**Figure 4**). The interface of the inner domain, outer domain, and bridging sheet contains a deep hydrophobic cavity, whose primary binding target is the Phe43 residue of CD4. The cavity is lined with highly conserved amino acids in the variable region, thereby exemplifying the critical nature of gp120 binding specificity to the Phe43 residue[23]. In all, the constant conformational rearrangements and heavy glycosylation make gp120 an elusive target.

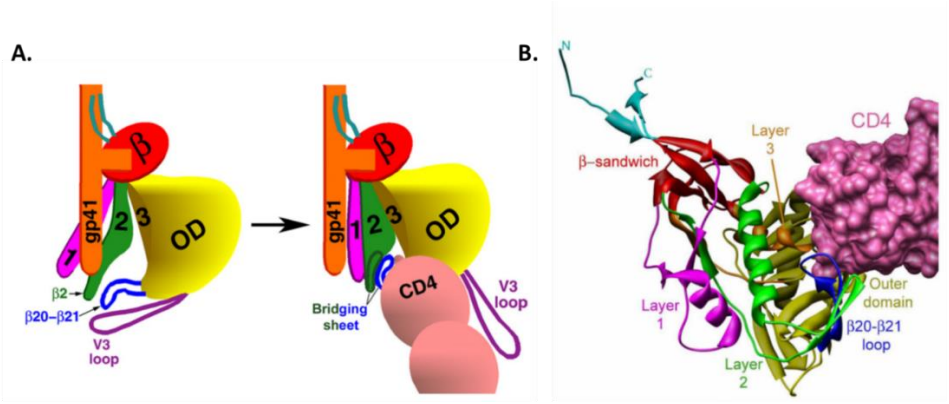

Figure 4. Model of HIV-1 gp120 monomer activation triggered by CD4 binding. A. The image is oriented to depict the viral membrane at the top of gp120[25]. The image displays the gp41 ectodomain (orange), β20-β21 loop (blue), gp120 outer domain (yellow), and the gp120 inner domain beta sandwich (red). The inner domain consists of three layers; layer 1(magenta), layer 2(green), and layer 3(yellow). Inner domain rearrangement after CD4 binding. V3 and β20-β21 loops move to form the bridging sheet post CD4 binding to allow gp120 availability for co-receptor binding. B. The structure of HIV-1 HXBC2 gp120 (ribbon) bound to a CD4 domain (pink surface)[24]. Copyright permission granted.

However, in 1998 the crystal structure of a deglycosylated gp120 "core" lacking some N and C termini as well as the variable loops bound to CD4 and 17b, a co-receptor surrogate, contributed to a much greater understanding of the structural biology of gp120[24,26]. Although this structure was not a complete representation of HIV-1 Env, it revealed potential new gp120 sites that could be

targeted by inhibitors. Due to the homology between HIV and SIV many researchers have found it useful to compare these structures to provide answers regarding the structural conformations of bound and unbound gp120. Crystal structure analysis of HIV ad SIV bound to the antibodies F105 and b12 as well as CD4 helped to show that hydrophobic residues in the V3 loop help maintain the gp120-gp41 association (**Figure 5**)[27]. Since this time several other gp120-liganded crystal structures have been determined which contain more domains of gp120, such as the V3 and V4 loops and some portions of the N and C termini (**Figure 5**)[27].

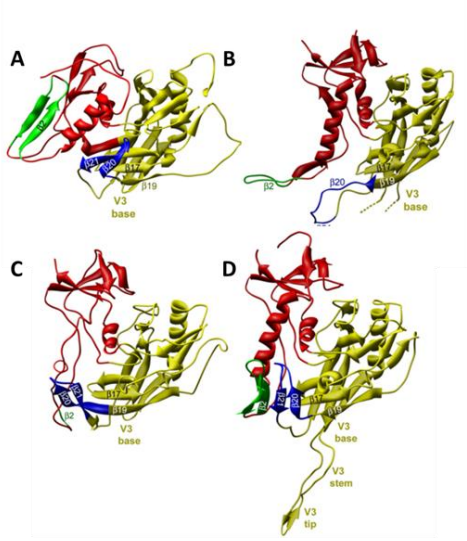

Figure 5. Various conformations of SIV or HIV crystallographically determined structures[27]. (A) Unliganded SIV. (B) F105 Bound HIV-1. (C) b12 Bound HIV-1. (D) CD4 Bound HIV-1. The HIV-1 HXBc2 core gp120 crystal structures observed in complex with Fab fragments of b12 or F105 neutralizing antibodies or with two-domain CD4. The HIV-1 domains are colored as follows: outer domain (yellow), inner domain (red), bridging sheet (blue) [blue for β20-β21 loop and green for β2-β3 of the V1/V2 region. Copyright permission granted.

Furthermore, cryo electron tomography produced a 6 - Å membrane bound, uncleaved, and fully glycosylated trimer structure and crystallography has produced the structure SOSIP (pdb structure-4NCO), a native cleaved trimer[28,29]. These detailed trimer structures have spurred the discovery of antibodies and the identification of immunodominant HIV envelope target sites, thereby spurring efforts for an HIV vaccine[30,31].

All together these newly emerging structures provide a more holistic depiction of gp120-CD4 interactions and have been a platform to gain more detailed information about the binding interactions of many inhibitors. These structures are also valuable because they are being using for computational modeling to develop novel drugs against the ultimate target, the HIV viral spike.

1.2 HIV Entry Inhibitors

HIV entry requires the coordinated conformational changes of the viral envelope spike and the gp41 transmembrane protein. These intricate events allow for the initial receptor and co-receptor binding, fusion of the viral and host membranes, and subsequent viral integration events leading to HIV protein production. The multi-step process of HIV entry has enabled researchers to target the life cycle from many angles, ranging from inhibiting entry, viral membrane fusion, reverse transcription and integration of the viral genome, all in hopes of eradicating HIV transmission.

1.2.1 HAART:

HIV-positive patients receiving HAART are administered a cocktail of inhibitors, therefore controlling the plasma levels of HIV-1 RNA below detectable limits. There are more than 30 FDA-approved inhibitors for HAART treatment, each of these inhibitors belonging to one of six classes[32]. These include protease inhibitors (PIs), fusion inhibitors (FIs), integrase inhibitors (IIs), non-nucleoside reverse transcriptase inhibitors (NNRTIs), nucleoside reverse transcriptase inhibitors (NRTIs), and chemokine receptor antagonists (CRAs)[32]. A series of patient- specific factors go into deciding which inhibitors are used in HAART, such as allergies of the patient and the viral load based on CD4 counts. After analysis of the patient diagnosis a minimum of two inhibitors are used in combination since these drugs target different stages of the viral life cycle[33]. However, there are still challenges that face HAART. Many HIV-1 patients report serious adverse effects because of HAART, so many discontinue use and patients who adhere to the treatment eventually no longer respond to the inhibitors due to viral resistance[33,34].

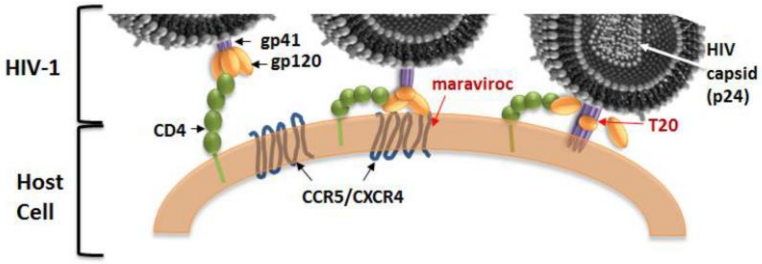

Figure 6. Mechanistic and therapeutic insights of HIV-1. Maraviroc and T20 (red) are current inhibitors that target HIV-1 fusion[35]. Maraviroc targets the CCR5 co-receptor, thereby inhibiting gp120 binding. T20 targets gp41, prevents six-helix bundle formation, subsequently inhibiting viral and host cell membrane fusion. Rosemary Bastian Dissertation 2014.

At the onset of viral resistance to HAART, patients are switched to salvage therapy, a treatment of inhibitors against HIV entry and fusion. Enfuvirtide, or T-20, is a 36 amino acid peptide that blocks the fusion process[36] (**Figure 6**). T-20 is comprised of a segment of the membrane proximal exposed region (MPER) of the gp41 protein. T-20 binds to the N- terminal heptad region (N-HR) of gp41 thereby preventing the assembly of the pre-hairpin intermediate and ultimately the six helix bundle, thus halting entry[37]. It is well documented that the N-HR of gp41 is transiently exposed, therefore T-20 has a limited time of action[38]. However, several escape mutations in the N-HR of gp41 have developed, which reduce the binding affinity of T-20 by nearly 50 fold. Side effects resulting from T-20 are similar to those of HAART, including diarrhea and nausea[39] additionally, because T-20 is administered twice daily subcutaneously, skin irritations and rash at the injection sites are also commonly reported. Lastly, the cost of production for peptides are extremely high, therefore T-20 is not used as a first line regimen of HAART, yet it is a salvage therapy.

Maraviroc is a Pfizer co-receptor inhibitor also FDA approved for salvage therapy. The small molecule binds to CCR5, a G-protein coupled receptor required for most HIV-1 clades, therefore preventing gp120 recognition[36]. Because Maraviroc solely inhibits R5-tropic viruses, candidate patients must initially undergo screening to confirm their co-receptor tropism. The limited viral scope of Maraviroc eventually leads to escape mutations as evidenced by the emergence of X4-tropic and X4R5-tropic viruses utilizing the CXCR4 co-receptor to gain entry into host cells[40]. Side effects of this orally administered drug include upper respiratory infections, rashes, and dizziness.

It is clear that the HAART represents the standard of care for HIV patients. However, it is also clear that there are still gaping holes in the field of viral entry and fusion inhibitors. This makes the need even more pressing to make major strides in the development of more potent entry inhibitors that yield less resistance.

1.2.2 CD4-Gp120 Interaction Inhibitors:

Gp120 engagement with CD4 is a critical stage for viral entry because it represents the virus' first encounter with a host cell. Therefore, disrupting gp120's interaction with CD4 has been at the forefront of HIV research. CD4 is a protein consisting of four extracellular domains. The N-terminal domain has a beta hairpin containing the Phe43 residue, thereby making this domain indispensable for gp120 binding[23,41]. The crystal structure from Kwong et al. of gp120 bound to CD4 highlighted the highly conserved residues in the span between 25 and 64 that outline the Phe43 cavity, importantly Arg59[23]. Researchers equipped with this newfound structural information of the g120 binding site in CD4 have made many attempts to block the CD4-gp120 interaction through the use of CD4 mimetics. However, this interaction has proven to be an elusive target.

One of the first attempts at disrupting this interaction was the development of a soluble CD4 (sCD4), engineered by the recombinant extracellular portion of the CD4 protein. sCD4 was found to be a potent therapeutic when tested in laboratory inhibition studies done in vitro. However, the hope of this becoming a successful drug was quickly halted when it did not display any efficacy in clinical trials[42,43]. The loss of efficacy is attributed to reduced affinity of sCD4 of primary HIV-1 isolates due to resistance mutations. Another approach has been to develop Phe43 cavity- targeting small molecules, examples include the BMS compounds and CD4 mimetics, like NBD inhibitors and the M33 peptide. The BMS class of inhibitors restructure gp120 making it unrecognizable for CD4 binding[44,45]. Despite the promising potency of BMS 448043, BMS 626529, and BMS 378806, these inhibitors did not progress further than phase 2 clinical trials due to poor pharmacokinetics[46]. The NBD class of compounds were originally identified by a screen. The lead drugs were improved upon by rational design to increase infection inhibition and gp120 binding potency[47]. However, further analysis of the NBD inhibitors demonstrated that they restructure gp120 in a manner very similar to that of CD4. This conformational entrapment of gp120 induced by NBD inhibitors led to enhanced co-receptor binding[48,49]. This was a highly disappointing result because it caused infection in CD4-negative cells[50]. Another CD4 mimetic was the 27 residue peptide, M33. M33 could not have been created without the detailed structural information about the gp120-CD4 binding interaction. CD4 consists of a beta hairpin that is responsible for most of its interaction with gp120. A structurally similar beta hairpin is found in scorpion and charybdotoxin, therefore the gp120 binding surface was placed onto the toxin scaffold, yielding M33[50,51]. The peptide bound directly into the Phe43 cavity, therefore preventing viral entry. However, its limitations were similar to the NBD class of compounds. It also induced the restructure gp120 in a manner similar to that seen with CD4, thereby causing enhanced co-receptor binding and subsequent enhanced infections[48,50].

Targeting the Phe43 cavity to disrupt the gp120-CD4 binding interaction is sought after because it remains one of the most highly conserved sites on gp120 where resistance mutations are unlikely to appear. However, the various attempts made to disrupt this critical interaction has taught us several things about the binding interaction. The efforts displayed in the era of CD4 mimetic development have shown that that designing Phe43 cavity inhibitors may still be a feasible route as long as they do not induce the gp120 structural rearrangements which allow co-receptor recognition and binding as we have seen that they led to enhanced infection.

1.2.3 Virucidal Agents and Microbicides:

Microbicides are generally pharmacologic or chemical agents that destroy microorganisms that cause human infection. Microbial activity can be utilized in numerous delivery systems, ranging from lotions, gels, tablets and films[52]. They can exert their action by detergents and surfactants, polyanion attachment strategies, nanoscale dendrimers, and anti-retrovirals (ARV) delivery[52,53]. Therefore, microbicides are a potentially useful method to prevent the transmission of HIV. Even further, microbicides that engage virions and cause specific viral lysis at the initial point of contact are known as virucidal agents. Virolytic microbicides of HIV-1 Env work by a mechanism which specifically targets Env in the absence of cells, thereby making them a potential prophylactic.

HIV-1 Env is of great importance for prophylactic development because these microbicides may have the ability to destroy virus particles before they engage target CD4 cells. For example, nonoxonyl-9 (N9), a nonionic detergent, was one of the first virucidal surfactants clinically tested[54,55]. Initially N9 was met with great promise because of its ability to disrupt viral membranes and because it could be manufactured cheaply. Although the FDA deemed N9 an effective vaginal contraceptive, it was not until later clinical trials analyzing the efficacy of N9 for sponge, gel, or

film formulations found the microbicide was not acceptable for general use. The clinical trial, COL-1492, administered between 1996 and 2000 most eloquently demonstrated precisely how inadequate N9 was for HIV prevention. COL-1492 displayed an increase in the incidence of HIV in the N9 group relative to the placebo group[56,57]. In subsequent laboratory studies N9 was shown to induce pro-inflammatory cytokines and have poor specificity for viral membranes and also caused damage to vaginal and rectal mucosa. After several surfactant microbicides failed clinical trials, there was a shift toward using polyanions as a microbicide source. Polyanions specifically bind to and inactivate viral particles, making them much more specific than surfactants. Like surfactants, polyanions are also cheap to produce, yet they have the additional feature of safety. The two efficacy trials using polyanions, cellulose sulfate and PRO 2000, were terminated after data revealed that they were not efficacious and they increased the risk of HIV infection[57,58]. Nanoscale dendrimers contain a multivalent display of microbicides, which lead to reducing HIV-1 replication upon contact. Microbial dendrimers have served as new age inhibitors for HIV, but also for reducing transmission of other sexually transmitted diseases. The broadly acting microbicide, VivaGel (SPL7013) was found to be a potent virucidal agent[59] not only against HIV, but also against human papilloma virus (HPV) and Herpes simplex virus (HSV). However, the utility of the microbicide varies depending on the drug toxicity to epithelial cells and the effect of semen on the protectiveness of the drug. Lastly, utilizing ARVs as microbicides has proven to be the safest and most potent method for preventing HIV-1 infection because it is most specific to the virus. The CAPRISA 004 clinical trial analyzed a gel formulation of the NRTI, tenofovir, also used in HAART[60]. The efficacy trials of 1% tenofovir gel displayed a greater than 50% reduction in HIV-1 acquisition[60,61]. Even more, the assessment did not display any changes to viral loads or adverse side effects.

There is a renewed enthusiasm in the HIV field for developing microbicide agents using other reverse transcriptase inhibitors. Researchers are hopeful that producing microbicides which

specifically target the virus will be a nontoxic mode of preventing HIV infection[57,58,60,62]. But, there are some concerns that are associated with using HAART inhibitors for microbicide treatments. It is risky to use a topical or oral treatment for pre-exposure prophylaxis treatment, which in many cases can lead to the emergence of escape mutations. The next goal in evolving microbicides should be directed towards using agents that specifically target the virus, but are not apart of current HIV therapy.

1.2.4 Peptide Triazole Thiols: Novel HIV-1 Entry Inhibitors

Previously, in an attempt to develop entry inhibitors, a phage display was used (8) to discover dual antagonists of gp120, which prevent CD4 and co-receptor binding. This effort led to the linear peptide precursor, **12p1** (12p1, RINNIPWSEAMM). Modifying proline 6 of **12p1** with an azide and subsequent copper-catalyzed (2+3) cycloaddition reactions of the azide with substituted acetylenes (Click Chemistry) led to production of a series of triazole peptide conjugates (**Figure 7**) with enhanced binding affinities to HIV-1 gp120[63-66]. The highest affinity candidate in the series of peptide triazole conjugates was the ferrocene triazole conjugate HNG-156. This derivative and related compounds are known as peptide triazole inhibitors. These were shown to bind to HIV-1 gp120 with an equilibrium dissociation constant K_D of 7 nM, in contrast to the 2600 nM K_D of the 12p1 precursor. The peptide triazole family of inhibitors binds gp120 and alters its conformation, thereby preventing it from engaging CD4 receptors as well as the co-receptor surrogate mAb 17b. Dual receptor site antagonism likely derives from allosteric action on the envelope protein[67,68]. In all, the HNG156 prototype of the peptide triazole class of entry inhibitors was found to bind to HIV-1 gp120 with nanomolar affinity[65], to suppress protein ligand interactions at both the CD4 and co-receptor binding sites of gp120[65,68] and to inhibit cell infection

of virus subtype A, B, C, and D isolates[69]. The peptide triazole does not exhibit any detectable toxicity in a tissue explant model at concentrations up to 100 μM[69]. Additionally, peptide triazoles cause gp120 shedding, therefore irreversibly inactivating HIV-1 Env[70]. Interestingly, a sub-class of peptide triazoles, peptide triazole thiols (PTTs), containing a C-terminal cysteine sulfhydryl group were found to cause viral lysis, evidenced by p24 release along with gp120 shedding.

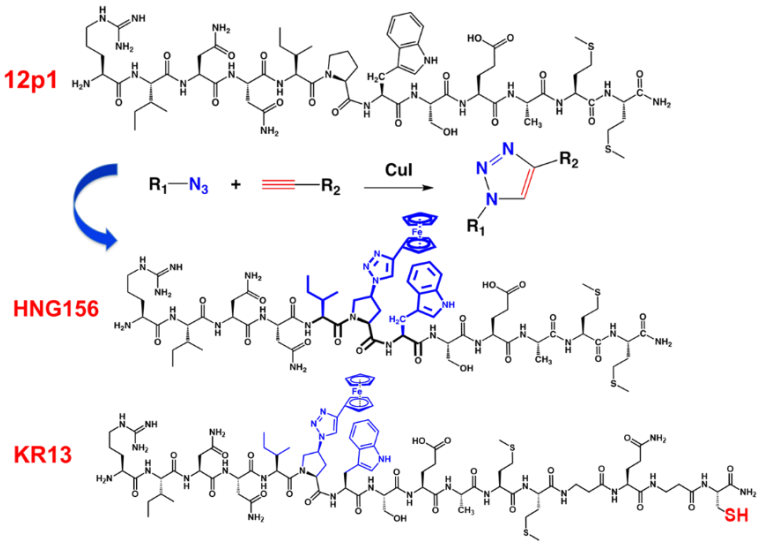

Figure 7. Conversion of linear peptide, 12p1, to peptide triazole, and next generation peptide triazole thiols. Ferrocenyl conjugates attached the Azido proline residue by Click Chemistry to generate potent peptide triazoles.

We have conducted site - directed mutagenesis experiments of the CD4 binding pocket of gp120 to identify the binding footprint of peptide triazoles with HIV-1 Env. Mutations in the residues of the inner and outer domain (D474A, T257A, and S375W) have shown a reduced binding affinity to peptide triazoles[70], therefore implicating their roles in initiating contact with peptide triazole inhibitors (**Figure 8**).

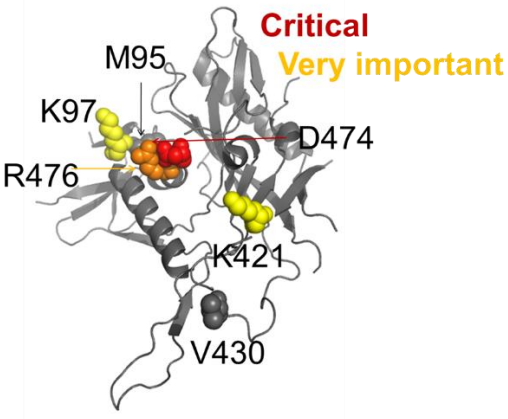

Figure 8. Functional epitope of PT in the context of gp120 in the mAb F105 bound state. Residues critical for PT binding are highlighted[71].

Thus, peptide triazole inhibitors bind to gp120, close to the Phe43 binding pocket, utilizing conserved residues in this region to alter its conformation, therefore preventing Env's recognition of both CD4 and co-receptor[68,72]. To further elucidate the role of these conserved residues we performed additional mutations (D474A, D474E, T257A, T257S, M475A, and S375W) in gp160

to determine their effects in cell infection and virolysis assays[71]. We have shown that peptide triazoles target HIV-1 Env specifically through conserved residues near the CD4 binding pocket, whereby the entry inhibitors undergo interactions with gp120 which disturbs the viral membrane. However, the events that cause viral membrane rupture are unknown.

The conformational entrapment trajectories induced by peptide triazole thiols will allow us to understand which Env epitope interactions and structural transitions lead to the most effective neutralization of the virion. Further, understanding the virolytic mechanism by analyzing disulfide exchange reactions will identify residues of Env that need to be targeted to optimize our entry inhibitors. The gp120 shedding and virucidal action of peptide triazoles has potential therapeutic use by preventing AIDS transmission and treating HIV-1 infected patients. The use of virolytic peptide triazoles as a potential therapeutic is based on their ability to inactivate virus before it engages host cells and the antigenicity of the retained gp41 on the residual virus particle. In the latter regard, peptide triazole thiols may possibly be used as an immunogen to develop an HIV vaccine.

1.3 The Biological and Biochemical Importance of the Sulfhydryl

Of the 20 proteinogenic amino acids, cysteine is special. Cysteine contains a reactive sulfhydryl group which is made possible by the sulfur atom found on its side chain, thereby making it a sulfur amino acid[73]. Methionine is also a sulfur amino acid, however its sulfur atom is attached to a methyl group which makes methionine more hydrophobic and the thiol less reactive than the one

found in cysteine. The reactivity of the sulfhydryl group on cysteine allows for the facile formation of a disulfide bond created by the oxidation of two bridging cysteines. This dimer of cysteine residues linked by a disulfide bond is referred to as a cystine, whose role is crucial in protein structure. Because of cysteine's thiol reactivity it is a potent nucleophile which can participate in disulfide-exchange, alkylation, and peptide hydrolysis reactions. In addition to the sulfhydryls role in protein structure, it also contributes to many biological processes by regulating enzymatic activity[73]. Further, more recently it has been shown that viruses maintain a balance of thiols and disulfides in a mechanism called, thiol-disulfide exchange, as another means to regulate the viral entry process.

1.3.1 Role of Cysteine and Sulfhydryls in Protein Structure

Protein structure and function are based on the protein's primary structure, which consists of the amino acid sequence and topology of disulfide bridges. The pattern of disulfide bridges is important to the three dimensional structure of the protein because they influence stability of secondary and tertiary structures, such as helices. For example, some proteins contain cysteine residues which are not involved in a disulfide, in this case the sulfhydryl group of the cysteine residue stabilizes alpha helix formation. However, more commonly cysteines are frequently found in pairs due to their propensity to form disulfides[73]. The strong forces which hold together the disulfide cause secondary structure motifs, such as "turns" and "loops"[73]. Of these motifs created by disulfides is the cystine knot. This protein structural motif is comprised of six cysteine residues, yielding three disulfide pairs and leading to the formation of several loops of polypeptide. The cystine knot motif

provides great stability to proteins across many species, including spider and snail toxins as well as plant cyclotides.

The cleavage and reformation of disulfides alter the stability of the tertiary structure, and without disulfide bridge formation between several protein chains, quaternary structure would not be possible. For this reason, disulfides are often referred to as "molecular staples" due to their ability to maintain structural motifs which are critical to the proper folding and subsequent function of proteins. The essential role of disulfides in reinforcing protein conformations, paired with the highly conserved nature of cysteine residues, explains why cysteines and disulfides are frequently used as regulatory tools.

1.3.2 Role of Cysteines and Sulfhydryls in Enzymatic Activity

Not only do cysteines contribute to the structural integrity of proteins, they are also involved in enzyme catalysis and affect in vivo redox potential, which influences downstream cellular processes and mechanisms [73-75]. For these reasons, cells maintain a distinct thiol/disulfide balance, in order to regulate biological processes. Cysteine is required for the activity of the thiol protease class of enzymes due to a reactive cysteine sulfhydryl group in the catalytic site. This feature is necessary to initiate the reaction with the substrate. Blocking a reactive sulfhydryl group, whether because of its use as a mixed disulfide, oxidation, or alkylation, can result in enzyme inactivity (71). There is a variety of classes of enzymes which use cysteine residues to exert and regulate their mechanisms. The thiol proteases, HIV protease, papain and caspases utilize their cysteinyl residues

for nucleophilic attack during peptide cleavage and the metabolic enzyme responsible for key regulatory steps in glycolysis, glyceraldehyde-3-phosphate dehydrogenase (GAPDH), contains a cysteine residue in its active site. Not only does the thiol in the catalytic site of GADPH have a direct influence on ATP production, but its activity is involved in transcriptional activation, vesicle shuttling from the ER to Golgi, and the initiation of apoptosis [76,77].

The equilibrium between the reduced and oxidized state of cysteine's sulfhydryl group impacts the redox potential in biological systems[74,75]. For example, the tripeptide antioxidant, glutathione, contains a cysteine residue which enables the peptide to maintain reduced cytoplasmic proteins[75]. This process oxidizes glutathione yielding glutathione disulfide, however NADPH is used as an electron donor to regenerate the reduced glutathione reductase peptide. The ratio of reduced and oxidized forms of NADPH goes on to regulate biosynthetic reactions, such as cholesterol and lipid synthesis.

The redox state of thiols affects further downstream events, such as post-translational modifications. Phosphorylation events are affected by redox modulation since oxidative environments inhibit phosphatase activity, which directly influences protein signaling[73]. Lastly, numerous processes require signal transduction which is transmitted through dimerized proteins made possible through the formation of a disulfide bond between the two protein subunits. The formation of the disulfide bond may require the oxidation of the cysteine in one subunit and the condensation of a cysteine in the other subunit, which is determined by the redox modulation[73].

Therefore, cysteine's role is vast because of its utility as a strong reducing factor and its thiol nucleophilic reactivity, thereby enabling it to act readily act as immediate "switch" to turn on and off enzyme activity as well as affect downstream processes. These attributes make the use of thiols essential as a regulatory action.

This work provides evidence HIV entry utilizes thiol/disulfides for regulation, through a mechanism called “disulfide exchange”, a process shown to be involved in several viral entry processes. Thiol- disulfide exchange is a reaction of a thiol interacting with and disrupting a disulfide to form a new disulfide and subsequently produces a newly derived thiol (**Figure 9**) [73,74,78].

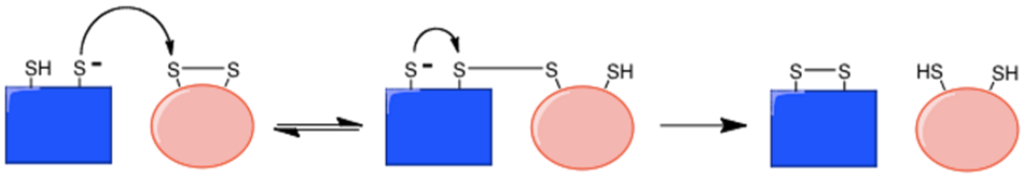

Figure 9. Cartoon depicting in the mechanism of thiol-disulfide exchange. For oxidoreductase cleavage, the active site sulfur ion nucleophile of the oxidoreductase attacks one of the sulfur atoms of the allosteric disulfide bond. The mixed disulfide then releases the oxidized oxidoreductase and the substrate protein contains a reduced allosteric disulfide. Pink circles represent gp120 containing disulfides and blue squares represent an oxidoreductase, which has a reactive thiol that initiates the disulfide-exchange mechanism.

CHAPTER 2: Exploring the Spatial Relationship between the Binding Pharmacophore and Sulfhydryl structural motifs of Peptide Triazole Thiols

2. Introduction

Inhibiting HIV-1 cellular entry remains an enticing strategy for HIV-1 intervention and prevention. The entry process is mediated by the interaction of the trimeric envelope glycoprotein (Env) on the virus membrane surface with the host cell receptors, CD4 and co-receptors CCR5 or CXCR4. Because Env is the only virus-specific protein on the virion surface and is essential for cell receptor interactions and subsequent virus-cell fusion, it is an important target for directly inhibiting and blocking the initial steps leading to host cell infection. Our lab previously developed a novel class of dual antagonistic peptide inhibitors of HIV-1 Env. Upon binding gp120, the peptide triazoles alter gp120 conformation to an inactive state, thereby disrupting protein-ligand interactions. These peptides potently inhibit cell infection and cause gp120 shedding from the virus. In addition, a subclass of PTs containing a free sulfhydryl group (SH) at the C terminus, denoted peptide triazole thiols or PTTs, was found to be virucidal as evidenced by release of the p24 capsid protein from the virus lumen. Here, we investigated the spatial relationship between the gp120-binding pharmacophore Ile-ferrocenyltriazolePro-Trp (denoted IXW) and the peptide C-terminal cysteine (Cys) residue that is required for lytic inactivation.

An obligatory dimer of KR13 formed by crosslinking of the Cys in KR13 with a bis-maleimide crosslinker did not cause viral lysis, although it did retain the ability to bind gp120 demonstrating that lysis requires the free Cys SH. PTT's with serially shortened linkers between functional groups IXW and CysSH were synthesized and their relative lytic activities vs. gp120 binding functions were determined. From a comparison of p24 release and antiviral activity, we observed a strong dependence of lysis activity on the length of the linker between the IXW pharmacophore and SH group. Molecular docking of PTT onto gp120 argued that, with sufficient linker length, the peptide SH could approach several gp120 disulfides. Furthermore, by performing competition p24 assays

with several distinct gp120 ligands, we found that the disulfide cluster located at the base of the V3 loop may have a role in PTT-induced disulfide disruption.

The results of our structure-activity analysis studies resulted in a greater understanding of the characteristic motifs of PTT required for lysis. We found that there is a required minimum C-terminal linker length after the pharmacophore residues, additionally the linker must terminate with a free C-terminal thiol group, which strongly supports the hypothesis that the p24 release of PTTs is promoted by disulfide exchange. Overall, the findings suggest that PTT binding, via its IXW pharmacophore residues, positions the peptide SH group to interfere with conserved disulfides clustered proximal to the CD4 binding site in gp120. It is possible that the close proximity of the peptide thiol group could lead to a rearrangement of the Env protein spike and ultimately disruption of the viral membrane.

2.1 MATERIALS AND METHODS

2.1.1 Peptide Synthesis and Click Conjugation

All sequences and denotations of peptides reported are given in **Table 1**. Peptides were synthesized manually by stepwise solid-phase peptide synthesis (SPPS) (**Figure 10**) on a Rink Amide Resin (NovaBiochem) with a substitution value of 0.25 mmole/gm as described previously[72]. The 9-fluorenylmethoxycarbonyl (Fmoc) group was employed for protection of the α-amino group during coupling steps. All α and β Fmoc amino acid derivatives and coupling reagents were purchased from Chem-Impex International, Inc. Side chain protecting groups were triphenylmethyl (Trt) for Asn, tert-butyl (tBu) for Ser and tertbutyloxycarbonyl (Boc) for Trp. Synthesis grade solvents were used in all procedures. Coupling of each residue was carried out using N, N, N′, N′-tetramethyl-

O-(1H-benzotriazol-1-yl) uronium hexafluorophosphate (HBTU) / hydroxybenzotriazole (HOBt) in dimethylformamide (DMF). Four equivalents of each Fmoc protected amino acid were used for coupling. The [3+2] cycloaddition reaction with ethynyl ferrocene (Sigma Aldrich) was carried out by an on-resin method. Completed peptides were cleaved from the resin by using a cocktail of 95:2:2:1 trifluoroacetic acid/1, 2-ethanedithiol/water/thioanisole. Crude peptides were purified using a semi-preparative column (Phenomenex Jupiter 10u C4 300A 250 x 10 mm, 3 ml/min) by HPLC (Beckmann Coulter, System Gold 126 Solvent Module and 168 Detector, 280 nm) with gradient between 95:5:0.1 and 5:95:0.1 water/acetonitrile/trifluoroacetic acid. Peptide purity and mass were confirmed using an analytical HPLC column (Phenomenex Luna 5u C18 100A 250 x 4.6 mm, 1 ml/min) and MALDI-TOF mass spectrophotometry, respectively (**Appendix Figures 1-30**).

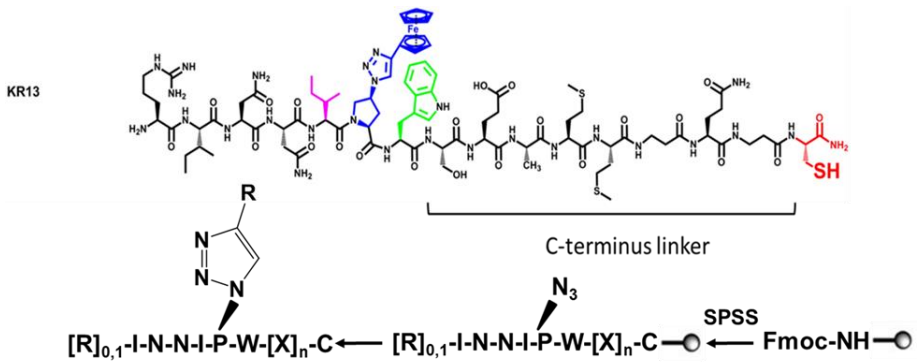

Figure 10. Scheme of Solid Phase Peptide Synthesis (SPPS). Peptide synthesis was performed on rink amide resin using Fmoc-α-amine-protected amino acids.

2.1.2 Chemoselective Ligation of KR13 by Bis-Maleimide

2.084 mg KR13 (**1**) (2.5 eq) was dissolved into 1000 µL of degassed phosphate buffer (50 mM, pH 6.6) prior to the addition of 0.574 mg Tris (2-carboxyethyl) phosphine hydrochloride (TCEP·HCl) (5 eq) (Thermo Fisher Scientific) to the reaction vessel. Peptide **1** was reduced with TCEP for 30 min under vacuum and nitrogen purging. 400 µL of 0.522g of Bis-Mal-dPeg$_3$ (Quanta Biodesign Limited) dissolved into 1000 µL ACN (1 eq) was added dropwise to the reaction vessel. The ligation process was monitored by analytical HPLC (Phenomenex Luna 5u C18 100A 250 x 4.6 mm, 1 ml/min) over a 30-95% ACN gradient, as the reaction mixture was stirred under N_2 at 37 °C for 2 hrs. After 2 hours, another 200 µl of Bis Mal dPeg was added to the reaction. Peptide purity and mass of the final ligation product, (**1a**, Peptide 1 dimer**)**, were confirmed using analytical HPLC (Phenomenex C18) and MALDI-TOF mass spectrophotometry, respectively.

2.1.3 Virus Infection Inhibition Assays

Modified human osteosarcoma cells engineered to express CD4 and CCR5 (HOS.T4.R5), as well as the vector for pNL4–3.Luc$^+$ R$^-$ E$^-$, were obtained through the NIH AIDS Repository from Dr. Nathaniel Landau, while the vector expressing the CCR5-targeting spike protein BaL.01 gp160 was obtained through the NIH AIDS Repository from Dr. John Mascola. The recombinant virus was produced by co-transfecting HEK-293T cells with the proviral envelope plasmid HIV-1$_{BaL}$ strain and the plasmid encoding the backbone sequence corresponding to an envelope-deficient pNL4–3.Luc$^+$ R$^-$ E$^-$ provirus. Post-transfection (72 hours), pseudovirus-containing supernatant was collected, filtered through a 0.45 µM syringe filter and concentrated using an Amicon spin filter (100 kDa MWCO) prior to being loaded on an Iodixanol gradient ranging from 6% to 20% in

phosphate-buffered saline (PBS)[79]. Samples were spun for 2 hours at 112,000 x g on an SW41 rotor in a Beckman Ultracentrifuge at 4 °C. Fractions containing the pseudovirus were collected, aliquoted in serum-free media and frozen at -80 °C.

Prior to cell infection experiments, virus samples were titered for p24 content and infectivity as described below. The viral stocks were first incubated with serial dilutions of the peptide at 37 °C for 30 min and then added to 96 well tissue culture plates, with HOS.T4.R5 cells, pre-seeded for 24 hrs at 8,000 cells per well. After 48 hours infection, with a growth medium wash step 24 hours post-treatment, the cells were lysed with passive lysis buffer (Promega) followed by 3 freeze–thaw cycles. Luciferase assays were performed using 1 mM d-Luciferin salt (AnaSpec) as substrate and detected on a 1450 Microbeta liquid scintillation and luminescence counter (Wallac and Jet). The single-round, pseudoviral infection luciferase reporter assay was conducted as previously described[69]. Nonlinear regression analysis was performed using Origin v.8.1 (OriginLab, Northampton, USA) to calculate the IC_{50} values. All experiments were performed at least in triplicate and results were expressed as relative infection with respect to cells infected with virus in the absence of inhibitor (100% infected).

2.1.4 Competition ELISA

The ability of peptides to inhibit sCD4 and mAb 17b binding to HIV-1_{YU2} gp120 was analyzed by competition ELISA[72]. First, 100 ng of HIV-1_{YU2} gp120 was adsorbed per well at 2 ng/µl to a 96-well high binding polystyrene plate (Fisher Scientific) for 12 hrs at 4 °C. The HIV-1_{YU2} gp120 was removed from the plate and blocked with 200 µL/well of 3% bovine serum albumin (BSA) (Research Products International, Corp) in 1× phosphate buffered saline (PBS) for 2 hours at 25 °C, followed by plate washing 3 times with 1× PBS containing 0.1% Tween-20 v/v (PBS-T). For

the CD4 competition experiments, 100 μL of 30 nM sCD4 was added to each well in the presence of increasing concentrations of peptide. This and all subsequent incubation steps were done in 0.5% BSA in PBS. After a 1 hour incubation period, the plate was washed 3 times with PBS-T followed by addition of 100 μL/well of biotinylated anti-CD4 antibody (eBioscience) at a 1:5000 dilution and the plate incubated for an additional 1 hour at 25 °C. After plate washing, streptavidin-bound HRP (AnaSpec) was added at a 1:5000 dilution and again incubated for 1 hour at room temperature. To determine effectiveness of peptides to inhibit antibody binding to gp120, 100 μL of 15 nM mAb 17b was added to the plate-immobilized gp120 in the presence of increasing concentrations of peptide. After a 1 hour incubation at room temperature, the plate was washed 3 times with PBS-T, followed by the addition of a horse radish peroxidase (HRP)-conjugated goat-antihuman antibody (CHEMICON) which was incubated for 1 hour at room temperature. The extent of HRP conjugate binding was detected in both assays by adding 200 μL of o-phenylenediamine dihydrochloride (OPD) (Sigma-Aldrich) reagent for 30 min followed by measuring optical density (OD) at 450 nm using a microplate reader (Molecular Devices). IC_{50} values were determined using non-linear regression analysis with Origin v.8.1 (Origin Lab, Northampton, USA).

2.1.5 Optical Biosensor Binding Assays

Surface Plasmon Resonance (SPR) kinetic interaction experiments were performed on a Biacore 3000 (GE) optical biosensor instrument. A CM5 sensor chip was derivatized by amine coupling using N-ethyl-N-(3-dimethylaminopropyl) carbodiimide/N- hydroxyl-succinimide with either soluble CD4 or 2B6R (antibody to human IL-5 receptor α as a control). Each of the ligands, sCD4 or 2B6R, were immobilized on the CM5 senor surface chip at a density of 2000 RU. For sCD4 competition experiments, serial dilutions of the peptides with a constant concentration of HIV-1_{YU2}

WT gp120 (200 nM) were injected over the sCD4 surface. The indicated analytes were injected over the surface at a flow rate of 100 µl/min with a 2.5 min association phase and a 2.5 min dissociation phase. Surfaces were regenerated with 10 mM HCl injection for 3 seconds. All experiments were conducted at 25 °C in filtered and degassed PBS pH 7.4 containing 0.005% Tween 20. SPR data analyses were performed using BIAEvaluvation 4.1.1 software (GE Healthcare). The responses from the buffer injection, and responses from the control surface to which the mAb 2B6R was immobilized, were subtracted to account for non-specific binding. Experimental data were fit to a 1:1 Langmuir binding model. The average kinetic parameters generated from a minimum of 3 data sets were used to define the equilibrium dissociation (K_D) constant. The evaluation method for SPR inhibition data included a calculation for the inhibitor concentration at 50% of the maximal response (IC_{50}). The inhibition curve was converted into a calibration curve by the using a fitting function. Data were fit to a four-parameter sigmoidal equation in Origin v.8.1 (Origin Lab, Northampton, USA).

2.1.6 Virolysis Assays

The ability of the peptide triazole thiols to cause virolysis of pseudotyped HIV-1_{BaL} virus was analyzed by quantifying p24 release. An equal volume of intact pseudotyped HIV-1_{BaL}, purified through gradient centrifugation, was added to a series of samples that contained a 1:4 serial dilution of peptide triazole thiols as well as non-lytic HNG156 at working concentrations determined from the cell infection assays. The control samples replaced the peptide with either phosphate-buffered-saline (PBS) (negative lysis control) as well as 1% Triton-X 100 (positive lysis control). All prepared samples were incubated for 30 min at 37 °C prior to a 2 hr spin at 16,000 x g and 4°C on a tabletop 5424R centrifuge (Eppendorf). The top 120-µL soluble fraction was collected and tested for p24 content by sandwich capture ELISA as follows. High binding polystyrene ELISA plates

(Fisher Scientific) were coated with 50 ng/well of mouse anti-p24 (Abcam) followed by blocking with 3% BSA for 2 hr at room temperature. This was followed by PBS-T rinsing three times for 5 min each time. Then the soluble fractions obtained from the peptide treated HIV-1_{BaL} diluted in 1:100 using 0.5% BSA, were loaded onto the plate and incubated for 2 hr. The p24 in the soluble fractions was quantified using 1:5000 dilutions of anti-rabbit p24 (Abcam) and then anti-rabbit IgG fused to horseradish peroxidase (HRP) (Invitrogen). The activity of the HRP conjugate binding was determined by adding 200 µL/well of o-phenylenediamine dihydrochloride (OPD) (Sigma-Aldrich) reagent for 30 min followed by measuring optical density (OD) at 450 nm using a transmission plate reader (Tecan, Infinite F50). The PBS treated virus signals were subtracted; net signals were then plotted as a function of p24 release, using the fully lysed virus control, treated with 1% Triton X-100, as the 100% value. Nonlinear regression analysis was performed using Origin v.8.1 (OriginLab, Northampton, USA) to calculate the EC_{50} values. All experiments were performed at least in triplicate.

2.1.7 Protein expression and purification of CVN

The CVN plasmids were transformed into BL21 (DE3) pLysS cells and scaled-up LB media. Protein expression was induced using 1mM isopropyl-B-D-thiogalactopyranoside (IPTG) for 9 hrs a 30 °C. In order to perform extraction of periplasmic proteins from the bacterial membrane, the cell suspension was pelleted and lysed before being sonicated using a microtip probe (Misonix 3000). The sonicated sample was spun down for 30 min at 10,000 x g to separate the bacterial debris from the protein containing supernantant. The protein was then purified by gravity flow affinity chromatography with nickel-nitriloacetic acid (Ni-NTA) beads (Qiagen), followed by gel filtration with a 26/60 Superdex 200 prep - grade column (GE Healthcare) using an AKTA fast protein liquid chromatograph (FPLC, GE Healthcare). Western blotting of the Ni-NTA and gel

filtration elution fractions along with enzyme - linked immunosorbent assays (ELISA) analysis were used to track protein content of eluates and functionality, respectively. Fractions containing target proteins were concentrated and buffer exchanged to phosphate-buffered saline pH 7.4 using a 5,000 molecular weight cut-off (MWCO) spin filter (Amicon). The final protein was examined on a 15% SDS-PAGE gel using Commassie blue and silver staining. Western blot analysis using a rabbit anti-CVN (Biosyn Inc.) was used to confirm the presence of the CVN component. The final concentration was determined using absorbance at 280 nm and an extinction coefficient at 280 nm of 39,740 M^{-1} cm^{-1}. Cyanovirin-N and gp120 were produced in E.Coli and CHO (Chinese hamster ovary cells respectively, as previously reported[80,81].

2.1.8 Assays for Protein Inhibition of Virolysis

The neutralization EC_{50} values of gp120 protein ligands were used as the starting concentrations for measuring inhibition of virolysis[82,83]. Serial dilutions of 2G12 antibody starting at 1 mg/mL, 1 µM of Cyanovirin, or 100 µg/mL of 697-30D antibody were incubated with the EC_{80} concentration of peptide, namely 10 µM peptide **1**, 14 µM peptide **2**, and 50 µM peptide **8**. The peptide and protein were added to a 1:4 working dilution of the purified pseudotyped HIV-1_{BaL} virions for 30 min at 37 ºC. The soluble fraction was separated, and the extent of p24 release was determined by the same protocol as the sandwich ELISA protocol described above. Virus in PBS was the negative control, while virus in 1% Triton-X 100 was the positive control. Quantified values from triplicate assays were plotted as a function of p24 released compared to the positive control. These values were fit using Origin v.8.1 (Origin Lab, Northampton, USA) to determine EC_{50}s.

2.1.9 Gp120 Shedding Assay

Serial dilutions of peptide triazole thiols **1**, **2**, **4**, **7**, and **9** starting from 50 µM were incubated for 30 minutes at 37 ºC with a 1:4 working dilution of the purified pseudotyped HIV-1_{BaL} virions. Next, the virus-peptide mixture was spun for 2 hr at 16,000 x g and 4 °C on a tabletop 5424R centrifuge (Eppendorf). Negative and positive control samples included, respectively, virus in PBS and virus in 1% Triton X-100. Next, 120 µl was removed from the soluble fraction to separate the viral pellet fraction. Western blot analysis with an anti-gp120 D7324 (Aalto) was used to quantify the amount of viral envelope gp120 retained in the pellet. The western blots were quantified using Image J software, and compared to the blots for the lysed virus fraction. Data for amount of gp120 shed from virus were analyzed by non-linear regression analysis with Origin v.8.1 (Origin Lab, Northampton, USA) to determine shedding EC_{50} values.

2.1.10 Origin Pro. 8 curve fitting of dose dependence data

Data analysis of dose-dependence measurements performed in this study was conducted by sigmoidal curve fitting using the Origin v.8.1 (Origin Lab, Northampton, USA) software. The formula used, which enables a sigmoidal logistic fit, was

$$y = \frac{A_1 - A_2}{1 + \left(\frac{X}{X_0}\right)^p} + A_2$$

where A_1 is the initial value (0), A_2 is the final value (based on the experimental data), p is the Hill coefficient, x is the concentration of the inhibitor used and X_0 is the IC_{50} value. The logistic nature of the fitting algorithm allows the p value to float freely. The differences in cooperativity we observe in the fitted plots likely arise from complexities of the peptide-virion and virion-cell interactions, a situation which is different than simple protein- protein and protein –peptide interactions.

2.1.11 Molecular Docking

***Peptide preparation for docking**:*

Peptide **8** was prepared and drawn using VIDA 4.2.0 (Openeye Scientific Software, Santa Fe, NM. http://www.eyesopen.com). The ferrocene containing peptide was energy-minimized using the MM2 forcefield (ChemBio3D Ultra 13.0) with RMS gradient of 0.001 and 10^4 alterations. The minimized structure was saved as a pdb file, and autodock tools graphical interface (Autodock tools 1.5.6rc3)[84] was used to prepare the minimized structure of **8** for docking.

Flexible docking:

The starting point for peptide **8** flexible docking to gp120 was the previously developed model of PT interactions using the F105 bound crystal structure of gp120 (PDB code 3HI1)[85]. The gp120 structure was extracted from this complex and was further energy refined using Szybki 1.8.0.2 (Openeye Scientific Software, Santa Fe, NM. http://www.eyesopen.com). The option (-max_iter)

in Szybki was set to 10^6 to make sure that the added hydrogen atoms are correctly optimized. The optimized gp120 structure was then prepared by Autodock tools graphical interface (Autodock tools 1.5.6rc3)[84], where non-polar hydrogen atoms were merged, Kollman charges added and Gasteiger charges calculated. Trp112 residue was set to be flexible for the docking such that the indole side chain can move during the docking simulation to accommodate the bulky ferrocene moiety. The grid box for the docking search was set to 52 x 52 x 52 points for the x, y and z dimensions with a spacing grid of 0.375 Å. Grid centers X, Y and Z were set to 55.784, 28.301 and -21.068, respectively. AutoGrid 4.2 algorithm was used to evaluate the binding energies between the peptide and gp120 and to generate the energy maps for the docking run. For docking **8** with gp120 in a high accuracy mode, the maximum number of evaluations ($25X10^6$) was used. Fifty runs were generated by using Autodock 4.2 Lamarckian genetic algorithm[84] for the searches. Cluster analysis was performed on docked results, with a root-mean-square tolerance of 2.0 Å. Visual inspection of the docked poses was done and compared to the mutagenesis analysis results[71,86] to select a low energy representative binding mode. The complex was then typed with the CHARMM forcefield with Discovery Studio 4.0 software (Accelrys Software Inc.: San Diego, CA, 2013) to relax the obtained pose within the protein pockets, visualized by VIDA 4.2.0 (Openeye Scientific Software, Santa Fe, NM. http://www.eyesopen.com).

2.1.12 2G12 Mechanism of Action Infection Assay

Modified human osteosarcoma cells engineered to express CD4 and CCR5 (HOS.T4.R5), vector for pNL4–3.Luc+ R- E-, as well as the recombinant virus was produced as previously explained. To allow HIV viral engagement with CD4 and co-receptors yet halt fusion, the initial part of the assay was performed under chilled conditions at 4 °C. The latter part of the assay was conducted at 37 °C to facilitate viral fusion. Viral stocks, growth medium, and HOS.T4.R5 cells, pre-seeded for 24 hrs at 8,000 cells per well, were pre-chilled to 4 °C. The virus was then incubated with the pre-

chilled cells for 4 hrs at 4 °C. The media was removed and cells were washed twice with freshly chilled growth medium to remove unbound virus. Then serial dilutions of 2G12 prepared in chilled medium and 1X PBS were incubated with cells at 30 min increments at 4 °C, then 23 °C, followed by a 37 °C incubation for 24 hrs, which concluded with a growth medium wash step. After 48 hours of infection the cells were lysed with passive lysis buffer (Promega) followed by 3 freeze–thaw cycles. The 6-helix bundle peptide, Enfurvutide (T20), was used as a control inhibitor for fusion. The luciferase activity for the infection assay was performed as described above. All experiments were performed at least in triplicate, and results were expressed as relative infection with respect to cells infected with virus in the absence of inhibitor (100% infected).

2.2 RESULTS

2.2.1 Synthesis and Characterization of Obligatory Dimer

Previous studies have shown that luminal p24 release is a phenotype of peptide triazoles containing a C-terminal thiol. The non-sulfhydryl containing peptide, (**10,** HNG156) (**Figure 12A**) and sulfhydryl blocked derivative, KR13b, do not cause viral lysis although they potently shed gp120 and inhibit infection[70]. We employed Michael Addition chemistry to crosslink the Cys residues of two monomers of peptide **1** using a bismaleimide linker to produce an obligate dimer, peptide **1a** (**Table 1** and **Figure 11**). We compared the effects of **1a** with control peptide **1** on gp120 binding, HIV-1 inhibition, and virolytic properties. Surface plasmon resonance (SPR) interaction analysis displayed that **1a** binds gp120 with affinity comparable to that of the control, **1**, seen by K_D values found to be 2.71 ± 1.4 nM and 3.02 ± 0.9 nM, respectively (**Figure 12**). Additionally, peptide **1a** was a potent inhibitor of HIV-1 infection as evidenced by pseudotyped HIV-1_{BaL} antiviral assays,

but did not cause p24 release (**Figure 13**). These results reaffirmed the requirement of a free sulfhydryl group for virolysis.

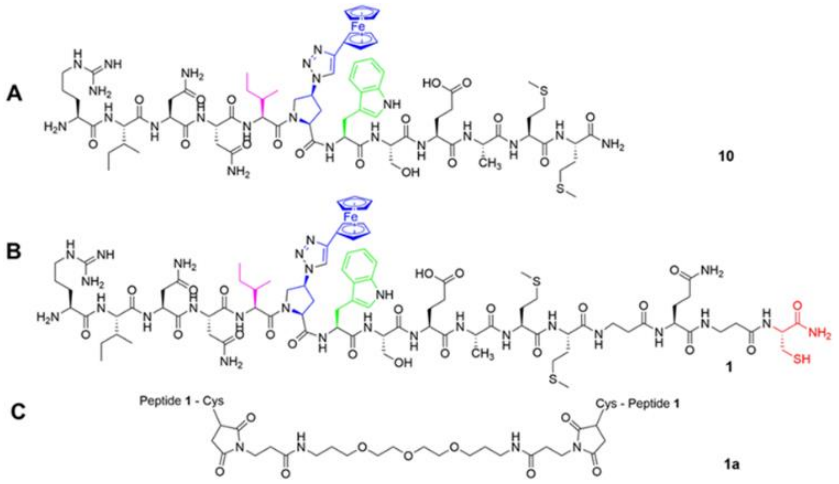

Figure 11. Structures of **10**, **1** and **1a**. (A) **10** is the non-lytic parental peptide triazole. (B) **1** is the lytic parent peptide of the library of peptide triazole thiol truncates. All PTs contain the signature pharmacophore, Isoleucine (magenta)-AzidoProline (blue)-Tryptophan (green). (C) Peptide **1a** is composed of Bis-Mal dPeg conjugated to the C-terminal sulfhydryl groups of two monomers of **1**.

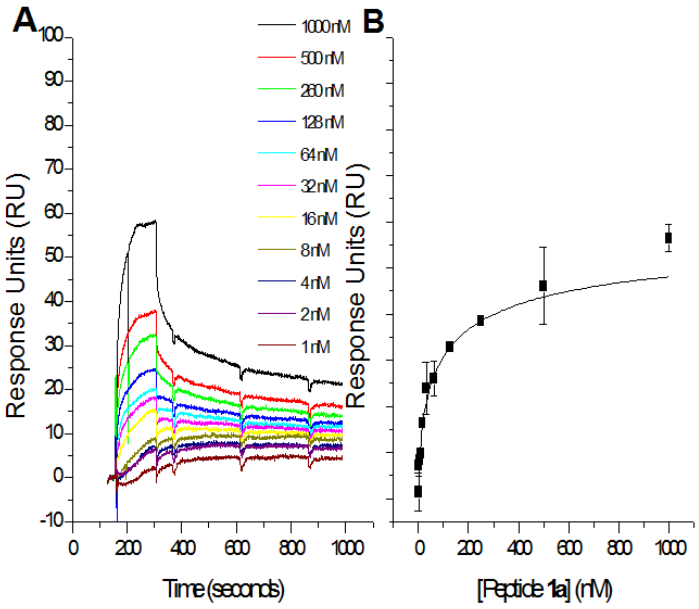

Figure 12. Functional Characterization of PTT dimer, **1a**. (A) Direct binding was measured to chip-immobilized WT YU2 gp120. Data show proportionally increasing binding responses to immobilized gp120 at increasing concentrations of **1a**. (B) Steady state fit analysis of the Req values for each concentration of the Peptide 1 from calculated using the BiaEvaluation software. Error bars represent standard deviation of the mean, n = 3.

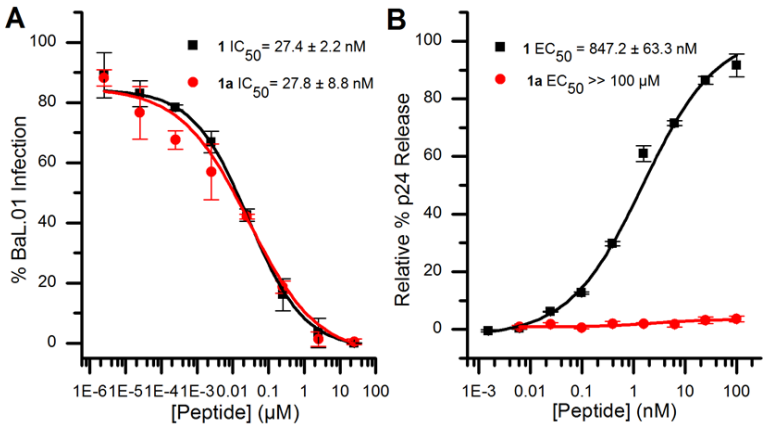

Figure 13. Dose response of the effects of **1** and **1a** on HIV-1_{BaL} pseudovirus antiviral functions. (A) Inhibition of cell infection analyzed using a single round pseudotyped assay. The IC_{50} values of **1** and **1a** inhibit HIV-1_{BaL} infection to the same extent. (B) Relative p24 release measured using ELISA. The calculated EC_{50} values for **1** and **1a** were and 847.2 ± 63 nM and >100,000 nM respectively. The data were normalized using untreated virus as a negative control (< 5% p24 release), and p24 release observed with 1% triton X treated virus was taken as 100% p24 content. Sigmoidal curve fits of data were obtained using Origin v.8.1 (Origin Lab, Northampton, USA). Error bars represent standard deviation of the mean, n = 3.

Table 1. Sequences of peptide triazole thiols, expected and observed mass and length of peptide chain between Trp α carbon and SH based on amide bond lengths. *N/A= not applicable due to a capped Cys or the absence of a Cys.

Code	Designation	Sequence	Mass (Da) Observed	Mass (Da) Calculated	Trp-SH Length Å
1	KR13	RINNIXW**S-E-A-M-M-βA-Q-βA-C**	2084.73	2085.22	35.96
1a	KR13 dimer	RINNIXWS-E-A-M-M-βA-Q-βA-C-**Mal Peg Mal**-C- βA-Q-βA-M-M-A-E-SWXINNIR	4694.95	4692.99	N/A
2	HL01	RINNIXW**S-EA-βA-Q-βA-βA-C**	1893.66	1893.82	38.99
3	HL02	RINNIXW**S-EA-βA-Q-βA-C**	1822.67	1822.82	33.14
4	HL03	RINNIXW**S-EA-βA-Q-C**	1751.78	1751.75	26.02
5	HL04	RINNIXW**S-EA-βA-C**	1623.70	1623.62	23.23
6	LB05	RINNIXW**S-EA-C**	1552.64	1552.54	18.70
7	LB04	RINNIXW**S-E-C**	1481.59	1481.46	14.52
8	LB03	RINNIXW**S-C**	1352.56	1351.16	10.07
9	LB02	RINNIXW-**C**	1265.48	1264.08	5.75
10	HNG156	RINNIXWS-**E-A-M-M**	1711.73	1711.49	N/A
11	KR13b	RINNIXW**S-E-A-M-M-βA-Q-βA-C(ACM)**	2155.8	2156.87	N/A
12	UM15	INNIXW	1006.31	1005.94	N/A

2.2.2 Synthesis and Characterization of PTT Truncates

To determine the optimal linker length between the peptide IXW pharmacophore and the PT-SH, we synthesized a family of eight virolytic truncates based on the PTT parent peptide, **1**. The PTT truncates contained the characteristic peptide triazole pharmacophore, however the C-terminus linkers were serially truncated followed by a terminal CysSH (**Figure 14**). The effects of the truncated linker lengths were determined by analyzing the peptide potencies in antiviral, ELISA (CD4 and 17b), SPR, gp120 shedding, and virolysis assays (**Table 2**). Peptide **1** served as a positive control and **10**, a peptide triazole which contains no free thiol group, served as the negative control (**Figure 11**). The gp120 binding activities were tested by performing competition ELISA assays using soluble CD4 (sCD4) and the co-receptor surrogate monoclonal antibody, 17b (**Figure 15**). The gp120 binding ability of these peptides were confirmed by sCD4 competition SPR, with IC_{50} values determined for **1-9** (**Figure 16A and Table 2**). Both methods displayed that the PTT truncates bind gp120 strongly, except the most severely truncated peptide, **9**, which displayed reduced binding affinity.

Peptide effects on the contents of virus were determined by incubating increasing concentrations of peptide with HIV-1_{BaL} virions and quantifying p24 release and gp120 shedding. Similar to the gp120 binding analyses, the peptides were relatively active in antiviral inhibition (**Figure 16B**) and all peptides caused gp120 shedding (**Figure 17 and Table 2**). In contrast, the peptides with the most severe linker truncations were inactive in p24 release assays (**Figure 16C**). The non-sulfhydryl containing peptide, **10**, was used as a negative control.

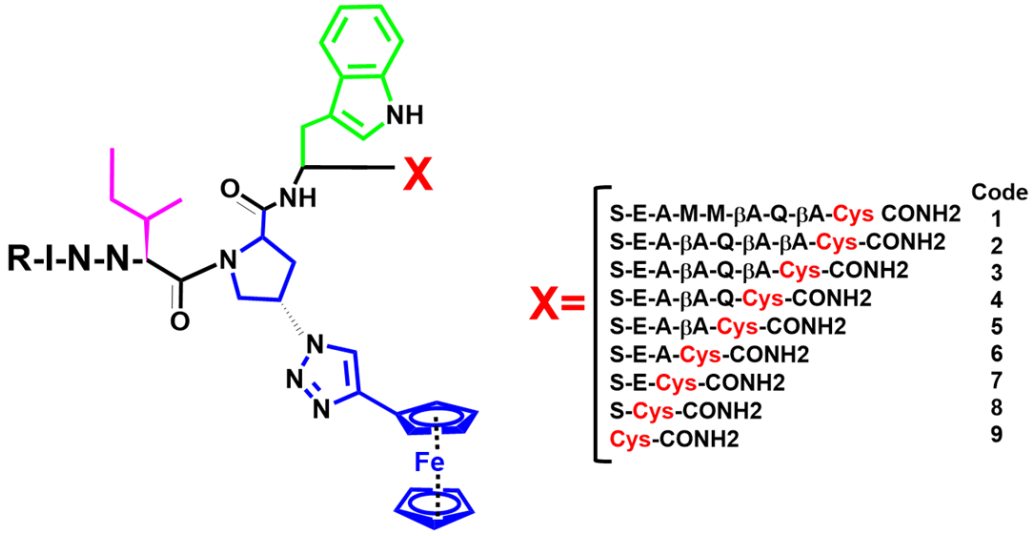

Figure 14. Chemical structures of PTTs with serially truncated linker between pharmacophore and C-terminal Cys. The pharmacophore sequence, composed of Isoleucine (magenta) - TriazoleProline (blue) - Tryptophan (green). The chemical structures were generated in ChemDraw Pro 13.0.

Table 2. Binding and Antiviral Properties of Peptide Triazole Thiols. *ND= not determined

Code	Designation	ELISA IC_{50} (nM) sCD4	ELISA IC_{50} (nM) 17b	SPR sCD4 IC_{50} (nM)	Inhibition of Infection IC_{50} (nM)	Gp120 shedding EC_{50} (nM)	p24 Release EC_{50} (nM)
1	KR13	28 ± 4	32 ± 6	93 ± 4	53 ± 19	32 ± 20	1065 ± 40
2	HL01	110 ± 8	153 ± 14	237 ± 8	143 ± 45	140 ± 37	1800 ± 91
3	HL02	123 ± 51	142 ± 25	153 ± 47	114 ± 40	ND	1321 ± 26
4	HL03	199 ± 23	198 ± 35	172 ± 66	197 ± 38	183 ± 37.9	2202 ± 61
5	HL04	183 ± 13	227 ± 30	ND	286 ± 13	ND	4762 ± 73
6	LB05	207 ± 29	195 ± 41	ND	469 ± 19	ND	26730 ± 82
7	LB04	218 ± 10	713 ± 144	344 ± 70	554 ± 7	288 ± 133	33210 ± 89
8	LB03	331 ± 11	939 ± 186	379 ± 16	550 ± 63	523 ± 97.6	38420 ± 49
9	LB02	589 ± 74	906 ± 128	2913 ± 798.8	7030 ± 2200	9366 ± 563	>> 500000

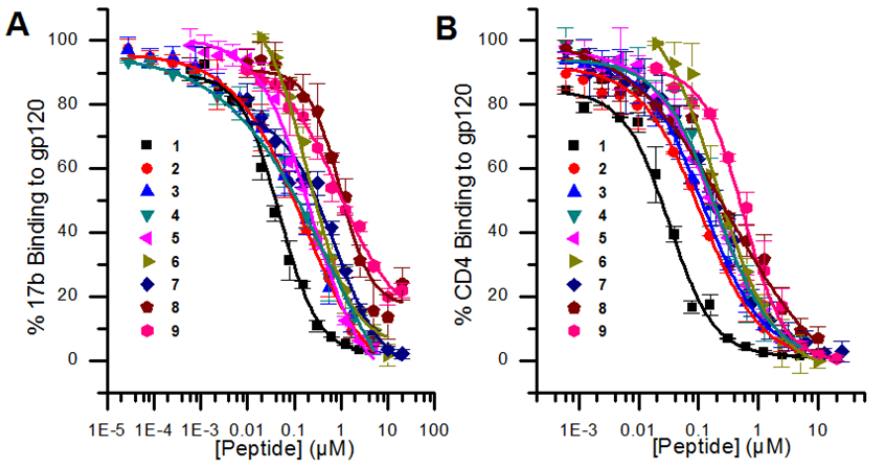

Figure 15. ELISA Competition of gp120 by PT thiol truncates. Sandwich ELISA was used to determine the extent of (A) 17b and (B) CD4 antagonism caused by largely truncated peptide triazole thiols. The data display that serially truncated PTT's retain gp120 binding affinity as the distance between the IXW pharmacophore and sulfhydryl group is shortened. Reduced gp120 binding affinity of **9** is due to complete elimination of the linker. IC_{50} values were determined by fitting the peptide data to logistic function in Origin (OriginLab) and are listed in Table 1. Error bars represent standard deviation of the mean, n = 3.

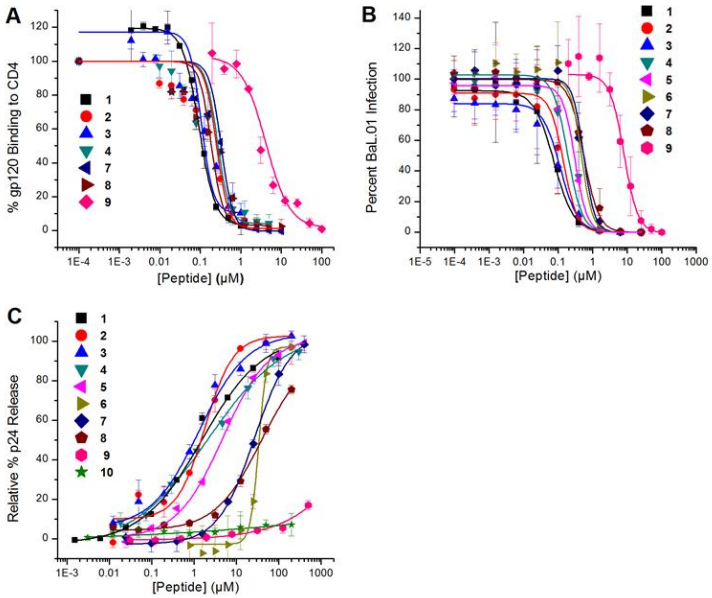

Figure 16. (A) Binding activity of peptide triazole thiols as determined by surface plasmon resonance CD4 Competition. Data points for response at steady state were extracted from sensorgrams and fit to a four-point parameter sigmoidal equation resulting in IC_{50} values listed in Table 1. (B) Dose response of the effects of peptide triazole thiol truncates on HIV-1_{BaL} pseudovirus cell infection. Inhibition of cell infection was analyzed using a single round pseudotyped assay. The IC_{50} values are reported in Table 1. The data show that serially truncated PTT's progressively lose antiviral potency as the distance between the IXW pharmacophore and sulfhydryl group is shortened. (C) p24 release from HIV-1_{BaL} pseudotyped virus caused by PTT's. Relative p24 release was measured using ELISA. The data were normalized using untreated virus as a negative control (< 5% p24 release), and p24 release observed with 1% triton X treated virus was taken as 100% p24 content. Sigmoidal curve fits of data were obtained using Origin v.8.1 (Origin Lab, Northampton, USA). Error bars represent standard deviation of the mean, n = 3.

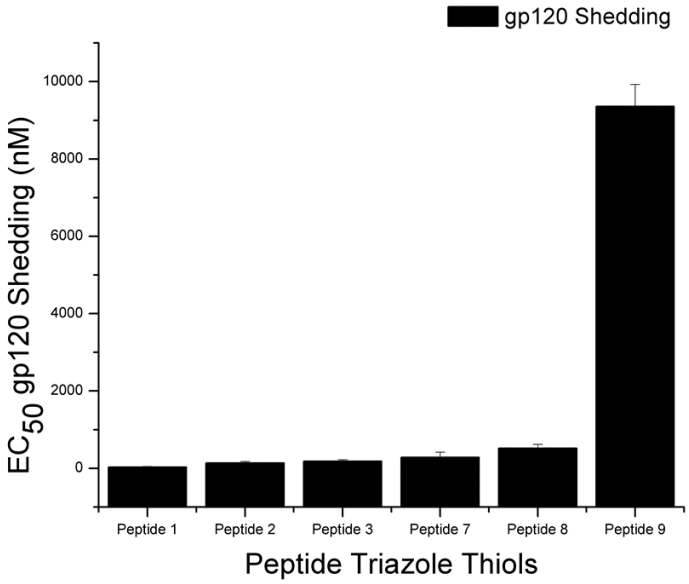

Figure 17. Gp120 shedding of virolytic peptides. Relative gp120 shedding was performed by western blot analysis (see Methods section). Bands of gp120 protein detected by chemiluminesence on film were quantified by Image J analysis. EC_{50} values obtained are in Table 2. The data were normalized by using untreated virus as a negative control (< 5% shedding) and 1% triton X treated virus was taken as 100% gp120 shedding.

2.2.3 Analysis of the Effect of PTT Linker Length on p24 Release

Using the serially truncated peptide triazole thiols, we compared the p24 release and antiviral activities, then assessed this relationship by analyzing the p24 release vs. binding-dependent properties as a function of the length of the linker between the IXW pharmacophore and SH group.

The results in **Table 3** show that the progressive truncation of the C-terminal linker suppresses the virolytic efficiency of PTTs (**Figure 18**).

We observed a discontinuous relationship between the length of the C terminus linker and p24 release. The proportionately greater effect of linker shortening on virolysis *versus* antiviral potency argues that a minimal length is required for efficient virolysis. It is well known that HIV-1 contains ten conserved disulfides', nine of them are located in gp120 and one in gp41. Observation of a minimum linker length between the peptide triazole pharmacophore and peptide triazole SH for p24 release supports the hypothesis that the virolytic effect of peptide triazole thiols is promoted by a disulfide exchange between the peptide C-terminal thiol group and a specific disulfide in gp120.

Table 3. Calculated Correlations between Virolysis and Binding of Peptide Triazole Thiols.

*ND= not determined.

Code	Designation	p24 EC_{50}/ ELISA IC_{50}		p24 EC_{50}/ Inhibition of Infection IC_{50}	p24 EC_{50}/ gp120 Shedding EC_{50}	p24 EC_{50}/ SPR sCD4 IC_{50}
		sCD4	17b			
1	KR13	38.0	33.3	20.1	3.3	11.5
2	HL01	16.4	11.8	12.6	12.9	7.6
3	HL02	10.7	9.3	11.6	ND	8.6
4	HL03	11.1	11.1	11.2	12	12.8
5	HL04	26.0	20.9	16.6	ND	ND
6	LB05	128.9	136.9	56.9	ND	ND
7	LB04	152.3	46.5	59.9	115.3	96.5
8	LB03	116.0	40.9	69.8	73.5	101.3
9	LB02	>>848.8	>>551.8	>> 71.1	>> 53.4	>> 171.6

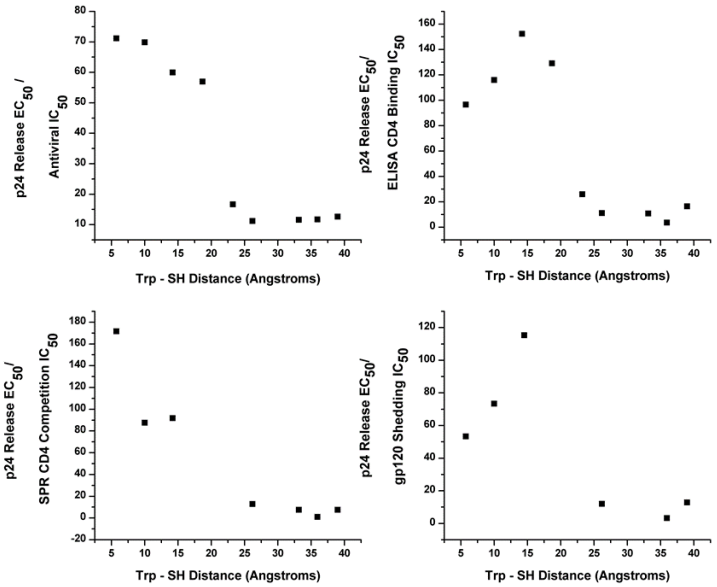

Figure 18. (A) Relative p24 release vs. length (based on cell infection inhibition) (B) Relative p24 release vs. length (based on ELISA). (C) Relative p24 Release vs. Length (based on SPR CD4 competition). (D) Relative p24 release vs. length (based on gp120 Shedding). Truncated peptide triazole thiols lose virolytic potency as the distance shortens between the thiol group and Trp residue of the IXW pharmacophore.

\

2.2.4 PTT Docking onto gp120 using Molecular Dynamics (MD) Simulation

We sought to identify possible sites of disulfide exchange within gp120 by determining the trajectory of the peptide SH group. Unfortunately, we do not have a crystal structure of a peptide triazole bound to gp120. Therefore, we performed a MD simulation and enhanced docking of PTT,

peptide **8**, to gp120 to identify nearby disulfide residues that may interact with the peptide sulfhydryl group (**Figure 19**). Modeling studies performed by Dr. Adel Rashad show there are several conserved disulfide bonds surrounding the CD4 binding pocket, which may be involved in the virolytic mechanism. We postulate that these residues participate in disulfide exchange with the sulfhydryl group of PTTs, a process which is known to be required for entry of several enveloped viruses[87].

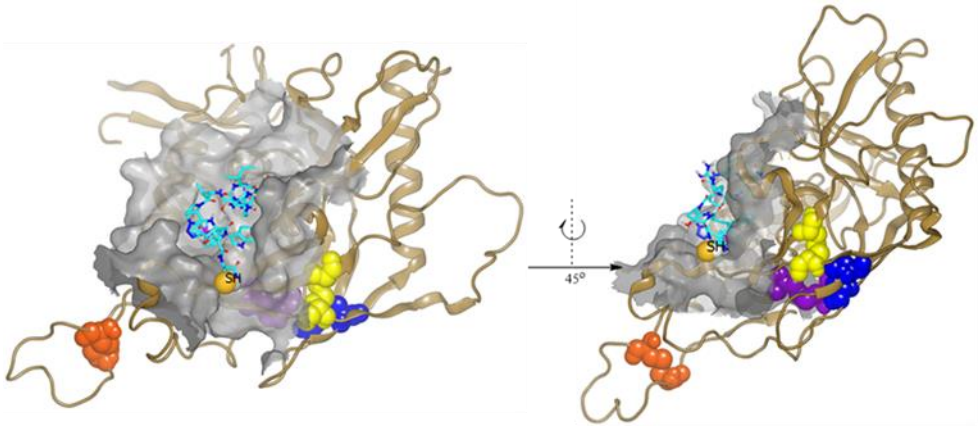

Figure 19. Molecular docking simulation of PTT, 8, in complex with gp120. The structure of 8 (carbons shown in cyan) was docked onto gp120 resulting in the binding model shown. Peptide 8 binds in a site overlapping the CD4 pocket (surface shown in grey), with the C-terminal Cys (SH shown as CPK) trajectory to the conserved disulfide cluster (blue; C296-C331, yellow; C385-C418, violet; C378-C445, orange; C119-C205) which encompasses possible sites of disulfide interaction. The model shows that the peptide SH group is well solvated and with the conformational flexibility can reach any of the disulfide bridges shown.

From prior molecular dynamics simulated model of peptide triazole-gp120 binding, it was shown that the hydrophobic motif (IXW) of peptide triazoles binds to specific residues that are buried within the CD4 binding cavity of gp120[88]. However, past modeling for peptide triazoles utilized phenyl-containing scaffolds instead of the ferrocenyl appendage found in high affinity peptide triazole thiols. The use of the phenyl substituent enabled the use of CHARMM, which possessed surface desolvation and energy parameters for a phenyl moiety and not those for ferrocene rings. The new, enhanced docking model (**Figure 19**) now displays the PT thiol truncate, **8**, which contains the ferrocenyl apppendage native to PT's, in complex with the core gp120. Molecular docking is most accurate when using small, rigid molecules. Because peptides are large and flexible, we performed these studies with the smallest PTT that was still capable of causing p24 release, **8**. The molecular docking model of **8** bound to gp120 predicted that pharmacophore binds in a site overlapping the CD4 binding site, which was also observed in the previous MD model[88]. Furthermore, the C-terminus of the PT was shown to project towards the CD4 exposed disulfide cluster in the variable loop of gp120 (**Figure 19**). From our model of PTT docked onto gp120, we speculate that PTTs interact with the CD4-exposed disulfide cluster in gp120, composed of C296-C331 (V3 loop) disulfide, C385-C418 (C4) disulfide, and C378-C445 (C3) disulfide.

2.2.5 gp120 Protein Ligands Used to Deduce Likely Disulfides Targeted

To probe the disulfide-containing gp120 region that is the contact site for the PT-SH group, we performed virolysis competition assays with several gp120 neutralizing antibodies (**Figure 20 and 21**). It is well known that the V3 loop of gp120 is necessary for proper folding conformation of mature Env, for this reason we initiated an investigation to determine if these disulfides are

involved in p24 release caused by PTTs[89,90]. We performed competition assays with 2G12, a broadly neutralizing conformational antibody of HIV-1. 2G12 has previously been shown to bind to the mannose rich epitope at the base of the gp120 V3 loop[91], where it binds to the glycans associated with N295, N332, and N392. Additional glycans that influence 2G12 binding are the mannose residues linked to N339 and N386. In all, these 2G12 binding-glycans occupy the same V3 loop region as the CD4 exposed disulfide cluster. The 2G12 p24 assays were performed with the control peptide, **1**, the longest of the truncated virolytic peptides, **2**, and the short linker truncate which still causes p24 release, **8**. These inhibition assays displayed that 2G12 inhibits the ability of all three virolytic peptides to cause p24 release (**Figure 21A)**. To address the possibility that 2G12 may inhibit six helix bundle formation we performed an infection assay where pre-chilled virus was added to cells while keeping cells at 4 °C and incubated for four hours to allow commitment of receptor binding to gp120 but to arrest the process in the pre-fusion step, preventing six-helix bundle formation. Then, after washing to remove unbound virus and adding serial dilutions of 2G12, we raised the temperature to 37 °C and carried out the assay accordingly as described in Methods section. We added 10 μM of T20 at the same time as 2G12, as a negative control to demonstrate that 6-helix bundle formation had not occurred at the time of 2G12 addition. This was verified by the complete inhibition observed, whereas the 2G12 treated cells showed no infection inhibition, verifying that 2G12 does not prevent six-helix bundle formation through direct interaction (**Appendix Figure 32**). These results suggest that the 2G12 antibody, which binds to glycans at the base of the V3 loop, effectively inhibits p24 release induced by virolytic peptides.

To confirm the specificity of 2G12 binding to the V3 loop glycosyl, we sought to perform this assay with a different protein which is also known to bind to glycans of HIV-1, yet in a location different from that of 2G12. Therefore, we chose to perform a p24 release assay with Cyanovirin, a protein produced from cyanobacterium Nostoc ellipsosporum and known to have antiviral activity against

several viruses[92,93]. Cyanovirin virucidal activity is caused by high affinity interactions with gp120 and specifically to high mannose residues found on the outer domain of HIV-1 Env[92]. Previously, we showed that Cyanovirin does not compete with peptide triazole binding. Here, we aimed to determine its' effect on PTT-induced p24 release. Our data displayed that Cyanovirin does not inhibit p24 release of virolytic peptide triazoles, **1**, **2**, or **8 (Figure 21B)**.

As mentioned above, there are several disulfides clustered around the V3 loop, however another possible site of disulfide exchange is located in the V1/V2 loop. The disulfide C119-C205 links the V1 and V2 loop and is also important for aiding in V3 loop access to the CD4 exposed conformation[82]. Further, our flexible docking suggested that the terminal Cys of PTT's could potentially extend past to the C119-C205 disulfide. For this reason, we aimed to determine the effect of the gp120 epitope antibody, 697-30D, on virolysis caused by peptide triazole thiols. The neutralizing antibody, 697-30D, is specific for the V2 region of gp120 and recognizes the epitope that spans the region 164-194[82]. The results of a p24 release inhibition assay showed that the conformational antibody 697-30D did not affect the ability of peptide triazole thiols to disrupt HIV-1 virions as shown in **Figure 21C**. In all, these data implicate the CD4 exposed disulfide cluster of the V3 loop as a possible contact site of PT-SH involved in the mechanism of PTT-induced virolysis.

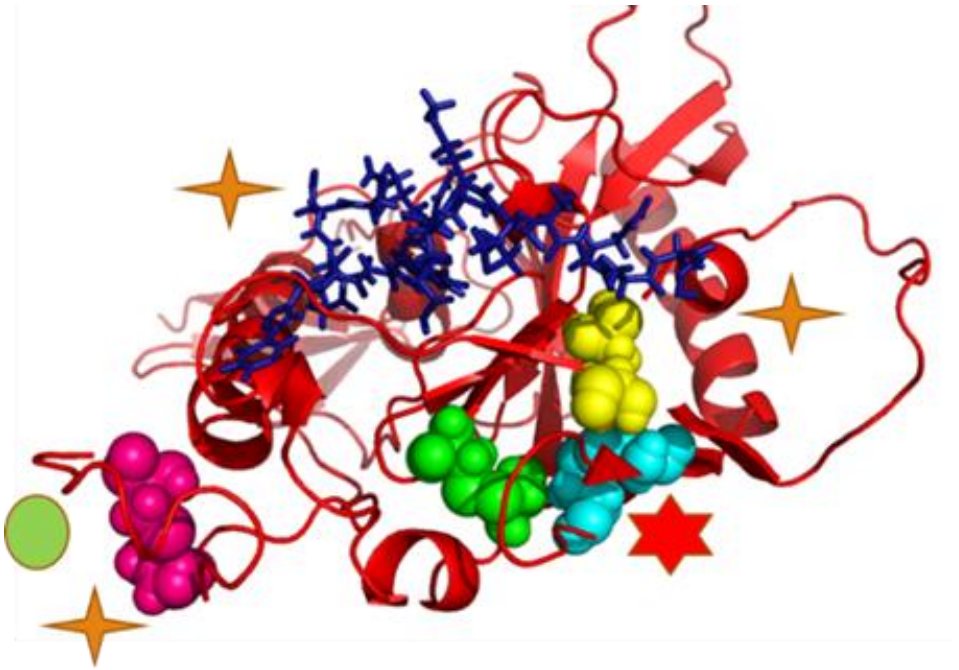

Figure 20. Cartoon of bound Gp120 Ligands in relation to possible disulfides involved in PTT "thiol-exchange". Sticks depiction of KR13 (navy blue) bound to the CD4 conformation of gp120 (red ribbon). 2G12 (red 6 point star) binds to asparagine-linked glycans located at the base of the V3 loop. Cyanovirin (orange 4 point star) binds to several mannose residues surrounding the outer domain. 697-30D (green circle) binds in the V1/V2 loop. Disulfide linkages C378-C445 (C3) shown in green, C385-C415 (C4) shown in yellow, C296-C331 (V3) shown in cyan, and C119-C205 (V1/V2) in magenta.

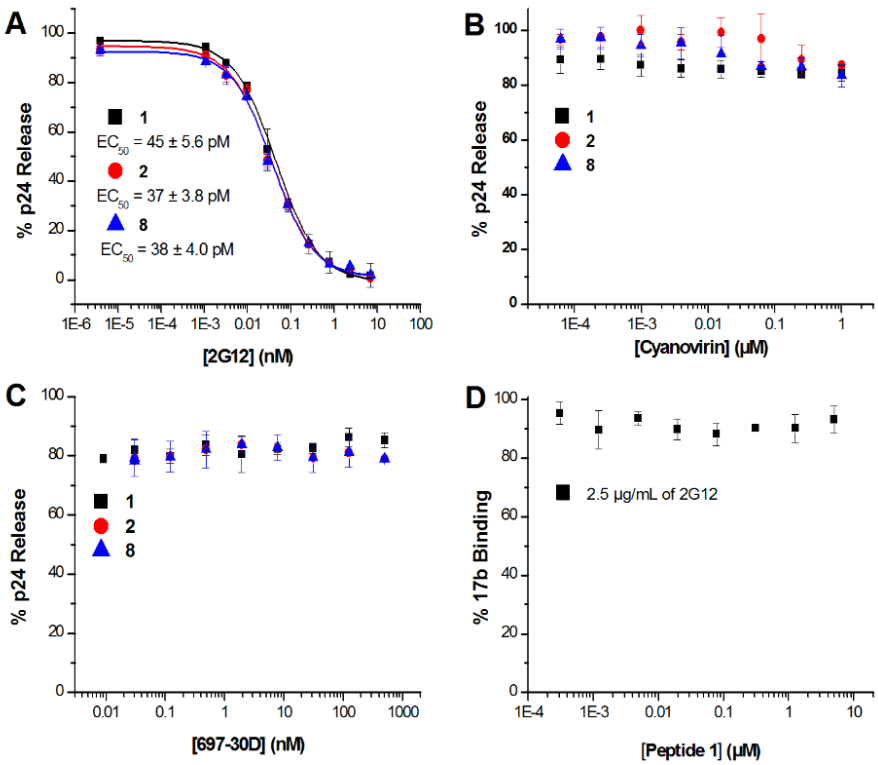

Figure 21. Effect of protein ligands on p24 release by PTTs. (A) Effect of conformational antibody 2G12 on p24 release. HIV-1_{BaL} pseudovirus was treated in the presence and absence of 10 µM **1,** 14 µM **2**, 50 µM **8** and serial dilution of 2G12 starting at 10 nM. (B) Effect of carbohydrate binding protein, Cyanovirin, on p24 release. HIV-1_{BaL} pseudovirus was treated in the presence and absence of the respective EC_{80} concentrations of **1**, **2**, and **8** and serial dilution of Cyanovirin starting at 1 µM. (C) Effect of conformational antibody, 697-30D, on p24 release. HIV-1_{BaL} pseudovirus was treated in the presence and absence of 10 µM **1**, 14 µM **2**, 50 µM **8** and serial dilution of 697-30D starting at 1 µM. (D) Effect of 2G12 on **1** binding to gp120. 17b Sandwich ELISA assay was performed with constant concentration of 2G12(2.5 µg/mL) and serial dilutions of **1**.

2.3 DISCUSSION

Previously, we reported a sub-class of peptide triazole inhibitors, which contain C- terminal sulfhydryl groups and irreversibly disrupt HIV-1 virions, evidenced by capsid p24 release[94]. Since the role of the thiol was implicated in the virolytic breakdown of Env, in a more recent study, we characterized a sulfhydryl blocked variant of **1**, (**11**, KR13b) [70]. **11** potently inhibited HIV-1 infection, but did not cause the release of protein capsid p24. These findings led us to characterize the mechanistic effects of the peptide triazole thiol, **1**, which was shown to cause gp120 shedding and p24 release. Furthermore, these molecular effects of **1** were examined in virolytic breadth studies using HIV-1 clades A, B, and C. Virolytic breadth studies displayed dose dependent p24 release, thereby confirming a conserved mechanism of action induced by peptide triazole thiols[70]. The ability of peptide triazole thiols to cause virolysis led to many questions concerning the role of the C-terminal thiol and the mechanism of virolysis induced by these peptides. In the current study, we initiated an inquiry of the structure - activity relationship of virolytic peptide triazoles by identifying the role of the thiol group and its mode of action once it encounters HIV-1 Env.

We started by reconfirming the role of the sulfhydryl by synthesizing an obligate dimer of (**1a**, KR13) a variant in which two molecules of **1** were linked on opposing sides of a bismaleimide, blocking both peptide Cys residues. We aimed to eliminate completely the possibility that viral membrane disruption may be an effect of peptide **1** self-dimerization, subsequently allowing each **1** monomer to potentially bind to two separate Env spikes simultaneously and stressing the viral membrane. From our data, we observed that KR13 dimer was a potent inhibitor of HIV-1 infection, however it was not lytically active (**Figure 14**). The inability of **1a** to disrupt viral particles ruled out the possibility that viral lysis was an artifact of peptide **1** self-dimerization. Instead, the results confirm that a free sulfhydryl group is indeed a requirement for peptide triazole thiol activated

virolysis. These results argue that there is a direct role of the free SH, possibly by exchange with disulfides of gp120.

We argued that if disulfide exchange occurs between the PT SH group and the gp120 disulfide cluster proximal to the CD4 binding site, then there must be a minimal length of C-terminal linker needed for the Cys-SH to contact the disulfides for efficient virolysis. Therefore, we speculated that decreasing the length of the peptide triazole thiol linker would suppress lysis but proportionally retain binding affinity, antiviral potency and gp120 shedding activity, all of which are caused by active core binding but not the free SH. To test this prediction, we synthesized and characterized a library of truncated peptide triazole thiols, based on the parent peptide **1** binding core structure, with serially truncated linker lengths at the C- terminal end. We found that once the C-terminus linker is reduced to less than 20 Å (**Table 1**) we observe a disproportionate loss of virolysis versus antiviral activity. This suggests that there is a minimal required spacing, between the peptide triazole pharmacophore and thiol group of 20 Å, which is necessary for virolysis. We found that even the most shortened peptides retain gp120 binding affinity and inhibit viral replication, however they do not possess the added feature of virolysis. **Figure 17** displays that the PTT library of peptides all potently bind HIV-1 at similar extents as, observed by cell infection and SPR CD4 competition assays. This is likely attributed to the active site pharmacophore (IXW), which is maintained in all peptide triazoles and has a strong binding affinity to the residues within the CD4 binding site. However, the virolysis assays strikingly display a distinct group of inhibitors which are potent virucides and another distinct group of inhibitors which do not have lytic capabilities. The data argues that the PT-SH may contact specific disulfides, and the inability to reach Env gp120 disulfides contributes to loss of the effect of viral lysis.

HIV-1 Env consists of ten conserved disulfides and of these disulfides the transmembrane protein, gp41, contains one, while gp120 contains the other nine disulfides. Disulfide linkages C378-C445

(C3), C385-C415 (C4), C296-C331 (V3), and C119-C205 (V1/V2) are of particular interest because they are found near the CD4 binding site, also the region of virolytic peptide triazole binding. For this reason, they are potential sites of "thiol exchange". To investigate the possible interaction of the PT thiol group with the disulfide cluster surrounding the CD4 binding site, we docked a PTT truncate to an F105- bound gp120 conformation and examined this spatial relationship. The docking study was in agreement with a previous MD simulation of PT's, which suggested that the IXW tripartite motif binds to residues lining the Phe43 cavity[88]. Additionally, the docking model showed that the C terminus linker and SH of the peptide do not project past gp120's V1/V2 region, yet it extends toward the disulfide linkages in the C3, C4, and V3 domains of gp120. In all, the molecular docking study confirmed the specificity of PT-gp120 binding, yet several possible disulfide candidates still remained.

We continued our SAR studies by using epitope specific protein ligands to map the trajectory of sulfhydryl contact with gp120 in viral lysis. 2G12, an antibody which binds to the base of the gp120 V3 loop, reduced the ability of virolytic peptides to cause p24 release in virolytic inhibition assays (**Figure 21A**). The data also show that the 2G12 antibody inhibited p24 release of peptide **1** with an IC_{50} of 45 ± 5.6 pM and similarly inhibited peptide truncates. 2G12 suppression of the release of capsid protein p24 of several PTT's of distinct lengths strongly indicates that PTT's exert their mechanism by interacting with a common contact site and that the contact site is near the V3 loop. This possibility was supported by finding that there was no inhibition of p24 release when viral particles were treated with the lectin Cyanovirin or antibody 697-30D (**Figures 21B and C**), therefore validating the importance of the V3 loop disulfides. Disturbance of this V3 loop disulfide has been found to be detrimental to gp120 folding, CD4 binding, and infectivity, thus is it not surprising that disulfide exchange in this region could cause complete loss of membrane integrity. Further support for the role of the V3 loop disulfide cluster in lysis was attributed by our molecular docking simulation of peptide **8** bound to gp120 (**Figure 20**), which showed that the trajectory of

the SH group extends toward the cluster of disulfides. Although the simulation cannot precisely extrapolate the PTT thiol contact with a specific disulfide, taken together with the epitope mapping, it can be inferred that the V3 loop disulfide cluster has a pertinent role in the activation of Env lysis induced by PTT's.

Peptide triazole thiols are novel virucides due to their specificity, inhibition potency, and ability to cause gp120 shedding. Additionally, PTT-induced viral inactivation results in residual antigenic virions, making them potential therapeutics. For this reason, minimized virolytic peptides could be used as drug leads, upon refining the pharmacophore by medicinal chemistry, prevention and therapeutic approaches to suppress the progression and transmission of AIDS and treating HIV-1 infected patients.

CHAPTER 3: Mechanism of Peptide Triazole Thiols Induced Virolysis by Mimicking HIV-1 Fusion Machinery

3. Introduction

In Chapter 2, I described experiments that provide evidence that peptide triazoles, specifically those with C-terminal Cys residues, are implicated in disrupting viral membrane integrity by disulfide bond interference. Based on those studies I investigated the hypothesis that the disruption leads to disulfide exchange in Env and the specific disulfide residues of the Env proteins in this process. I further sought to correlate the thiol/disulfide reaction properties in lysis with those reported to occur during virus cell infection.

3.1 MATERIALS AND METHODS

3.1.1 Reagents

Escherichia coli strain XL-10 gold (Agilent) and Stbl2 cells (Invitrogen) were products of Novagen Inc. (Madison, WI). Thermostable DNA polymerase (pfu ultra™) was obtained from Stratagene Inc (La Jolla, CA). Custom-oligonucleotide primers were supplied by Integrated DNA technologies (IDT). DNA plasmids encoding HIV-1_{BaL} Env (catalog # 11445) and NL4-3 R^- E^- Luc^+ were obtained from the NIH AIDS Reagent Program, Division of AIDS, NIAID and were a kind gift of Dr. J Mascola and Dr. N Landau respectively. All other reagents used were of the highest analytical grade available.

3.1.2 Peptide Synthesis and Click Conjugation

All sequences and denotations of peptides reported are given in **Table 1**. Peptides were synthesized manually by stepwise solid-phase peptide synthesis (SPPS) and purified as described in Chapter 2. Bt-KR13 was synthesized and purified by SciLight peptide.

3.1.3 Viral Inhibition Assays

The luciferase activity for the infection assay was performed as described in Chapter 2. All experiments were performed at least in triplicate, and results were expressed as relative infection with respect to cells infected with virus in the absence of inhibitor (100% infected).

3.1.4 Sulfhydryl Reagent "Treat/Wash" Viral Infection Assays

Modified human osteosarcoma cells engineered to express CD4 and CCR5 (HOS.T4.R5), as well as the vector for pNL4–3.Luc+ R- E-, were obtained through the NIH AIDS Repository from Dr. Nathaniel Landau, while the vector expressing the CCR5-targeting spike protein BaL.01 gp160 was obtained through the NIH AIDS Repository from Dr. John Mascola. The recombinant virus was produced as previously explained. The viral stocks were first incubated with serial dilutions of Dithiothreitol (DTT), Iodoacetamide (IAAm), and (tris(2-carboxyethyl)phosphine) (TCEP) at 37 °C for 30 min, then transferred to 30 kDa centrifuge filters (Amicon) and spun at 2000 x g at 37° C for 7 min. After the 7 min spin, 165 µL of 1 x PBS was added to the samples and mixed thoroughly via pipetting. The centrifugation and PBS wash were repeated 3 times; at this point, the treated virus was added to 96 well tissue culture plates, with HOS.T4.R5 cells, pre-seeded for

24 hrs at 8,000 cells per well. After 48 hours infection, with a growth medium wash step 24 hours post-treatment, the cells were lysed with passive lysis buffer (Promega) followed by 3 freeze–thaw cycles. Luciferase assays were performed using 1 mM d-Luciferin salt (AnaSpec) as substrate and detected on a 1450 Microbeta liquid scintillation and luminescence counter (Wallac and Jet). The single-round, pseudoviral infection luciferase reporter assay was conducted as previously described[69]. Nonlinear regression analysis was performed using Origin v.8.1 (OriginLab, Northampton, USA) to calculate the IC_{50} values. All experiments were performed at least in triplicate, and results were expressed as relative infection with respect to cells infected with virus in the absence of inhibitor (100% infected).

3.1.5 Optical Biosensor Binding Assays

Surface Plasmon Resonance (SPR) kinetic interaction experiments were performed and analyzed as explained in Chapter 2.

3.1.6 Virolysis Assays

The ability of the peptide triazole thiols to cause virolysis of pseudotyped HIV-1_{BaL} virus was analyzed by quantifying p24 release as explained in Chapter 2.

3.1.7 Assays for Sulfhydryl Reagent Inhibition of Virolysis

1mM DTT and TCEP and 0.02 mM IAAm were incubated with a 1:4 working dilution of purified pseudotyped HIV-1_{BaL} virions for 30 min at 37 ºC. Reagents were removed from virions by centrifugation at 2000 x g for 7 min at 37 °C in 30 kDa centrifugation filters (Amicon). The retained HIV-1_{BaL} virions were washed with 165 µL PBS, and this was repeated three times. The virus particles were then treated with serial dilutions of **1, 11,** and **12** for 30 min at 37 ºC. The soluble fraction was separated, and the extent of p24 release was determined by the same protocol as the sandwich ELISA protocol described above. Virus in PBS was the negative control, while virus in 1% Triton-X 100 was the positive control. Quantified values from triplicate assays were plotted as a function of p24 released compared to the positive control. These values were fit using Origin v.8.1 (Origin Lab, Northampton, USA) to determine EC_{50} values.

3.1.8 Western Blot Analysis of Biotinylated PTT Interaction with gp120 and HIV-1_{BaL}

For western blot detection of peptide triazole effects on gp120 protein, 5 µM of peptide triazoles Bt-KR13, Bt-KR13b, KR13, and KR13b were stirred and incubated with 100 nM soluble HIV-1_{Yu2} gp120 at 37 °C for 4 hrs. After the 4 hr incubation, non-reducing western blot analysis was performed by adding 15 µL of reaction samples to 15 µL of 1x Laemmli buffer. Biotinylated Bovine Serum Albumin (Thermo Scientific), 5 and 20 nM, was used for biotin controls. Reducing western blot analysis was performed by adding 15 µL of reaction samples to 15 µL of 1x Laemmli buffer in 5% β-mercaptoethanol. Gp120 was detected with 1:3000 dilution of anti-gp120 D7324 (Aalto) and anti-sheep IgG conjugated HRP (Life Technologies) and biotin was detected by 1:3000

dilution of mouse anti-biotin (Jackson Immuno Research Labs, Inc) and anti-mouse IgG conjugated HRP (Dako). For western blot detection of peptide triazole effects on pseudotyped HIV-1_{BaL}, a 1:2 working dilution of purified HIV-1_{BaL} virions was incubated and stirred with 5 μM of peptide triazoles Bt-KR13, Bt-KR13b, KR13, and KR13b at 37 °C for 4 hrs. Gp120 and biotin detection were performed as mentioned above. A standard curve using monomeric HIV-1_{YU2} gp120 serially diluted (1:2, v/v) starting at 100 ng/ml was used to determine the working dilution of pseudotyped HIV-1_{BaL}.

3.1.9 Design and construction of various HIV-1_{BaL} Env mutants

Wild-type (WT) HIV-1_{BaL} Env construct in a pcDNA3.1D vector (NIH AIDS reagent program). This construct was used to prepare HIV-1_{BaL} Env substitution mutants. Mutants of HIV-1_{BaL} Env were created using Quick-change site-directed mutagenesis reagents and methods (Stratagene). The primers used for mutagenesis were custom synthesized at IDT DNA. The following forward primers and their reverse complements were used in the 5′-3′ direction:

C598A Forward: 5’ - ggg gat ttg ggg tgc ctc tgg aaa act c

C598A-Reverse: 5’ - gag ttt tcc aga ggc acc cca aat ccc c

C604A Forward: 5’ - gga aaa ctc atc gcc acc act gcc g

C604A Reverse: 5’ - cgg cag tgg tgg cga tga gtt ttc c

C385V Forward: 5’ - ggg aat ttt tct acg cta att caa cac aac tg

C385V Reverse: 5’ - cag ttg tgt tga att agc gta gaa aaa ttc cc

C415S Forward: 5’ - cac aat cac act ccc agc cag aat aaa ac

C415S Reverse: 5’ - cac aat cac act ccc agc cag aat aaa ac

C378S Forward: 5’ - gtg acg cac agt ttt aat agt gga ggg gaa

C378S Reverse: 5’ - cac tgc gtg tca aaa tta tca cct ccc ctt

C445S Forward: 5’ - ccc atc aga gga caa att aga agt tca tca aa

C445S Reverse: 5’ - ggg tag cct gtt taa tct tca agt agt tt

C296E Forward: 5’ - gaa tct gta gaa att aat gag aca aga ccc aac aac

C296E Reverse: 5’ - gtt gtt ggg tct tgt ctc att aat ttc tac aga ttc

C331K Forward: 5’ - ata aga caa gca cat aag aac ctt agt aga gca

C331K Reverse: 5’ - tgc tct act aag gtt ctt atg tgc ttg tct tat

Mutagenesis was confirmed by sequencing (Genewiz Inc.) using the BGHR primer or custom-made primers that span the Env cassette (IDT).

3.1.10 Mutant HIV-1$_{BaL}$ Binding to CD4 and 17b ELISA

The ability of the HIV-1$_{BaL}$ mutants C296-C331, C378-C445, C385-C415, and C598A-C604A to bind sCD4 and mAb 17 was analyzed by ELISA[72]. Gradient-purified viruses were added to a 100 kDa concentrator (Amicon) followed by centrifugation at 2,000 x g at 4 °C for 3 minutes on a tabletop 5424R centrifuge (Eppendorf). The retained HIV-1$_{BaL}$ virions were washed with 250 µL 1 × PBS. The wash step was repeated three times and the flow through was discarded. 100 µL of concentrated and washed virus was added to 100 µL fixative mixture comprised of 0.2% Glutaraldehyde in 2% Paraformaldehyde. The mixture was incubated at 4 °C for 15 min followed by the addition of 100 µL 0.1 M Glycine followed by another incubation at 4 °C for 15 min to quench the reaction. HIV-1$_{BaL}$ virus-fixative sample was added back to 100 kDa concentrators (Amicon) and spun at 2,000 x g for 3 minutes at 4 °C to perform a buffer exchange with 1 × PBS. HIV-1$_{BaL}$ was adsorbed at 50 µL per well to a 96-well high binding polystyrene ELISA plate (Corning) for 12 hrs at 4 °C with gentle rocking. The HIV-1$_{BaL}$ was then removed from the plate

and the latter was blocked with 200 μL/well of 3% BSA (Research Products International, Corp) in 1× PBS for 2 hrs at 25 °C, followed by a plate washing step with 1× PBS-T. For the CD4 binding experiments, 50 μL/well of 30 nM sCD4 in 0.5 % BSA dissolved in 1x PBS was added to the plate and incubated for 1 hr at 25 °C. This and all subsequent incubation steps were done in 0.5% BSA in PBS. After a 1 hour incubation period, the plate was washed 3 times with PBS-T followed by addition of 100 μL/well of biotinylated anti-CD4 (OKT4) antibody (eBioscience) at a 1:5000 dilution and the plate incubated for an additional 1 hr at 25 °C. After plate washing, streptavidin-bound HRP (AnaSpec) was added at a 1:5000 dilution and again incubated for 1 hr at room temperature. For the 17b binding experiments, 50 μL of 15 nM mAb 17b was added to the plate-immobilized HIV-1_{BaL}. After a 1 hr incubation at 25 °C, the plate was washed 3 times with PBS-T, followed by the addition of a horse radish peroxidase (HRP)-conjugated goat anti-human antibody (CHEMICON) which was incubated for 1 hour at room temperature. The extent of HRP conjugate binding was detected colorimetrically in both assays by adding 200 μL/well of 0.4 mg/ml of o-phenylenediamine dihydrochloride (OPD) (Sigma-Aldrich) dissolved in Sodium Citrate with Perborate (Sigma-Aldrich) for 30 min in the dark. Capsid p24 was quantified on a separate plate using the concentrated virus collected after the quenching step. Quantification was done using 1:5000 dilutions of anti-rabbit p24 (Abcam) and then anti-rabbit IgG fused to horseradish peroxidase (HRP) (Invitrogen). Gp120 was quantified using the same virus after the quenching step by western blot analysis with 1:5000 dilution of anti-gp120 D7324 (Aalto) and anti-sheep IgG conjugated HRP (Life Technologies). The western blots were quantified using Image J software. Plates were read at 450 nm using a microplate reader (Molecular Devices). The optical density (OD) units generated from either CD4 or 17b binding to the pseudovirus samples were normalized based on the p24 content of each mutant and the gp120 content determined by Western blot to allow for comparison between the mutants. Each experiment for CD4 or 17b binding contained a standard curve using sCD4 and 17b binding to monomeric HIV-1_{YU2} gp120 serially diluted (1:2, v/v) starting at 100 ng/ml.

3.1.11 Origin Pro. 8 curve fitting of dose dependence data

Data analysis of dose-dependence measurements performed in this study was conducted by sigmoidal curve fitting using the Origin v.8.1 (Origin Lab, Northampton, USA) software as explained in Chapter 2.

3.2 RESULTS

3.2.1 The Effect of sulfhydryl reagents on p24 release by KR13

Previous work has shown that cysteine reduction and alkylation impairs the ability of HIV-1 to bind CD4[95], thereby suggesting that the conserved disulfides are critical to the function of the virus and may play a role in the infection process[96,97]. Due to the close proximity of the PTT thiol to disulfides and the requirement of a free SH for lysis, we examined the role of disulfide exchange within gp120 by using sulfhydryl blockers and reducers to analyze their effects on p24 release induced by **1**. The sulfhydryl blocker, Iodoacetamide (IAAm), is an irreversible alkylating reagent, known for its ability to bind free sulfhydryls. We also evaluated the effect of Dithiothreitol (DTT), a reducing agent which undergoes two sequential disulfide-exchange reactions when reducing the typical disulfide bond,[98] and the irreversible non-thiol reducing agent, tris(2-carboxyethyl)phosphine (TCEP). Prior to assessing the effect of these reagents on PTT-induced virolysis, we determined their effects on HIV-1 virions. In agreement with previous findings, these sulfhydryl blocking and reducing reagents were found to inhibit HIV infection[95]. However, we showed that the viral infectivity was regained after pre-treatment and wash removal of reagents ("treat/wash") before assays (**Figure 22A**).

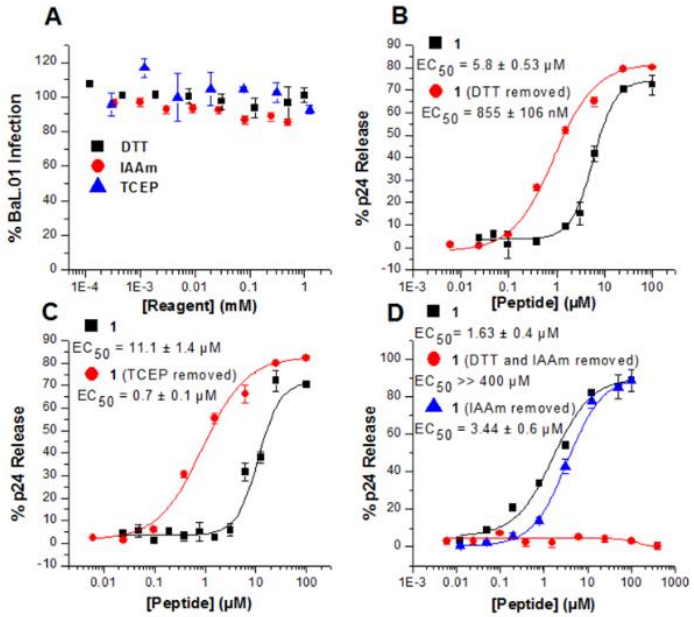

Figure 22. Effect of sulfhydryl reagents on PTT induced p24 release. (A) Effect of Sulfhydryl reagents on HIV-1_{BaL} infectivity. DTT, TCEP and IAAm treated HIV-1_{BaL} virions added to HOS cells to test infectivity. (B) Effect of HIV-1_{BaL} treatment and removal of DTT, followed by **1** treatment and p24 release analysis (C) Effect of HIV-1_{BaL} treatment and removal of TCEP, followed by 1 treatment and p24 release analysis. (D) Effect of HIV-1_{BaL} treatment of DTT serial dilutions and removal with subsequent treatment of 0.02mM IAAm. Followed by **1** treatment and p24 release analysis.

Additionally, these reagents did not cause p24 release. Therefore, we performed virolysis assays in which the virions were exposed to DTT, TCEP, or IAAm, in the "treat/wash" protocol before p24 analysis with **1**. Interestingly, DTT and TCEP pre-treatment of pseudotyped HIV-1_{BaL} caused

greater sensitivity to peptide **1**-induced p24 release (**Figures 22B and C**). Additionally, we showed that the enhanced p24 release potency caused by reducing agent pre-treatment was specific to thiol containing peptides (**Figure 23**).

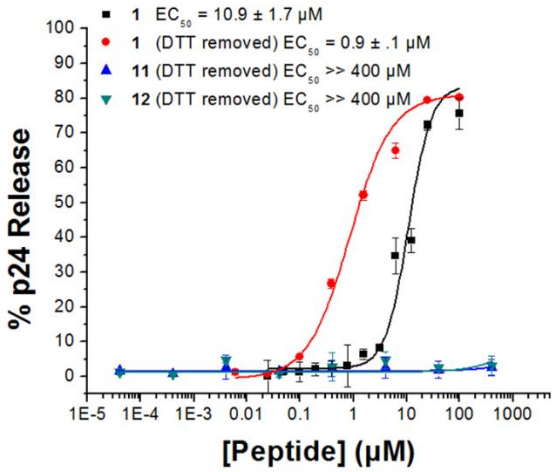

Figure 23. Peptide Triazole Specificity of DTT-induced enhancement of HIV-1_{BaL}. Effect of DTT treated HIV-1_{BaL} was compared with 1 and non-thiol containing peptides, 11 and 12 and analyzed for p24 release. Error bars represent standard deviation of the mean, n = 3.

Furthermore, we showed that virions exposed to DTT and subsequent IAAm, "treat/wash" after each reagent, were not capable of causing p24 release when treated with KR13 (**Figure 22D**). The enhanced lytic potency of **1** on DTT treated virions in comparison to untreated virions suggest that disulfide reduction in the HIV-1 Env protein augments the efficiency of peptide triazole thiol lysis activity. These data argue that PTTs cause virolysis by reducing disulfides and the free sulfhydryl group initiates a cascade of disulfide exchange reactions leading to virolysis.

3.2.2 Functional Properties of Biotinylated KR13

Based on the current hypothesis that PTT's cause p24 release by propagating disulfide exchange, we postulated that the PTT C-terminal thiol group covalently binds to a free gp120 cysteine or interacts with a cysteine of a disulfide pair, leading to HIV-1 viral lysis. To test this, we synthesized a peptide **1** derivative that contained a Lys (Biotinyl) residue at the N-terminus, denoted Bt-KR13 (**Figure 24A**) as well as a biotinylated control peptide derived from **11**, denoted Bt-KR13b. Bt-KR13b also contained a Lys (Biotinyl) residue at the N-terminus as well as an Acetamidomethyl (Acm) capped cysteine residue at the C-terminus (**Figure 24B**). We assessed the functionality of Bt-KR13 and Bt-KR13b with their respective parent peptides, **1** and **11**, for gp120 binding, HIV-1 infectivity and p24 release.

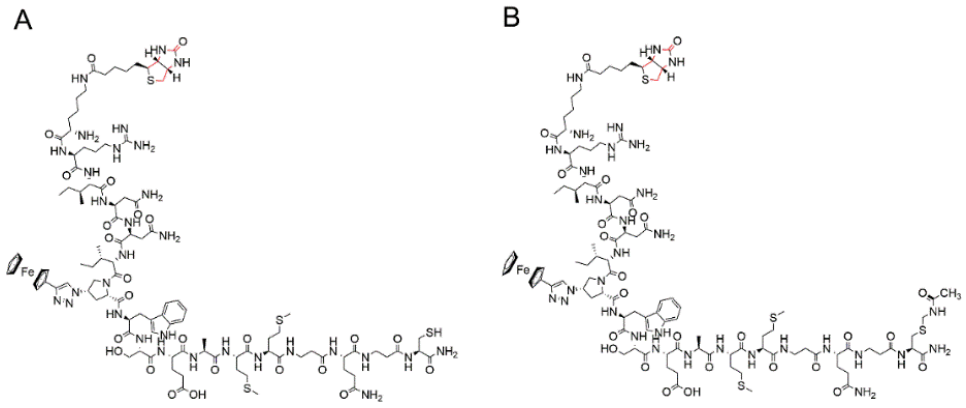

Figure 24. Chemical Structure of Biotinylated PTTs. (A) Bt-KR13 is the biotinylated variant of **1** (KR13) containing a biotinyl (Lysine) amino acid at the N-terminus. (B) Bt-KR13b is the biotinylated variant of **11** (KR13b) containing a biotinyl (Lysine) amino acid at the N-terminus and Cys(Acm) at the C-terminus. Biotinyl group displayed in red outline.

Peptide effects on virus were determined by treating gradient-purified HIV-1_{BaL} with increasing concentrations of peptide in cell infection and p24 release analyses. We found that Bt-KR13 and Bt-KR13b were both powerful inhibitors of HIV-1 infection comparable to that of **1** and **11** as displayed by their respective IC_{50} values of 136 ± 44 nM and 186 ± 38 nM. Additionally, Bt-KR13 induces p24 release as efficiently as its parent peptide, KR13, 0.99 ± 15 μM and 1.63 ± 16 μM

respectively (**Figure 25A and B**). Neither Bt-KR13b nor **11** caused p24 leakage as expected due to the unavailability of a free thiol because of the acetamidomethyl - sulfhydryl protection on their respective cysteine residues.

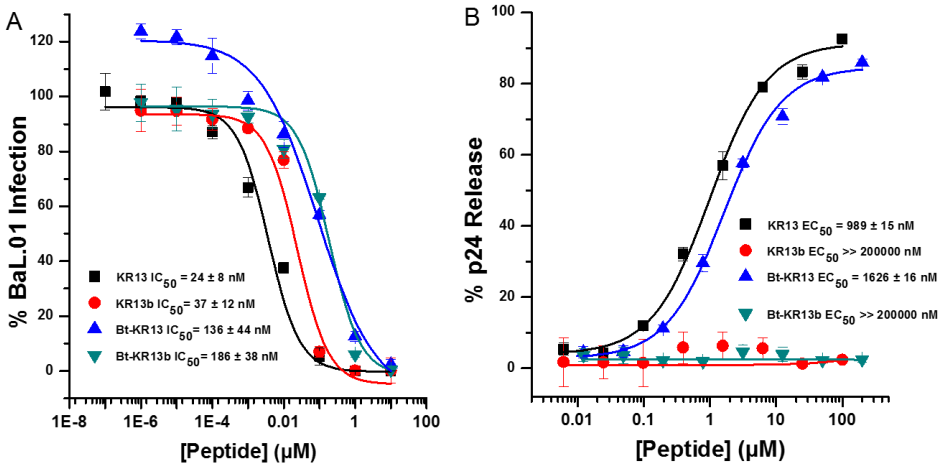

Figure 25. Functional Characterization of PTT Biotinylated variants on HIV-1_{BaL} pseudovirus antiviral functions. (A) Inhibition of cell infection analyzed using a single round pseudotyped assay. The IC_{50} values of Bt-KR13 and Bt-KR13b inhibit HIV-1_{BaL} infection to the same extent of their parent peptides, 136 ± 44nM and 186 ± 38 nM. (B) Relative p24 release measured using ELISA. The calculated EC_{50} values for **1** and Bt-KR13 were 0.989 ± 15 μM, 1.63 ± 16 μM respectively. **11** and Bt-KR13b did not display p24 lysis at 200 μM. The data were normalized using untreated virus as a negative control (< 5% p24 release), and p24 release observed with 1% triton X treated virus was taken as 100% p24 content. Sigmoidal curve fits of data were obtained using Origin v.8.1 (Origin Lab, Northampton, USA). Error bars represent standard deviation of the mean, n = 3.

3.2.3 Bt-KR13 effects on gp120 and HIV-1$_{BaL}$

After confirming that Bt-KR13 exhibited potencies similar to previous peptide triazoles by several characterization assays, we aimed to analyze the effect of the biotinylated peptides' Cys residue on gp120, by exploiting the biotin group for detection. The biotinylated peptides were incubated with soluble YU2 gp120, then the peptide/gp120 mixture was fractionated on a non-reducing gel along with several peptide controls also incubated with gp120, including a thiol-blocked variant, **11**. Separate western blots were performed to detect the presence of gp120 and biotin. We found that gp120 was present in all samples, however the only biotin detected was that of the Bt-BSA controls and a biotin blot in BT-KR13/gp120 mixture, which was at the same molecular weight of gp120 (**Figure 26A and B**).

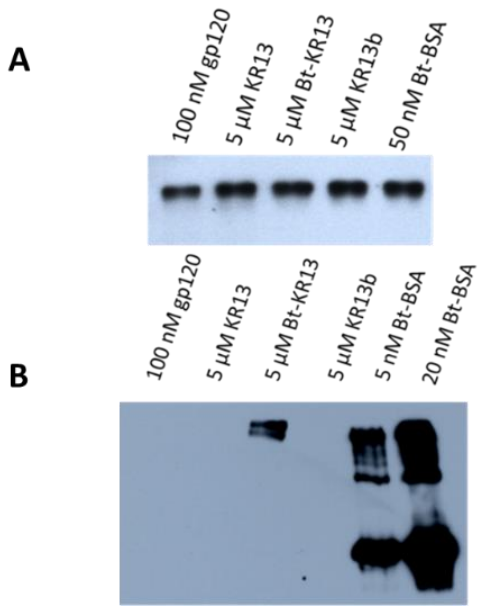

Figure 26. Non-Reducing Western Blot of Bt-KR13 Incubation with HIV-1_{BaL}. (A) anti- Gp120 and (B) anti-Biotin western blot of peptide samples Bt-KR13, KR13, and KR13b. Bt-KR13 detected at the gp120 MW under non-reducing conditions, however peptides without a free SH group were not detected with gp120. Yu2 gp120 and Biotinylated-BSA were used as gp120 and biotin controls, respectively.

Next, we repeated the Western blot detection under reducing conditions, to analyze the effect of the peptide attachment to gp120. Here we observed biotin detection of the Bt-BSA controls, however the biotin positive band was not detected in the Bt-KR13/gp120 mixture (**Figure 27**) suggesting that the disulfide bond between peptide and protein was cleaved.

Furthermore, to ensure that the biotin positive band we observed was due to a specific covalent attachment between the peptide thiol and gp120, we performed several control experiments

utilizing the non-thiol containing peptide (**12**, UM15). Peptide **12** at a concentration of 5 µM and 50 µM was co-incubated with a 5 µM concentration of Bt-KR13 and gp120 simultaneously. The western blot analysis of biotin detection showed that **12** competed with Bt-KR13 binding to gp120, once again confirming that the IXW pharmacophore of peptide triazoles specifically binds gp120, yet the sulfhydryl group is responsible for the covalent attachment (**Figure 28**). In addition, we performed a Western Blot using a biotinylated peptide with a blocked thiol group, denoted Bt-KR13b, to once again confirm the specificity of the thiol group. Bt-KR13b was co-incubated with gp120 and was then run on a 12% non-reducing gel, followed by Western blot analysis to detect gp120 and biotin. Biotin was not detected in the Bt-KR13b sample, thereby again displaying that a functional free thiol is required for covalent attachment (**Figure 28**). These results with soluble gp120 were similar to those using pseudotyped HIV-1_{BaL} virions.

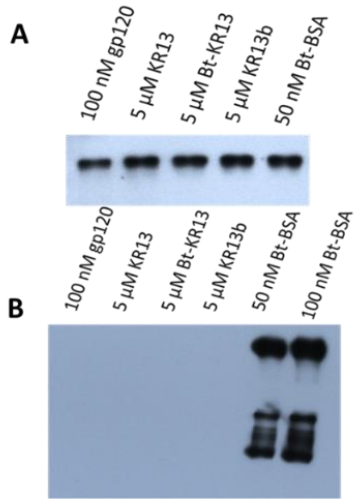

Figure 27. Reducing Western Blot of Bt-KR13 Incubation with HIV-1_{BaL}. (A) anti- Gp120 and (B) anti-Biotin western blot of peptide samples Bt-KR13, **1** (KR13), and **11** (KR13b). Bt-KR13 no longer detected at the gp120 MW under reducing conditions. Yu2 gp120 and Biotinylated-BSA were used as gp120 and biotin controls, respectively.

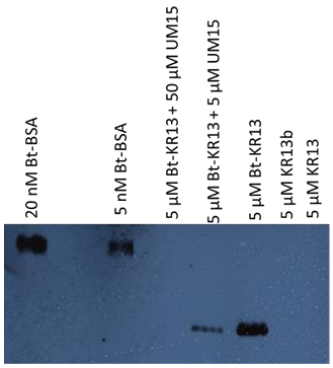

Figure 28. Western Blot of **12** (UM15) Competition with Bt-KR13 Incubation with HIV-1_{BaL}. Biotin detection in peptide samples Bt-KR13 with increasing concentrations of **12**. 1 (KR13), **11** (KR13b), and Biotinylated-BSA were used as controls.

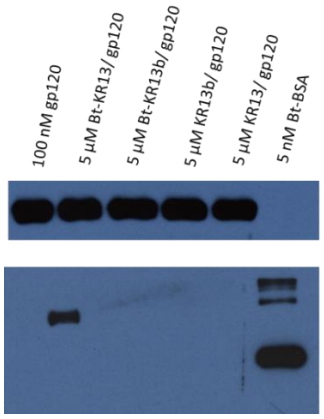

Figure 29. Non-Reducing Western Blot of Bt-KR13b Incubation with HIV-1_{BaL}. (A) anti- Gp120 and (B) anti-Biotin western blot of peptide samples Bt-KR13, KR13, and KR13b. Bt-KR13b not detected at the gp120 MW under non-reducing conditions, nor are the peptides without a free SH group are detected with gp120. Yu2 gp120 and Biotinylated-BSA were used as gp120 and biotin controls, respectively.

3.2.4 Effects of KR13 on disulfide mutations of HIV-1_{BaL}

To further investigate PTT-induced lysis, we aimed to identify specific gp120 disulfides involved in the lytic process. Therefore, we examined the role of several conserved cysteine residues which form disulfide bonds in gp120 and gp41. Based on the thiol trajectory of the PTT-gp120 docked structure in our MD model, V3 region disulfide bonds were of great interest. The peptide Cys residue approached disulfide linkages C378-C445, C385-C415 and C296-C331. These disulfides are commonly referred to as the "CD4 exposed disulfide cluster" due to their proximity to the CD4 binding site, thereby making them potential sites of disulfide exchange in the virus infection process. For that reason, we mutated each cysteine residue in a single disulfide pair to yield mutant

HIV-1_{BaL} virions. We prepared intact viruses for the gp120 disulfides, C296E-C331K, C378S-C445S and C385V-C415S. Taking into consideration previous findings that displayed that KR13 induces 6-helix bundle formation in gp41[70], we also mutated gp41 disulfide C598-C604A to yield the C598A-C604A mutant. These mutant virions were gradient purified as previously described and quantified for gp120 and p24 content. Mutant HIV-1_{BaL} virions were tested for infectivity and displayed low infection levels, therefore we examined the ability of the mutant virions to bind sCD4 and co-receptor surrogate, 17b, by ELISA. The ELISA displayed that the mutant virions were capable of binding sCD4 and 17b to various extents (**Figure 30**).

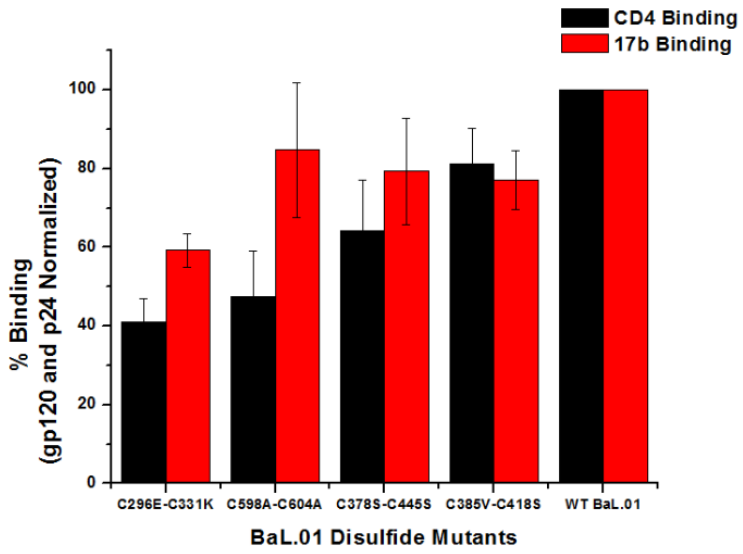

Figure 30. ELISA CD4 and 17b Binding of HIV-1_{BaL} pseudovirus disulfide mutants. Sandwich ELISA used to determine binding potencies of immobilized virus to anti-CD4 and mAb 17b antibodies. Percent binding values were normalized based on the p24 content of each mutant and the gp120 content. Error bars represent standard deviation of the mean, n = 3. Bailey et al. 2015.

We performed p24 release analysis of peptide **1** treated mutant virions and displayed that **1** maintained lytic potency comparable to WT HIV-1_{BaL} in mutant HIV-1_{BaL} C378S-C445S and C385V-C415S virions. Strikingly, HIV-1_{BaL} mutations C296E-C331K and C598A-C604A repressed p24 release normally elicited by **1** (**Figure 31**).

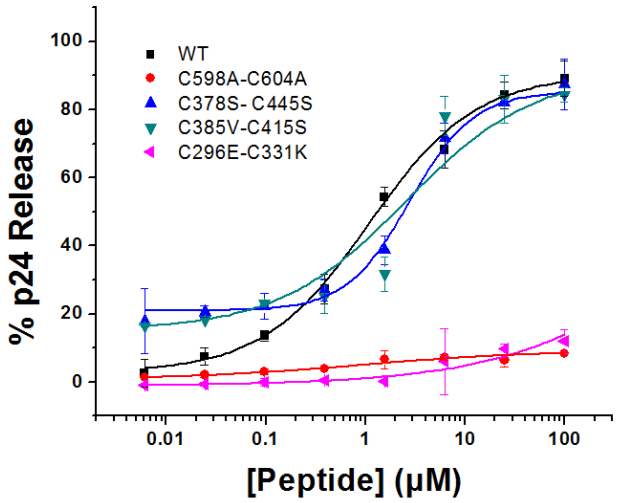

Figure 31. Effect of HIV-1_{BaL} disulfide mutations on p24 release by **1**. Effect of HIV-1_{BaL} mutations C296E-C331K (magenta) C378S-C445S (blue), C385V-C415S (cyan), and C598A-C604A (red) on p24 release. Relative p24 release was measured using ELISA. The data were normalized using untreated virus as a negative control (< 5% p24 release), and p24 release observed with 1% triton X treated virus was taken as 100% p24 content. Sigmoidal curve fits of data were obtained using Origin Pro.8 (Origin Lab). Error bars represent standard deviation of the mean, n = 3. Bailey et al. 2015.

These data imply that PTT- induced lysis is initiated within gp120 at C296-C331 and the role of the gp41 disulfide, C598-C604A, is to stabilize the 6 helix bundle for virolysis. We suggest the latter because C598-C604 links the N and C-helices of gp41, which is critical for the proper structural and functional rearrangements of Env and previous studies have shown that an intact gp41 disulfide is a prerequisite for fusion and infection[99,100]. However, we do recognize that our data do not determine the redox state of the gp41 disulfide, therefore it cannot be ruled out that C598-C604A is reduced during PTT-induced lysis.

3.3 DISCUSSION

The release of the capsid p24 protein caused by peptide triazole thiols led us to investigate the virucidal mechanism of action of peptide triazole thiols. We hypothesized that upon peptide Cys-SH encounter with HIV-1 Env, the thiol interferes with conserved disulfides clustered proximal to the CD4 binding site in gp120 through "disulfide exchange", ultimately leading to a rearrangement of the Env protein spike and disrupting the viral membrane. Based on our prior conclusions that displayed the importance of the V3 region of gp120, an area populated by several disulfide clusters, we examined the contribution of these disulfides to PTT-induced virolysis. In agreement with our proposed hypothesis of a PTT-triggered disulfide exchange reaction within gp120, we found that virions pre-treated with reducing agents DTT or TCEP prior to peptide treatment displayed augmented p24 release profiles. We also showed by mutagenic analysis of conserved HIV-1 envelope disulfides, that gp41 has an undefined role that is implicated in the lytic process.

To understand disulfide exchange in the context of PTT viral lysis, we assessed the effect of reducing agents on p24 release. DTT and TCEP pre-treated virions did not lose viral infectivity after reagent removal (**Figure 22A**), conversely the treated and washed virions displayed enhanced PTT- induced lysis (**Figure 22B and C**). The reductive enhancement caused by DTT and TCEP was diminished when those virions were subsequently treated with IAAm (**Figure 22D**). These results provide evidence that reducing agents, DTT and TCEP, produce free sulfhydryl groups within gp120 and these thiols are used to catalyze the disulfide exchange cascade.

The gp160 envelope protein contains 10 disulfide linkages; nine of these are found in gp120 and the last is within gp41. Our previous docking analysis of PTT truncate, 8, complexed with gp120, placed the peptide SH group at an equidistant location from the disulfides C378-C445 (C3), C385-C415 (C4), C296-C331 (V3). For this reason we explored the participation of these disulfides in the PTT lysis process by mutagenic analysis. We found that p24 release capability by **1** was retained in disulfide mutants C378S-C445S and C385V-C415S, but mutants C296E-C331K and C598A-C604A abolished lytic potency of **1 (Figure 31)**. The C296-C331 disulfide is located in the V3 loop, a region of gp120 which is displaced upon receptor binding to allow for further conformational changes of gp120 required for viral fusion. The C598-C604 disulfide is in a critical location of gp41, found in a loop between the N- and C- helices of the viral transmembrane protein. After engaging CD4, gp41's N- and C- helices reorganize to form a 6-helix bundle. The 6-helix bundle conformation is needed for virus fusion with host cells, thereby making these regions essential in the HIV infection process.

In all, these results collectively show that disulfide disruption is an integral part of the PTT lytic mechanism. We speculate that PTTs initiate a cascade of disulfide exchange reactions from gp120 to gp41, which subsequently induces 6-helix bundle formation, leading to lysis. This proposed

mechanism is buttressed by research showing that 6-helix bundle formation occurs during PTT-induced lysis[70]. In prior work, we found that Enfuvirtide, the fusion inhibitor that blocks 6- helix bundle assembly by targeting the N-terminal heptad repeat region of gp41, inhibits PTT-induced lysis. Enfuvirtide inhibition of virolysis suggests a relationship between viral membrane disruption and gp41 fusion-6 helix bundle formation. These findings have led us to believe that virolysis induced by PTTs is related to the native physiological events, within the Env trimer, which require triggering gp41 fusion machinery through the viral membrane. Investigating the mechanism of virolysis will provide insight into understanding how the chemical perturbation of the HIV Env protein results in HIV membrane destabilization. Additionally, understanding the virolytic mechanism will identify residues of Env that need to be targeted to optimize our entry inhibitors.

Chapter 4: Other Experiments

4. Introduction

Peptide triazole thiols were first developed by Dr. Kantharaju Kamanna, with the intention of utilizing the C-terminal cysteine residue as a strategy for peptide conjugation to gold nanoparticles[94]. The lytic effect of these inhibitors, a surprising finding on their own, led us on a quest to understand the mechanism of action and to use the lytic feature to develop other novel anti-HIV drug candidates. The experiments described below were aimed towards both of these thrusts and represent ongoing efforts in the Chaiken lab.

4.1 MATERIALS AND METHODS

4.1.1 Peptide Synthesis and Click Conjugation

All sequences and denotations of peptides reported are given in **Table 1**. Peptides were synthesized manually by stepwise solid-phase peptide synthesis (SPPS) and purified as described in Chapter 2.

4.1.2 Western Blot Analysis of PTT interaction with BG505 SOSIP.664 gp140

20 μM and 100 nM KR13 were incubated with BG505 SOSIP.664 gp140 as well at 37 °C for 35 min at 23 °C. After the incubation, a non-reducing western blot analysis was performed by adding 15 μL of reaction samples to 15 μL of 1x Laemmli buffer. Incubation of 20 μM UM15 was used as a negative control as well as 100 nM SOSIP and YU2 gp120. Gp120 was detected with 1:3000 dilution of anti-gp120 D7324 (Aalto) and anti-sheep IgG conjugated HRP (Life Technologies).

4.2 RESULTS

4.2.1 KR13 Effects on BG505 SOSIP.664 gp140

Previously, we aimed to determine if PTT-induced disulfide exchange initiated a cascade from gp120 disulfides to those in gp41. The SOSIP.664 trimer was used as a tool to investigate disulfide exchange. SOSIP.664 is a soluble cleaved gp140 trimer, composed of gp120 and the ectodomain of gp41 ($gp41_{ecto}$) in which the hydrophobic MPER sequence is removed[101] (**Figure 32**). Like the native envelope glycoprotein, SOSIP.664 has exposed epitopes that generate bNabs capable of neutralizing gp140 trimers. This is attributed to the T332N substitution, which yields a glycan needed for epitope recognition by several bNabs[101]. Additionally, SOSIP.664 is unique from other trimer mimics in that it is a stable variant. This was achieved by an I559P mutation, as well as the introduction of a mutant disulfide bond at position A501C-T605C which covalently connects gp120 and gp41[101] (**Figure 32).**

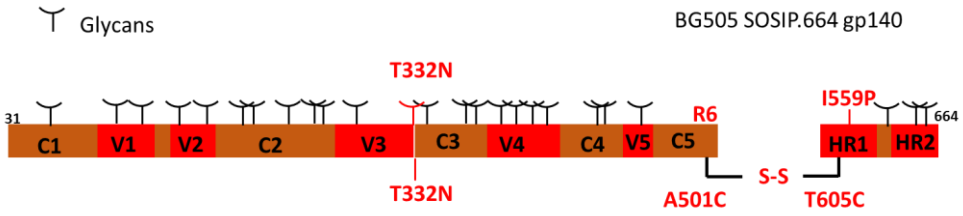

Figure 32. Design of BG505 SOSIP.664 gp140 trimer. Linear representation of BG505 SOSIP.664 gp140 trimer. Several modifications displayed including A501C-T605C, T332N, and I559P. These substitutions are required for stability and production of bNabs of envelope trimer.

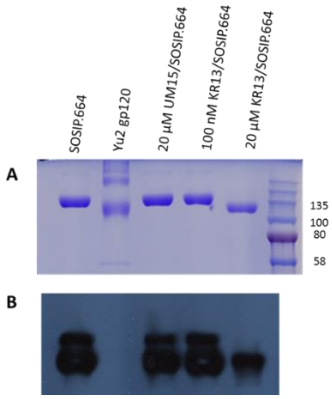

Figure 33. Effect of peptide triazole treatment on gp140 SOSIP.664. KR13 and the non-thiol containing peptide triazole, UM15, were incubated with SOSIP prior to analysis by (A**)** Coomassie staining and (B**)** Western Blot analysis.

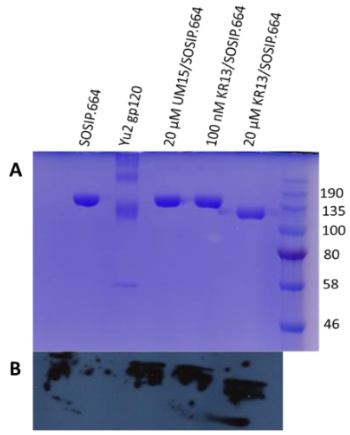

Figure 34. Effect of peptide triazole treatment on gp140 SOSIP.664. KR13 and the non-thiol containing peptide triazole, UM15, were incubated with SOSIP prior to analysis by (A) Coomassie staining and (B) Gp120 and gp41 Western Blot analysis.

The cleavage of the A501C-T605C disulfide conjoining gp120 and $gp41_{ecto}$ would be readily detected by the separation of these proteins, thereby making it a useful tool to analyze PTT induced disulfide reduction. We found that SOSIP.664 treatment with PTT caused cleavage of the gp140 trimer into the monomeric proteins, gp120 and $gp41_{ecto}$ (**Figure 32 and 33**) by disruption of the mutant SOS disulfide, A501C-T605C. However, it is important to note that the A501C-T605C disulfide which links gp120 and gp41 in SOSIP.664 is not native to HIV-1 Env, but its placement is in the same gp41 region of the naturally occurring gp41 disulfide, C598-C604. From our data it is not possible to conclude how PTTs cause disulfide bond cleavage in SOSIP. For example, it is very possible that the cysteine SH group of **1** merely cleaves the A501C-T605C disulfide as a reducing agent, much as DTT would. To fully determine the mode of the gp140 cleavage, future

work must include KR13S, a scrambled PTT, treatment with SOSIP.664 to assess the specificity of the disulfide cleavage.

4.3 Optimizing PTTs for enhanced proteolytic stability and formulating vehicles for delivery

4.3.1 Synthesizing non-natural virolytic peptides

Peptide triazoles hold great therapeutic promise as entry inhibitors, however in peptide form they are unstable. Therefore, we must develop new methodologies to optimize the proteolytic stability of PTTs, thereby making them accessible to HIV patients. The first method for increasing the stability of these peptides is to develop non-natural peptides. This can be achieved by replacing natural L-amino acids with their D-amino acid counterparts and also utilizing amino acid analogs. The rationale behind these studies is that these substitutions were based on the hypothesis that limiting peptide bonds would make the inhibitors less recognizable to proteases. By replacing the natural residues of UM-24 with D-amino acids and substituting Bta for Trp, a non-natural mimic of UM-24 was produced, denoted KR-42, as well as KR-42's lytic variant containing a C-terminal Cys, denoted LB-07 (**Table 4**). KR-42 displayed a reduced inhibition profile in comparison to its' parent peptide, UM-24, however adding the cysteine residue (LB-07) regained potency comparable to UM-24, thereby reaffirming the significance the thiol group.

Table 4. Non-Natural Peptide Triazoles and Corresponding Amino Acid Sequences.

Peptide	Amino Acid Sequence								
UM-24	^{L}Cit,	^{L}Asn,	^{L}Asn,	^{L}Ile,	AzidoPro,	^{L}Trp,	^{L}Ser,	NH_2	
KR-41	^{L}Cit,	^{L}Asn,	^{L}Asn,	^{L}Ile,	AzidoPro,	^{L}Bta,	^{L}Ser,	NH_2	
KR-42	^{D}Cit,	^{D}Asn,	^{D}Asn,	^{D}Ile,	AzidoPro,	^{L}Bta,	^{D}Ser,	NH_2	
LB-07	^{D}Cit,	^{D}Asn,	^{D}Asn,	^{D}Ile,	AzidoPro,	^{L}Bta,	^{D}Ser,	^{L}Cys,	NH_2
LB-08	^{D}Cit,	^{D}Asn,	^{D}Asn,	^{D}Ile,	AzidoPro,	^{L}Bta,	^{D}Ser,	^{D}Cys,	NH_2

Pilot studies were planned to investigate the proteolytic stability of natural PTs, non- natural PTs, and non-natural virolytic PTs. Initial peptide digestion studies performed by former PhD Candidate, Pamela Kubinski, using a 1:20 weight ratio of protease to peptide revealed a rapid degradation of the natural peptide UM-24 (**Figure 35**). Although Trp substitution with Bta and D-amino acid replacement did produce peptides with reduced proteolytic stability profiles, they have also shown to be less potent than their natural L-amino acid counterparts. Protease studies of non-natural virolytic PTs have yet to be completed. Therefore, we must explore other strategies to target stability, yet do not compromise potency. Importantly, such a strategy has recently been accomplished in the Chaiken lab[102], with the discovery of macrocyclic peptide triazoles.

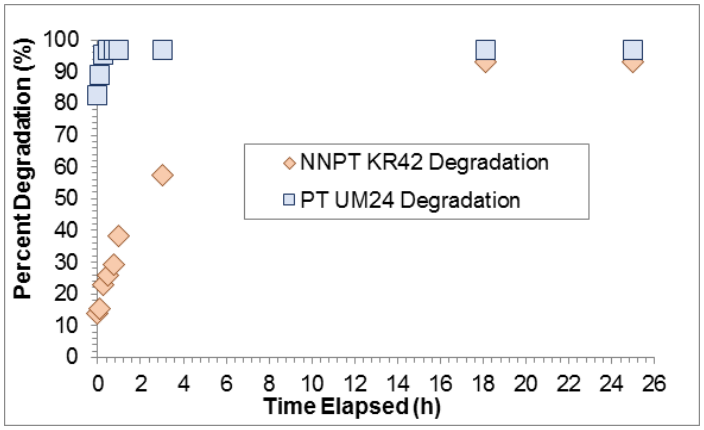

Figure 35. Natural and non-natural peptide percent degradation over 25 hours. Exposure of peptides UM-24 and its non-natural counterpart, KR-42, to α-chymotrypsin resulted in >95% degradation of UM-24 after 30 min, compared to retention of 75% of undigested non-natural peptide, KR-42, after 30 min. Trytophan analog (L-Bta), found in KR-42, resisted protease degradation. Data acquired from Pamela Kubinski.

CHAPTER 5: Future Directions

5. Introduction

The work described herein uncovering the mechanism of peptide triazole thiols has made defining contributions to the HIV field. The value of this research was recognized by the National Institute of Health, which awarded me an F31 Ruth Kirchstein fellowship to complete this exploration of gp120 disulfide dynamics in the HIV-1 antagonism. As previously explained, peptide triazole thiols irreversibly inactivate HIV-1 virions by their ability to cause gp120 shedding and virolysis, thereby making them novel inhibitors. As a result of the work elaborated in this thesis, we have made several conclusions regarding the virolytic mechanism of PTTs. We have determined the following, (a) The lytic action of PTTs is not a mere function of peptide self-dimerization, instead viral lysis requires a free thiol. (b) Lytic action is dependent on the length of the C-terminus linker. (c) Finally, one of the most significant outcomes of this project, PTTs cause virolysis by inducing exchange of gp120 disulfides.

Although, we determined a significant amount regarding the structure-activity relationship of PTTs and their mechanism of action, there is still more to be determined. These innovative inhibitors have a broad scope of utility for their potential as drug candidates as well as their role in vaccine development. Furthermore, PTTs have shed light on disulfide exchange, a process not frequently discussed as a feature of viral entry. Attaining a more detailed understanding of virus-related disulfide exchange will help propel rational design of drugs and provide researchers with a more holistic view of lentiviral infection.

5.1 Therapeutic Delivery of Peptide Triazoles

5.1.1 Pegylated Liposomal Delivery of NNPTs

Despite the efficacy of HAART, there is still a pressing need for a long-acting HIV drug. To this end, we aim to develop an effective, yet safe formulation for PTT delivery. Therefore, as described above, we used the combined synthesis and functional screening to identify a structure-minimized, maximally non-natural peptide triazole virucide (NNPT) and to design its scale-up synthesis as a lead microbicide development candidate. We further aimed to derive a hydrogel-encapsulated form of the NNPT virucide and identify formulations for in vivo testing. Anti-retrovirals have previously been delivered by using liposome encapsulation methods. This has proven to be an advantageous strategy for delivery because it offers multiple layers of protection for the drug. Liposomes prevent peptide/drug degradation while in transport. Additionally, liposomes can be modified with polymers, such as polyethyleneglycol (PEG), which protect the liposomal integrity. Decorating encapsulated liposomes with sCD4 and 17b co-receptor surrogate, will specifically engage HIV particles (**Figure 36**). After engagement, controlled release of PTT entry inhibitors will exert their mechanism of action causing irreversible viral inactivation. Therefore, Dr. Rachna Arora has been leading studies in hopes of developing HIV-1-targeting liposome formulations. These pegylated liposomes represents another potential use of PTTs due to their ability to inactivate virus in the absence of cells.

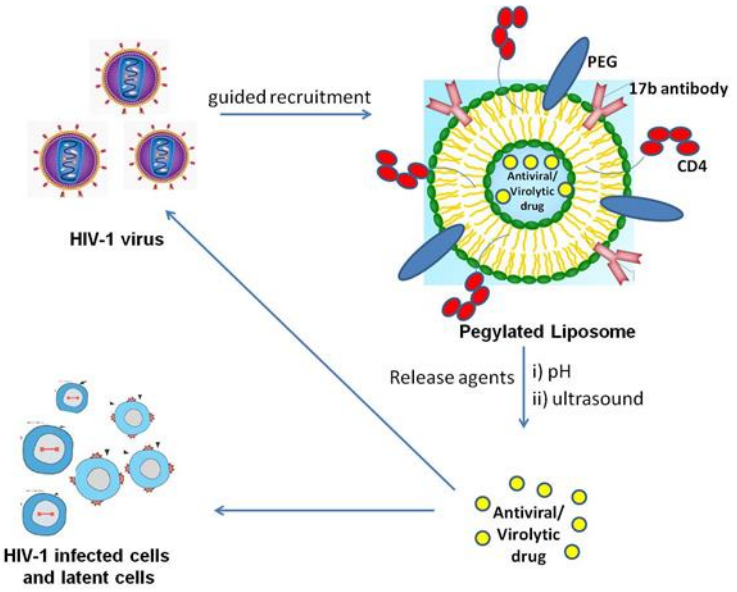

Figure 36. Proposed mode of action of pegylated liposomal drug delivery vehicle. Image by Rachna Arora.

5.2 Understanding the Role of Disulfide Exchange in viral entry processes

5.2.1 The Role of Thiols in Regulating Viral Entry

HIV-1 and other enveloped viruses require a series of coordinated conformational rearrangements of the viral envelope and transmembrane proteins to ensure efficient viral infection. These synchronized chemical and structural changes between the viral and host cell proteins are regulated by a myriad of factors which ultimately result in transfer of the viral genetic material into target

cells. The role of thiols as a means of regulation in virus entry processes is a new field, yet growing evidence suggests that many viruses utilize thiol-disulfide exchange reactions as a sensory mechanism to enhance viral entry. Several lentiviruses including, Sindbis virus (SV), murine leukemia virus (MLV), human T-cell lymphotropic virus (HTLV-1), and HIV-1 appear to execute disulfide cleavage by thiol-exchange during their respective viral entry processes[100,103,104]. This reliance on redox-induced changes to their disulfides is an additional layer of regulation to ensure successful viral membrane fusion.

5.2.2 Oxidoreductase Activity Involvement in Viral Thiol Exchange

Gp120 disulfide exchange has been previously observed and may be an integral step in native HIV entry. Mounting evidence[96,105-107] has demonstrated that oxidoreductase inhibition impairs HIV infection, CD4 binding, and fusion events, thereby implicating redox exchange as a mechanism used in HIV entry. Oxidoreductases are a class of enzymes that utilize cofactors, NADP or NAD+, to transfer electrons from one molecule to another (**Figure 37**) [108].

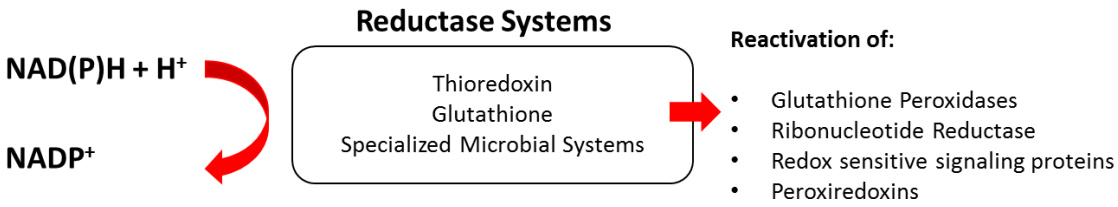

Figure 37. Electron flow displaying the reductive recycling of NADPH and NAD utilized by cellular oxidative proteins. Reductase systems shown are the thioredoxin (Trx) system, including thioredoxin reductase (TrxR); the glutathione (GSH) system, including glutathione reductase, which recycles oxidized glutathione (GSSG). Also included are the microbial reductase systems.

The body uses oxidoreductases to catalyze the formation and cleavage of disulfide bonds in cells. Common oxidoreductases are thioredoxin (Trx) and protein disulfide isomerase (PDI), known for their catalysis of thiol-disulfide exchange reactions employed in the protein maturation process in the endoplasmic reticulum. However, oxidoreductases also are commonly trafficked to the cell-surface and exert their catalytic functions in disulfide cleavage of surface-bound macromolecules and viral proteins. One of the first studies that alluded to the reductive function of mammalian cells was the analysis of the activation of the diphtheria toxin (DT) protein[109]. DT is a homodimer linked by a disulfide bridge, which is cleaved upon binding to its cell surface receptor. The disulfide cleavage activates DT, thereby enabling the protein to exert cytotoxic properties[109]. Intriguingly, the membrane impermeant thiol reagents p-chloromercuribenzene sulfonate (pCMBS) and 5,5'-

dithiobis-(2-nitrobenzoic acid) (DTNB) were found to inhibit the reductive cleavage of DT, thereby preventing cytotoxicity[109]. More recently, PDI inhibitors and monoclonal antibodies to PDI have shown similar inhibitions, suggesting that the reductive cleavage events on the cell membrane are attributed to PDI[110].

Further analysis of these thiol blocking reagents has shown that DTNB inhibits Sindbis and HIV infection in a dose- dependent manner. Both of these viruses contain many disulfide bonds. It is postulated that DTNB and other thiol reagents inhibit the cleavage of viral disulfide bonds that are required for infection, which implies that cell surface redox activity is a requirement of viral entry. Furthermore, the IC_{50} values of HIV inhibition by DTNB is comparable to its IC_{50} value for PDI inhibition[87]. These data suggest that DTNB inhibits HIV infection by inhibiting PDI, leading to the hypothesis that gp120 disulfide cleavage is required for viral entry. Further buttressing this argument is research from Markovic et al., which displayed that only oxidized gp120 is capable of binding to CD4 and co-receptor[111]. After these binding events, the resulting gp120 has 4 free thiols, indicating that 2 disulfides are reduced during HIV entry[111].

In all, the disulfide-exchange literature is vast and diverse; and although cell-surface secreted oxidoreductases are implicated in the process, there are still many lingering questions. There has been much debate in literature regarding whether cell lines utilize various oxidoreductase enzymes or if a single oxidoreductase is the sole initiator of these reactions[96]. Also, it is still unknown if oxidoreductases directly undergo disulfide exchange with gp120 disulfides or if other partners are involved. Cerutti et al. showed that the gp120 binding to CD4 required a reduced disulfide in either domain 1 or domain 2 of the latter[105]. These results suggest that membrane-associated oxidoreductases “prime” CD4 for gp120 interaction and suggest the possibility that the redox state of the CD4 receptor is critical to HIV entry. Moving forward, it will be useful to identify the oxidoreductase involvement in HIV entry by comparing the PTT antiviral potencies with various

PDI–deficient cell lines in antiviral infection assays. Additionally, useful information will be obtained from characterizing structural details of CD4 domains and determining gp120's CD4 redox preference during virus entry.

In an effort to further elucidate the role of disulfide exchange in HIV entry, previous researchers have used active site mutants of PDI to capture the mixed disulfide intermediate of PDI and its substrate, gp120. These results showed that PDI formed a covalent disulfide cross-linked intermediate with soluble gp120 protein, which was not observed in the presence of PDI inhibitors[112]. Together, these results provided additional evidence of the role of disulfide exchange in HIV entry. Although PDI and Trx are the most common oxidoreductases implicated in facilitating viral entry, there has not been a robust study evaluating the utility of the entire 22 subclasses of these enzymes and their effects on virus entry. Therefore, assessing HIV infectivity capability on cell lines that are deficient of oxidoreductases through the use of siRNAs or CRISPR/Cas9 technology, may further clarify their roles.

Additional experiments may include detecting and quantifying free sulfhydryls of gp120 before and after its incubation with cell lines expressing PDI and PDI-deficient cell lines. The thiols of gp120 can be quantified by the use of a maleimide biotin probe followed by a co-immunoprecipitation pull-down assay with Streptavidin-HRP to retrieve and visualize the protein.

What is known is that the conserved disulfides of the HIV envelope are pertinent to CD4 binding, gp120 binding, and infectivity[97,113]. It is also known that thiol-exchange is a prerequisite for CXCR4 tropic HIV entry[111] and because cell membrane oxidoreductases are readily accessible to Env disulfides, their enzymatic function is linked to disulfide exchange[114].

5.3 Understanding Disulfide Exchange in the context of PTT Lysis

5.3.1 Identify occurrence and nature of covalent attachment of PTT to gp120 during virus lysis

We were able to define the mechanism of action of PTTs as "disulfide exchange" through the use of various methodologies. Western blot analysis allowed us to determine that PTTs covalently bind Env, however we still have not been able to determine the specific disulfide contact site on gp120 that is targeted for covalent attachment by the PT-SH group. Therefore, future studies of PTTs will include pinpointing and displaying PTT attachment to a defined disulfide site of Env. Mass spectroscopy digestion assays utilizing the biotinylated PTTs, Bt-KR13 and Bt-KR13b, will be useful tools. These peptides can be used to form conjugates with gp120, followed by trypsin digestion, and subsequent LC-MS/MS, can then be used to detect peptides corresponding to Cys containing regions of gp120.

Furthermore, identifying the path of disulfide exchange induced by PTTs may also be accomplished through the use of affinity labeling techniques. Another option to detect PTT attachment to gp160 is using Activity-Based Protein Profiling (ABPP), a synthetic methodology where probes contain a reporter tag, C-terminal reactive group, and a peptide pharmacophore that targets the protein of interest. To identify the contact site of PT- thiol engagement, ABPP probes can be designed and then incubated with gp160. Such probes can be designed so that they contain the characteristic peptide triazole, IXW pharmacophore, a photocrosslinker for the reactive group would allow the labeling of gp120 disulfides/cysteines and this covalent attachment could easily be visualized by in-gel fluorescence scanning by using a rhodamine group for the reporter tag. Benjamin Cravatt displayed the utility of the ABPP approach in verifying target identification in several structurally diverse proteins [115].

5.3.2 Further identify HIV-1 Env Cysteine mutations involved in PTT lytic mechanism

The findings of PTT-induced disulfide exchange were intriguing, however there are still facets of the cascade process that are unknown. We still do not know the exact path of disulfide exchange. Further we do not know if PTT-induced virolysis yields a single disulfide exchange reaction or multiple reactions resulting in a cascade. To address these questions combinatorial disulfide mutagenesis experiments in HIV-1 Env will be useful. Performing p24 release assays with gp120 containing multiple cysteine mutations may help to identify the regions of gp120 responsible for PTT-induced lysis and explain the path of disulfide exchange.

5.3.3 Analyzing 6 helix bundle formation after PTT treatment in comparison to native 6 helix bundle formation after cell-fusion events

Additionally, we found that mutating the gp41 disulfide led to inefficient virolysis, thereby suggesting the role of disulfide exchange in the native cell-fusion process. The discovery of the involvement of the gp41 disulfide in PTT-induced virolysis was striking due to previous findings[70] which displayed MPER exposure after virus-PTT treatment. These results taken together advocate for our current working model of PTT mechanism of action (**Figure 38**). We propose that PTTs trigger disulfide exchange in gp120 , which leads to a conformational change in the HIV envelope that has similar structural properties to that occurring in the virus cell fusion process[70]. Analysis of the native 6-helix bundle formation in comparison to the 6-helix bundle thought to be induced by PTT treatment is necessary to more clearly define the structural mechanisms induced by PTTs.

In particular, the hydrophobic gp41 loop region is of special interest. This region contains a characteristic CXXKXXC amino acid sequence found in the fusogenic proteins of numerous retroviruses[116-118]. In turn, this suggests a conserved mechanistic role of this sequence in the fusion process. Furthermore, the basic amino acid, Lysine 601, centered in the conserved sequence is hypothesized to provide a balance of polarity and hydrophobicity that allows for the proper functioning of the gp41 loop during membrane fusion[99]. Previously, gp41 peptides consisting of K601 mutations, have shown the importance of a basic residue, such as Lys or Arg in the gp41 loop, for efficient six-helix bundle formation and entry[99]. However, alanine mapping mutagenesis of the CXXKXXC gp41 loop region in virus has yet to be analyzed. Subsequent Env treatment with PTT will be a useful study to understand the virus-cell fusion process in the context the PTT mechanism.

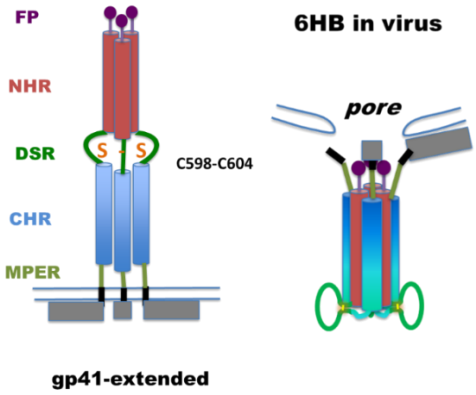

Figure 38. Working Model of Peptide Triazole Thiol Virolytic Mechanism of Action. PTTs hijack the fusion mechanism of the HIV entry process. PTT binding to Env initiates disulfide disruption in gp120, causing similar conformational arrangements that occur upon the virus fusion process. Gp41 fusion peptide is stabilized by C598-C604, which protrudes and ruptures the viral membrane, therefore causing HIV to release its cellular contents. Gp41 NHR (red), gp41 CHR (blue), viral membrane (grey), six-helix bundle (blue/red cylinder), disulfide region-DSR (dark green), MPER (lime green). Image from Andrew Holmes.

Bibliography

(1) Weiss, R. A. *Clinical and Experimental Immunology* **2008**, *152*, 201.

(2) Weiss, R. A. *Science* **1993**, *260*, 1273.

(3) Blattner, W.; Gallo, R. C.; Temin, H. M. *Science* **1988**, *241*, 515+.

(4) Quashie, P. K.; Mesplede, T.; Wainberg, M. A. *Current infectious disease reports* **2013**, *15*, 85.

(5) Lieberman-Blum, S. S.; Fung, H. B.; Bandres, J. C. *Clinical therapeutics* **2008**, *30*, 1228.

(6) Adefolaju, G. A.; Theron, K. E.; Hosie, M. J. *Biomedicine & pharmacotherapy = Biomedecine & pharmacotherapie* **2013**.

(7) Suvada, J. *Neuro endocrinology letters* **2013**, *34*, 5.

(8) Barouch, D. H. *Nature* **2008**, *455*, 613.

(9) Barouch, D. H.; Korber, B. *Annu Rev Med* **2010**, *61*, 153.

(10) Frankel, A. D.; Young, J. A. T. *Annual Review of Biochemistry* **1998**, *67*, 1.

(11) Borradale, D. *Australian Science* **2013**, *24*.

(12) Wilen, C. B.; Tilton, J. C.; Doms, R. W. *Cold Spring Harbor Perspectives in Medicine* **2012**, *2*.

(13) Wilen, C.; Tilton, J.; Doms, R. In *Viral Molecular Machines*; Rossmann, M. G., Rao, V. B., Eds.; Springer US: 2012; Vol. 726, p 223.

(14) Weiss, C. D.; Levy, J. A.; White, J. M. *Journal of virology* **1990**, *64*, 5674.

(15) Gallo, S. A.; Finnegan, C. M.; Viard, M.; Raviv, Y.; Dimitrov, A.; Rawat, S. S.; Puri, A.; Durell, S.; Blumenthal, R. *Biochimica et biophysica acta* **2003**, *1614*, 36.

(16) Uchil, P. D.; Mothes, W. *Cell*, *137*, 402.

(17) Wyatt, R.; Moore, J.; Accola, M.; Desjardin, E.; Robinson, J.; Sodroski, J. *Journal of virology* **1995**, *69*, 5723.

(18) Liu, J.; Bartesaghi, A.; Borgnia, M. J.; Sapiro, G.; Subramaniam, S. *Nature* **2008**, *455*, 109.

(19) Mao, Y.; Wang, L.; Gu, C.; Herschhorn, A.; Xiang, S.-H.; Haim, H.; Yang, X.; Sodroski, J. *Nature structural & molecular biology* **2012**, *19*, 893.

(20) Frey, G.; Chen, J.; Rits-Volloch, S.; Freeman, M. M.; Zolla-Pazner, S.; Chen, B. *Nature structural & molecular biology* **2010**, *17*, 1486.

(21) Poignard, P.; Saphire, E. O.; Parren, P. W.; Burton, D. R. *Annual Review of Immunology* **2001**, *19*, 253.

(22) Wyatt, R.; Thali, M.; Tilley, S.; Pinter, A.; Posner, M.; Ho, D.; Robinson, J.; Sodroski, J. *Journal of virology* **1992**, *66*, 6997.

(23) Kwong, P. D.; Wyatt, R.; Robinson, J.; Sweet, R. W.; Sodroski, J.; Hendrickson, W. A. *Nature* **1998**, *393*, 648.

(24) Pancera, M.; Majeed, S.; Ban, Y.-E. A.; Chen, L.; Huang, C.-c.; Kong, L.; Kwon, Y. D.; Stuckey, J.; Zhou, T.; Robinson, J. E.; Schief, W. R.; Sodroski, J.; Wyatt, R.; Kwong, P. D. *Proceedings of the National Academy of Sciences of the United States of America* **2010**, *107*, 1166.

(25) Kwong, P.; Wyatt, R.; Robinson, J.; Sweet, R.; Sodroski, J.; Hendrickson, W. *Nature* **1998**, *393*, 648

(26) Finzi, A.; Xiang, S.-H.; Pacheco, B.; Wang, L.; Haight, J.; Kassa, A.; Danek, B.; Pancera, M.; Kwong, P. D.; Sodroski, J. *Molecular cell* **2010**, *37*, 656.

(27) Xiang, S.-H.; Finzi, A.; Pacheco, B.; Alexander, K.; Yuan, W.; Rizzuto, C.; Huang, C.-C.; Kwong, P. D.; Sodroski, J. *Journal of virology* **2010**, *84*, 3147.

(28) Lyumkis, D.; Julien, J.-P.; de Val, N.; Cupo, A.; Potter, C. S.; Klasse, P. J.; Burton, D. R.; Sanders, R. W.; Moore, J. P.; Carragher, B.; Wilson, I. A.; Ward, A. B. *Science (New York, N.Y.)* **2013**, *342*, 1484.

(29) Mao, Y.; Wang, L.; Gu, C.; Herschhorn, A.; Désormeaux, A.; Finzi, A.; Xiang, S.-H.; Sodroski, J. G. *Proceedings of the National Academy of Sciences of the United States of America* **2013**, *110*, 12438.

(30) Kumar, R.; Tuen, M.; Liu, J.; Nàdas, A.; Pan, R.; Kong, X.; Hioe, C. E. *Vaccine* **2013**, *31*, 10.1016/j.vaccine.2013.09.010.

(31) Schiffner, T.; Kong, L.; Duncan, C. J. A.; Back, J. W.; Benschop, J. J.; Shen, X.; Huang, P. S.; Stewart-Jones, G. B.; DeStefano, J.; Seaman, M. S.; Tomaras, G. D.; Montefiori, D. C.; Schief, W. R.; Sattentau, Q. J. *Journal of virology* **2013**, *87*, 10163.

(32) Bartlett, J. A.; Fath, M. J.; DeMasi, R.; Hermes, A.; Quinn, J.; Mondou, E.; Rousseau, F. *AIDS* **2006**, *20*, 2051.

(33) Volberding, P. A.; Deeks, S. G. *The Lancet*, *376*, 49.

(34) Jin, Y.; Liu, Z.; Wang, X.; Liu, H.; Ding, G.; Su, Y.; Zhu, L.; Wang, N. *International Journal of STD & AIDS* **2014**, *25*, 771.

(35) Bastian, A. R. Doctorate, Drexel University, 2014.

(36) Tilton, J. C.; Doms, R. W. *Antiviral Research* **2010**, *85*, 91.

(37) Berkhout, B.; Eggink, D.; Sanders, R. W. *Current opinion in virology* **2012**, *2*, 50.

(38) Pan, C.; Liu, S.; Jiang, S. *Journal of the Formosan Medical Association*, *109*, 94.

(39) Hawkins, T. *AIDS Patient Care and STDs* **2006**, *20*, 6.

(40) Moore, J. P.; Kuritzkes, D. R. *Current opinion in HIV and AIDS* **2009**, *4*, 118.

(41) Wyatt, R.; Sodroski, J. *Science* **1998**, *280*, 1884.

(42) Daar, E. S.; Li, X. L.; Moudgil, T.; Ho, D. D. *Proceedings of the National Academy of Sciences of the United States of America* **1990**, *87*, 6574.

(43) Schooley, R. T.; Merigan, T. C.; Gaut, P.; Hirsch, M. S.; Holodniy, M.; Flynn, T.; Liu, S.; Byington, R. E.; Henochowicz, S.; Gubish, E.; Spriggs, D.; Kufe, D.; Schindler, J.; Dawson, A.; Thomas, D.; Hanson, D. G.; Letwin, B.; Liu, T.; Gulinello, J.; Kennedy, S.; Fisher, R.; Ho, D. D. *Annals of Internal Medicine* **1990**, *112*, 247.

(44) Madani, N.; Perdigoto, A. L.; Srinivasan, K.; Cox, J. M.; Chruma, J. J.; LaLonde, J.; Head, M.; Smith, A. B.; Sodroski, J. G. *Journal of virology* **2004**, *78*, 3742.

(45) Ho, J.; Moir, S.; Malaspina, A.; Howell, M. L.; Wang, W.; DiPoto, A. C.; O'Shea, M. A.; Roby, G. A.; Kwan, R.; Mican, J. M.; Chun, T.-W.; Fauci, A. S. *Proceedings of the National Academy of Sciences of the United States of America* **2006**, *103*, 19436.

(46) Nettles, R. E.; Schürmann, D.; Zhu, L.; Stonier, M.; Huang, S.-P.; Chang, I.; Chien, C.; Krystal, M.; Wind-Rotolo, M.; Ray, N.; Hanna, G. J.; Bertz, R.; Grasela, D. *Journal of Infectious Diseases* **2012**, *206*, 1002.

(47) Liu, T.; Huang, B.; Zhan, P.; De Clercq, E.; Liu, X. *European Journal of Medicinal Chemistry* **2014**, *86*, 481.

(48) Zhao, Q.; Ma, L.; Jiang, S.; Lu, H.; Liu, S.; He, Y.; Strick, N.; Neamati, N.; Debnath, A. K. *Virology* **2005**, *339*, 213.

(49) Martin, L.; Stricher, F.; Misse, D.; Sironi, F.; Pugniere, M.; Barthe, P.; Prado-Gotor, R.; Freulon, I.; Magne, X.; Roumestand, C.; Menez, A.; Lusso, P.; Veas, F.; Vita, C. *Nat Biotech* **2003**, *21*, 71.

(50) Stricher, F.; Huang, C.-c.; Descours, A.; Duquesnoy, S.; Combes, O.; Decker, J. M.; Kwon, Y. D.; Lusso, P.; Shaw, G. M.; Vita, C.; Kwong, P. D.; Martin, L. *Journal of molecular biology* **2008**, *382*, 510.

(51) Vita, C.; Vizzavona, J.; Drakopoulou, E.; Zinn-Justin, S.; Gilquin, B.; Ménez, A. *Peptide Science* **1998**, *47*, 93.

(52) Krakower, D. S. *Clinical Infectious Diseases* **2015**.

(53) Das, K.; Arnold, E. *Current opinion in virology* **2013**, *3*, 111.

(54) Schreiber, C. A.; Meyn, L. A.; Creinin, M. D.; Barnhart, K. T.; Hillier, S. L. *Obstetrics and gynecology* **2006**, *107*, 136.

(55) Burke, A. E.; Barnhart, K.; Jensen, J. T.; Creinin, M. D.; Walsh, T. L.; Wan, L. S.; Westhoff, C.; Thomas, M.; Archer, D.; Wu, H.; Liu, J.; Schlaff, W.; Carr, B. R.; Blithe, D. *Obstetrics and Gynecology* **2010**, *116*, 1265.

(56) Vandebosch, A.; Goetghebeur, E.; Ramjee, G.; Alary, M.; Ettiegne-Traore, V.; Chandeying, V.; Van Damme, L. *Sexually Transmitted Infections* **2004**, *80*, 241.

(57) Van Damme, L.; Govinden, R.; Mirembe, F. M.; Guédou, F.; Solomon, S.; Becker, M. L.; Pradeep, B. S.; Krishnan, A. K.; Alary, M.; Pande, B.; Ramjee, G.; Deese, J.; Crucitti, T.; Taylor, D. *New England Journal of Medicine* **2008**, *359*, 463.

(58) Karim, S. S. A.; Richardson, B. A.; Ramjee, G.; Hoffman, I. F.; Chirenje, Z. M.; Taha, T.; Kapina, M.; Maslankowski, L.; Coletti, A.; Profy, A.; Moench, T. R.; Piwowar-Manning, E.; Mâsse, B.; Hillier, S. L.; Soto-Torres, L. *AIDS (London, England)* **2011**, *25*, 957.

(59) Rupp, R.; Rosenthal, S. L.; Stanberry, L. R. *International Journal of Nanomedicine* **2007**, *2*, 561.

(60) Abdool Karim, Q.; Abdool Karim, S. S.; Frohlich, J. A.; Grobler, A. C.; Baxter, C.; Mansoor, L. E.; Kharsany, A. B.; Sibeko, S.; Mlisana, K. P.; Omar, Z.; Gengiah, T. N.; Maarschalk, S.; Arulappan, N.; Mlotshwa, M.; Morris, L.; Taylor, D.; Group, C. T. *Science* **2010**, *329*, 1168.

(61) Denton, P. W.; Othieno, F.; Martinez-Torres, F.; Zou, W.; Krisko, J. F.; Fleming, E.; Zein, S.; Powell, D. A.; Wahl, A.; Kwak, Y. T.; Welch, B. D.; Kay, M. S.; Payne, D. A.; Gallay, P.; Appella, E.; Estes, J. D.; Lu, M.; Garcia, J. V. *Journal of virology* **2011**, *85*, 7582.

(62) Skoler-Karpoff, S.; Ramjee, G.; Ahmed, K.; Altini, L.; Plagianos, M. G.; Friedland, B.; Govender, S.; De Kock, A.; Cassim, N.; Palanee, T.; Dozier, G.; Maguire, R.; Lahteenmaki, P. *The Lancet*, *372*, 1977.

(63) Gopi, H. N.; Tirupula, K. C.; Baxter, S.; Ajith, S.; Chaiken, I. M. *ChemMedChem* **2006**, *1*, 54.

(64) Gopi, H.; Cocklin, S.; Pirrone, V.; McFadden, K.; Tuzer, F.; Zentner, I.; Ajith, S.; Baxter, S.; Jawanda, N.; Krebs, F. C.; Chaiken, I. M. *J Mol Recognit* **2009**, *22*, 169.

(65) Gopi, H.; Umashankara, M.; Pirrone, V.; LaLonde, J.; Madani, N.; Tuzer, F.; Baxter, S.; Zentner, I.; Cocklin, S.; Jawanda, N.; Miller, S. R.; Schon, A.; Klein, J. C.; Freire, E.; Krebs, F. C.; Smith, A. B.; Sodroski, J.; Chaiken, I. *Journal of medicinal chemistry* **2008**, *51*, 2638.

(66) Ferrer, M.; Harrison, S. C. *Journal of virology* **1999**, *73*, 5795.

(67) Cocklin, S.; Gopi, H.; Querido, B.; Nimmagadda, M.; Kuriakose, S.; Cicala, C.; Ajith, S.; Baxter, S.; Arthos, J.; Martin-Garcia, J.; Chaiken, I. M. *Journal of virology* **2007**, *81*, 3645.

(68) Biorn, A. C.; Cocklin, S.; Madani, N.; Si, Z.; Ivanovic, T.; Samanen, J.; Van Ryk, D. I.; Pantophlet, R.; Burton, D. R.; Freire, E.; Sodroski, J.; Chaiken, I. M. *Biochemistry* **2004**, *43*, 1928.

(69) McFadden, K.; Fletcher, P.; Rossi, F.; Kantharaju; Umashankara, M.; Pirrone, V.; Rajagopal, S.; Gopi, H.; Krebs, F. C.; Martin-Garcia, J.; Shattock, R. J.; Chaiken, I. *Antimicrob Agents Ch* **2012**, *56*, 1073.

(70) Bastian, A. R.; Contarino, M.; Bailey, L. D.; Aneja, R.; Moreira, D. R.; Freedman, K.; McFadden, K.; Duffy, C.; Emileh, A.; Leslie, G.; Jacobson, J. M.; Hoxie, J. A.; Chaiken, I. *Retrovirology* **2013**, *10*, 153.

(71) Tuzer, F.; Madani, N.; Kamanna, K.; Zentner, I.; LaLonde, J.; Holmes, A.; Upton, E.; Rajagopal, S.; McFadden, K.; Contarino, M.; Sodroski, J.; Chaiken, I. *Proteins* **2013**, *81*, 271.

(72) Umashankara, M.; McFadden, K.; Zentner, I.; Schon, A.; Rajagopal, S.; Tuzer, F.; Kuriakose, S. A.; Contarino, M.; Lalonde, J.; Freire, E.; Chaiken, I. *ChemMedChem* **2010**, *5*, 1871.

(73) Poole, L. B. *Free Radical Biology and Medicine* **2015**, *80*, 148.

(74) Whitesides, R. S. a. G. M. *Thiol- Disulfide Interchange*; John Wiley and Sons: Cambridge. MA, 1993.

(75) Winterbourn, C. C.; Hampton, M. B. *Free Radical Biology and Medicine* **2008**, *45*, 549.

(76) Tarze, A.; Deniaud, A.; Le Bras, M.; Maillier, E.; Molle, D.; Larochette, N.; Zamzami, N.; Jan, G.; Kroemer, G.; Brenner, C. *Oncogene* **2006**, *26*, 2606.

(77) Zala, D.; Hinckelmann, M.-V.; Yu, H.; Lyra da Cunha, Marcel M.; Liot, G.; Cordelières, Fabrice P.; Marco, S.; Saudou, F. *Cell* **2013**, *152*, 479.

(78) Hogg, P. J. *Nat Rev Cancer* **2013**, *13*, 425.

(79) Gluschankof, P.; Mondor, I.; Gelderblom, H. R.; Sattentau, Q. J. *Virology* **1997**, *230*, 125.

(80) Contarino, M.; Bastian, A. R.; Kalyana Sundaram, R. V.; McFadden, K.; Duffy, C.; Gangupomu, V.; Baker, M.; Abrams, C.; Chaiken, I. *Antimicrobial agents and chemotherapy* **2013**, *57*, 4743.

(81) McFadden, K.; Cocklin, S.; Gopi, H.; Baxter, S.; Ajith, S.; Mahmood, N.; Shattock, R.; Chaiken, I. *Proteins: Structure, Function, and Bioinformatics* **2007**, *67*, 617.

(82) Gorny, M. K.; Moore, J. P.; Conley, A. J.; Karwowska, S.; Sodroski, J.; Williams, C.; Burda, S.; Boots, L. J.; Zolla-Pazner, S. *J. Virol.* **1994**, *68*, 8312.

(83) Huskens, D.; Férir, G.; Vermeire, K.; Kehr, J.-C.; Balzarini, J.; Dittmann, E.; Schols, D. *J. Biol. Chem.* **2010**, *285*, 24845.

(84) Morris, G. M.; Huey, R.; Lindstrom, W.; Sanner, M. F.; Belew, R. K.; Goodsell, D. S.; Olson, A. J. *J. Comput. Chem.* **2009**, *30*, 2785.

(85) Chen, L.; Do Kwon, Y.; Zhou, T.; Wu, X.; O'Dell, S.; Cavacini, L.; Hessell, A. J.; Pancera, M.; Tang, M.; Xu, L.; Yang, Z.-Y.; Zhang, M.-Y.; Arthos, J.; Burton, D. R.; Dimitrov, D. S.; Nabel, G. J.; Posner, M. R.; Sodroski, J.; Wyatt, R.; Mascola, J. R.; Kwong, P. D. *Science* **2009**, *326*, 1123.

(86) Aneja, R.; Rashad, A.; Li, H.; Kalyana Sundaram, R. V.; Bailey, L. D.; Duffy, C.; and Chaiken, I. In *Journal of the American Chemical Society* 2014 (in progress).

(87) Ryser, H. J.; Levy, E. M.; Mandel, R.; DiSciullo, G. J. *Proc. Natl. Acad. Sci. U. S. A.* **1994**, *91*, 4559.

(88) Emileh, A.; Tuzer, F.; Yeh, H.; Umashankara, M.; Moreira, D. R.; Lalonde, J. M.; Bewley, C. A.; Abrams, C. F.; Chaiken, I. M. *Biochemistry* **2013**, *52*, 2245.

(89) Yokoyama, M.; Naganawa, S.; Yoshimura, K.; Matsushita, S.; Sato, H. *PloS one* **2012**, *7*, e37530.

(90) Ivanoff, L. A.; Dubay, J. W.; Morris, J. F.; Roberts, S. J.; Gutshall, L.; Sternberg, E. J.; Hunter, E.; Matthews, T. J.; Petteway, S. R. *Virology* **1992**, *187*, 423.

(91) Calarese, D. A.; Scanlan, C. N.; Zwick, M. B.; Deechongkit, S.; Mimura, Y.; Kunert, R.; Zhu, P.; Wormald, M. R.; Stanfield, R. L.; Roux, K. H.; Kelly, J. W.; Rudd, P. M.; Dwek, R. A.; Katinger, H.; Burton, D. R.; Wilson, I. A. *Science* **2003**, *300*, 2065.

(92) Esser, M. T.; Mori, T.; Mondor, I.; Sattentau, Q. J.; Dey, B.; Berger, E. A.; Boyd, M. R.; Lifson, J. D. *Journal of virology* **1999**, *73*, 4360.

(93) Balzarini, J.; Van Laethem, K.; Peumans, W. J.; Van Damme, E. J. M.; Bolmstedt, A.; Gago, F.; Schols, D. *J. Virol.* **2006**, *80*, 8411.

(94) Bastian, A. R.; Kantharaju; McFadden, K.; Duffy, C.; Rajagopal, S.; Contarino, M. R.; Papazoglou, E.; Chaiken, I. *ChemMedChem* **2011**, *6*, 1335.

(95) McDougal, J. S.; Nicholson, J. K.; Cross, G. D.; Cort, S. P.; Kennedy, M. S.; Mawle, A. C. *J. Immunol.* **1986**, *137*, 2937.

(96) Stantchev, T. S.; Paciga, M.; Lankford, C. R.; Schwartzkopff, F.; Broder, C. C.; Clouse, K. A. *Retrovirology* **2012**, *9*.

(97) Clements, G. J.; Price-Jones, M. J.; Stephens, P. E.; Sutton, C.; Schulz, T. F.; Clapham, P. R.; McKeating, J. A.; McClure, M. O.; Thomson, S.; Marsh, M.; et al. *AIDS Res. Hum. Retroviruses* **1991**, *7*, 3.

(98) Cleland, W. W. *Biochemistry* **1964**, *3*, 480.

(99) Qiu, J.; Ashkenazi, A.; Liu, S.; Shai, Y. *J. Biol. Chem.* **2013**, *288*, 29143.

(100) Ashkenazi, A.; Viard, M.; Wexler-Cohen, Y.; Blumenthal, R.; Shai, Y. *FASEB J.* **2011**, *25*, 2156.

(101) Sanders, R. W.; Derking, R.; Cupo, A.; Julien, J.-P.; Yasmeen, A.; de Val, N.; Kim, H. J.; Blattner, C.; de la Peña, A. T.; Korzun, J.; Golabek, M.; de los Reyes, K.; Ketas, T. J.; van Gils, M. J.; King, C. R.; Wilson, I. A.; Ward, A. B.; Klasse, P. J.; Moore, J. P. *PLoS Pathog* **2013**, *9*, e1003618.

(102) Rashad, A. A.; Kalyana Sundaram, R. V.; Aneja, R.; Duffy, C.; Chaiken, I. *J. Med. Chem.* **2015**.

(103) Mulvey, M.; Brown, D. T. *J. Virol.* **1994**, *68*, 805.

(104) Glomb-Reinmund, S.; Kielian, M. *Virology* **1998**, *248*, 372.

(105) Cerutti, N.; Killick, M.; Jugnarain, V.; Papathanasopoulos, M.; Capovilla, A. *J. Biol. Chem.* **2014**, *289*, 10455.

(106) Auwerx, J.; Isacsson, O.; Söderlund, J.; Balzarini, J.; Johansson, M.; Lundberg, M. *Int. J Biochem. Cell. Biol.* **2009**, *41*, 1269.

(107) Reiser, K.; François, K. O.; Schols, D.; Bergman, T.; Jörnvall, H.; Balzarini, J.; Karlsson, A.; Lundberg, M. *Int J. Biochem. Cell Biol* **2012**, *44*, 556.

(108) Holztman, J. L. *Prolyl Hydroxylase, Protein Disulfide Isomerase and Other Structurally Related Proteins*; Taylor & Francis, 1997.

(109) Ryser, H. J.; Mandel, R.; Ghani, F. *Journal of Biological Chemistry* **1991**, *266*, 18439.

(110) Mandel, R.; Ryser, H. J.; Ghani, F.; Wu, M.; Peak, D. *Proc. Natl. Acad. Sci. U. S. A.* **1993**, *90*, 4112.

(111) Markovic, I.; Stantchev, T. S.; Fields, K. H.; Tiffany, L. J.; Tomiç, M.; Weiss, C. D.; Broder, C. C.; Strebel, K.; Clouse, K. A. *Thiol/disulfide exchange is a prerequisite for CXCR4-tropic HIV-1 envelope-mediated T-cell fusion during viral entry*, 2004; Vol. 103.

(112) Wang Z, Z. Z., Guo ZY, Chi CW. *Acta Biochim Biophys Sin (Shanghai).* **2010**, *42*, 358.

(113) van Anken, E.; Sanders, R. W.; Liscaljet, I. M.; Land, A.; Bontjer, I.; Tillemans, S.; Nabatov, A. A.; Paxton, W. A.; Berkhout, B.; Braakman, I. *Mol. Biol. Cell.* **2008**, *19*, 4298.

(114) Cerutti, N.; Mendelow, B. V.; Napier, G. B.; Papathanasopoulos, M. A.; Killick, M.; Khati, M.; Stevens, W.; Capovilla, A. *J. Biol. Chem.* **2010**, *285*, 25743.

(115) Barglow, K. T.; Cravatt, B. F. *Chemistry & Biology*. **2004**, *11*, 1523.

(116) Maerz, A. L.; Center, R. J.; Kemp, B. E.; Kobe, B.; Poumbourios, P. *Journal of virology* **2000**, *74*, 6614.

(117) Li, K.; Zhang, S.; Kronqvist, M.; Wallin, M.; Ekström, M.; Derse, D.; Garoff, H. *J. Virol.* **2008**, *82*, 7135.

(118) Wallin, M.; Ekström, M.; Garoff, H. *EMBO J.* **2004**, *23*, 54.

Appendix

Appendix Figure 1. Peptide 1a Chromatogram

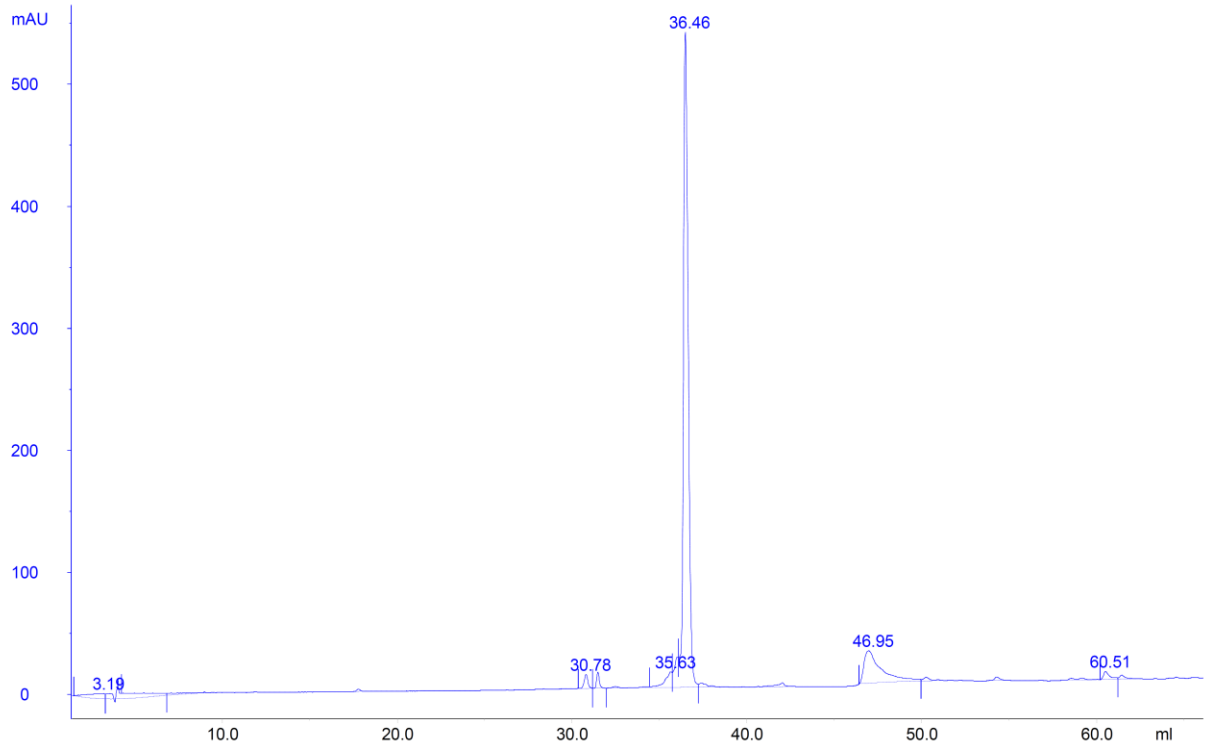

Appendix Figure 2. Peptide 1a Mass Spectrum

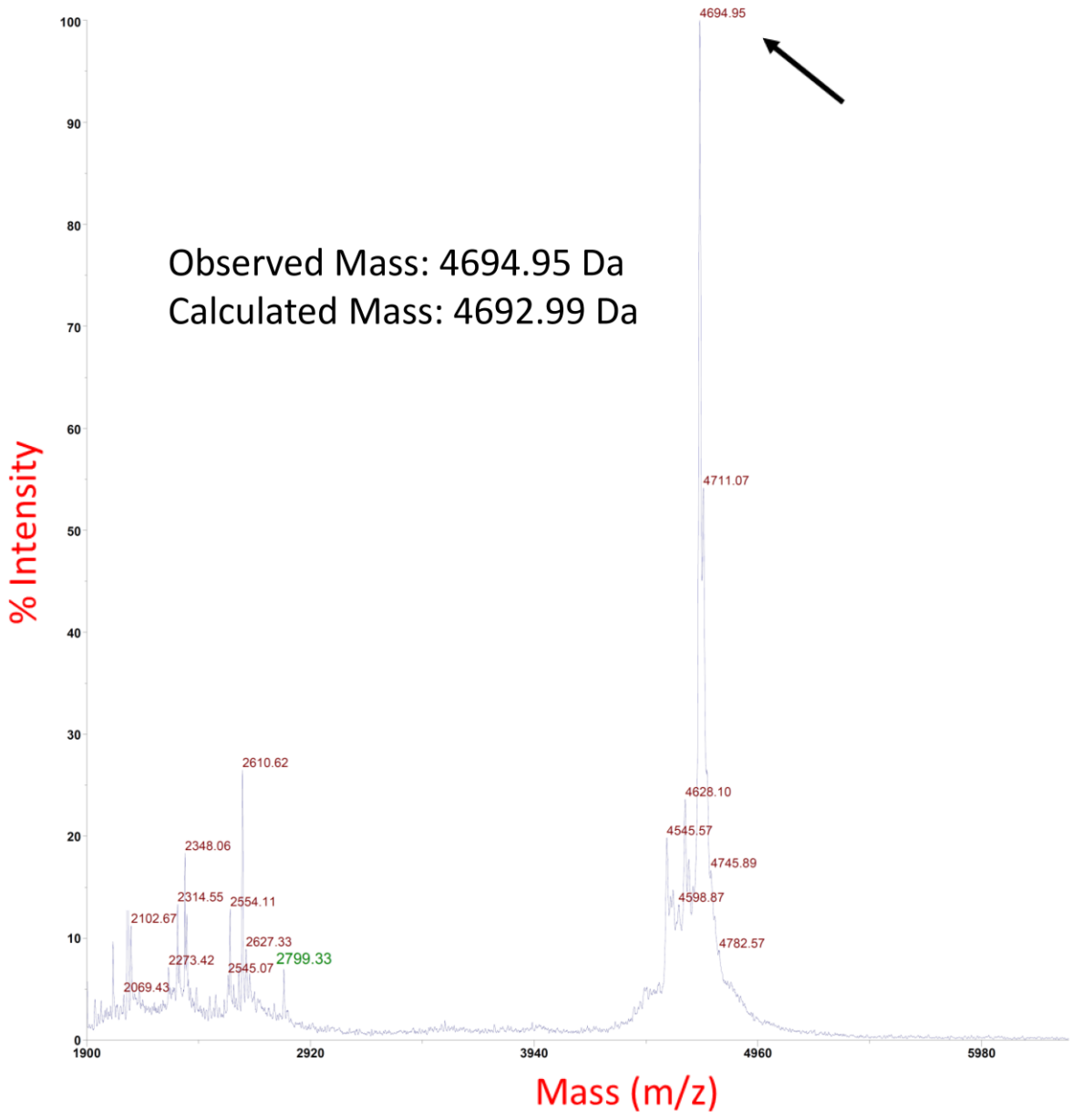

Appendix Figure 3. Peptide 1 Chromatogram

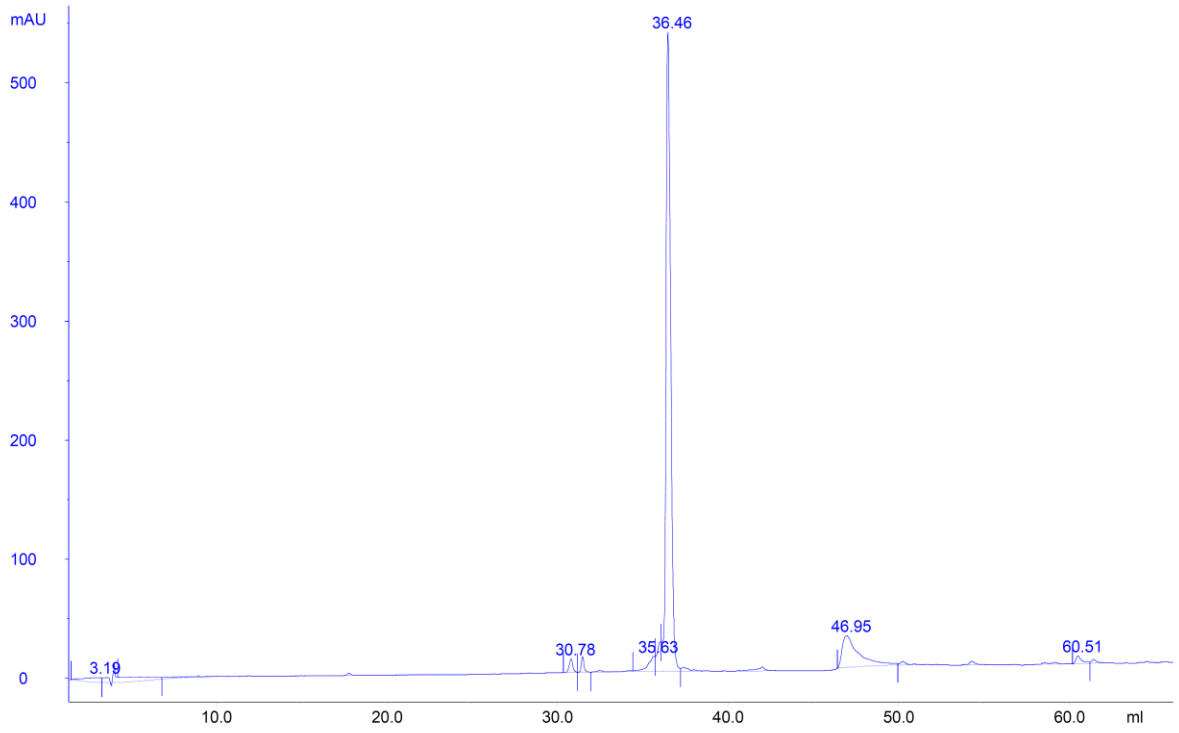

Appendix Figure 4. Peptide 1 Mass Spectrum

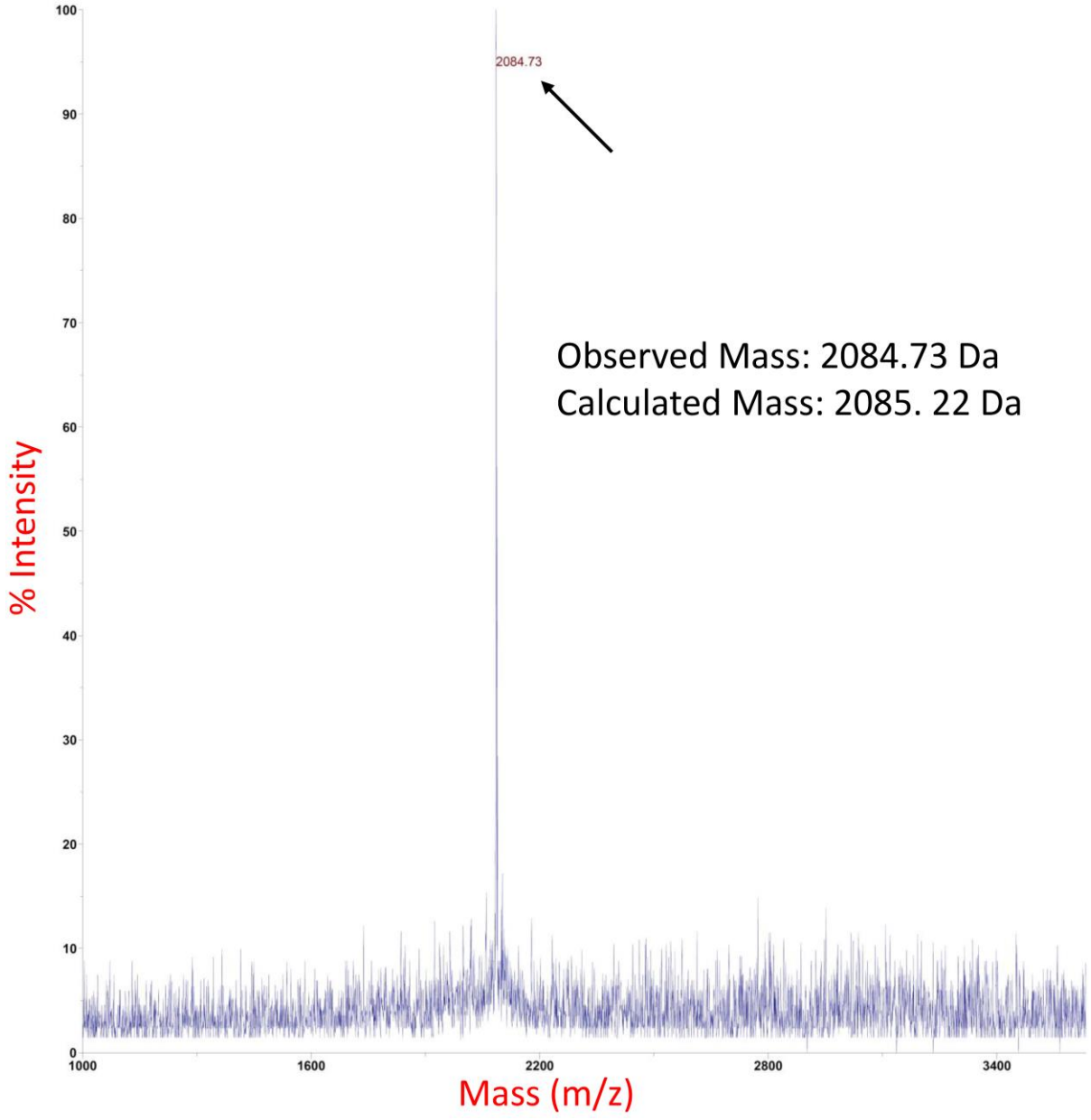

Appendix Figure 5. Peptide 2 Chromatogram

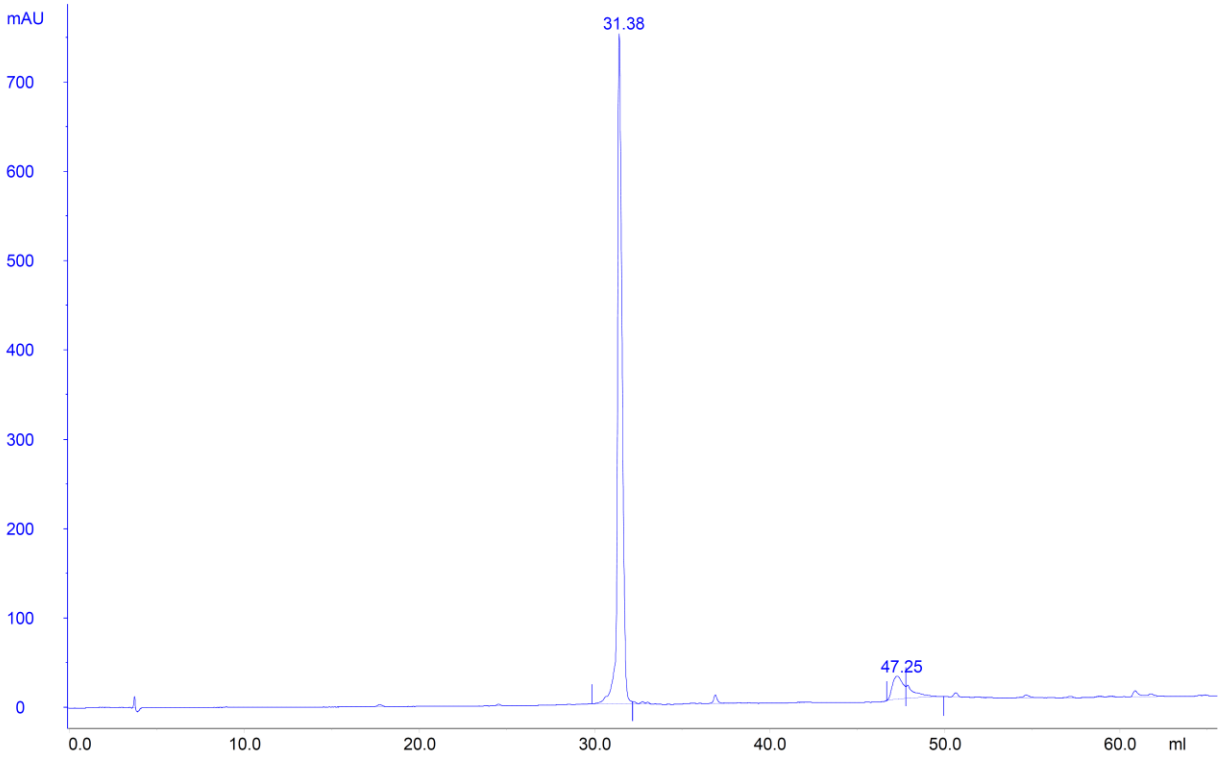

Appendix Figure 6: Peptide 2 Mass Spectrum

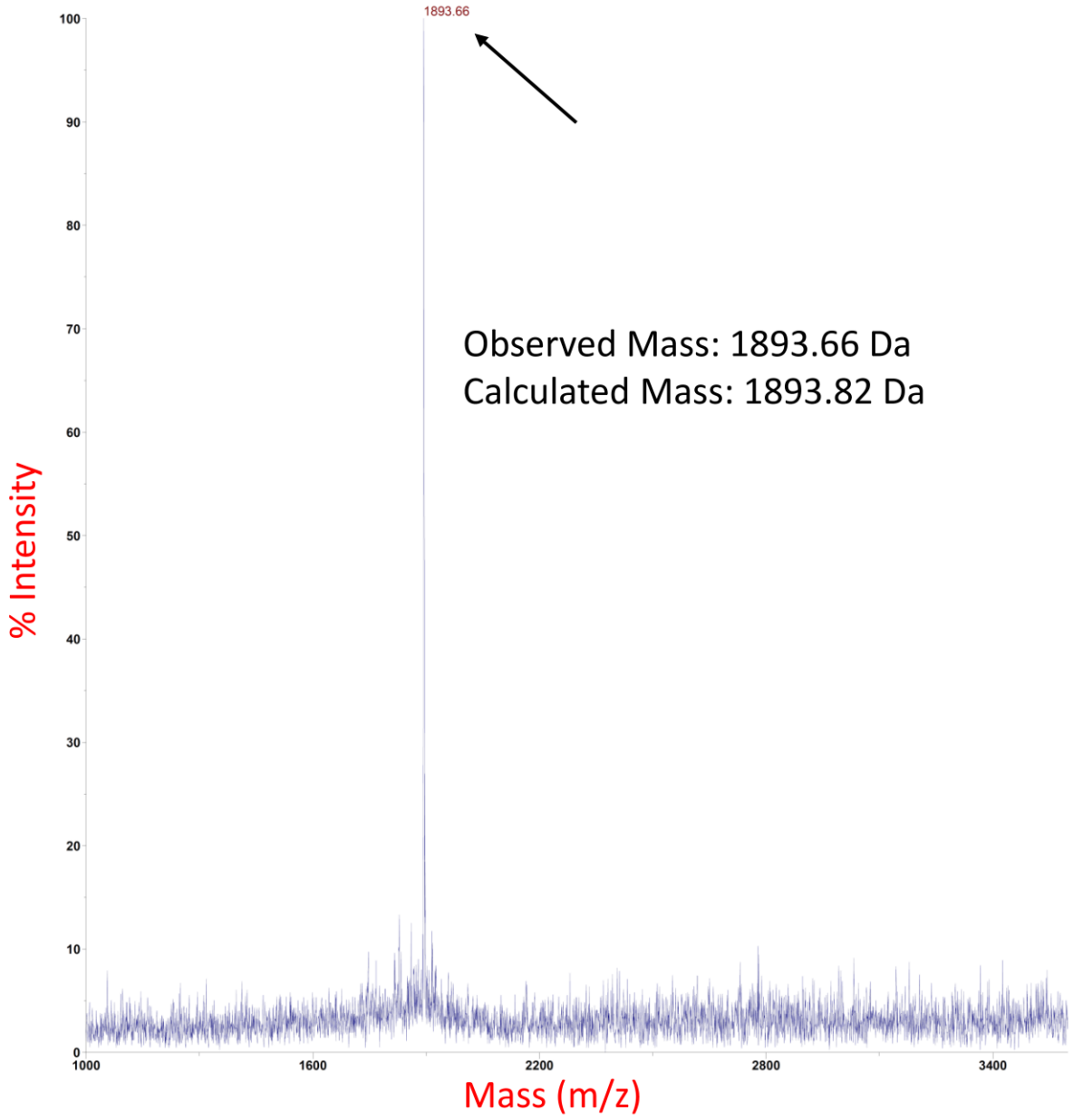

Appendix Figure 7. Peptide 3 Chromatogram

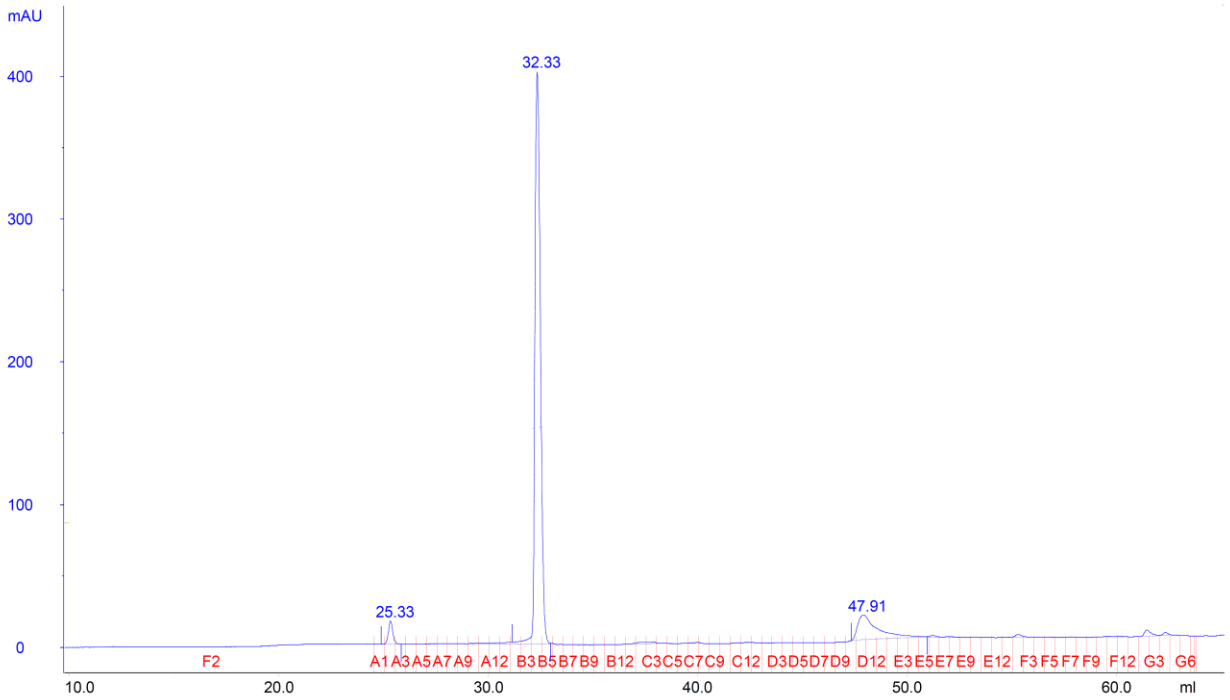

Appendix Figure 8: Peptide 3 Mass Spectrum

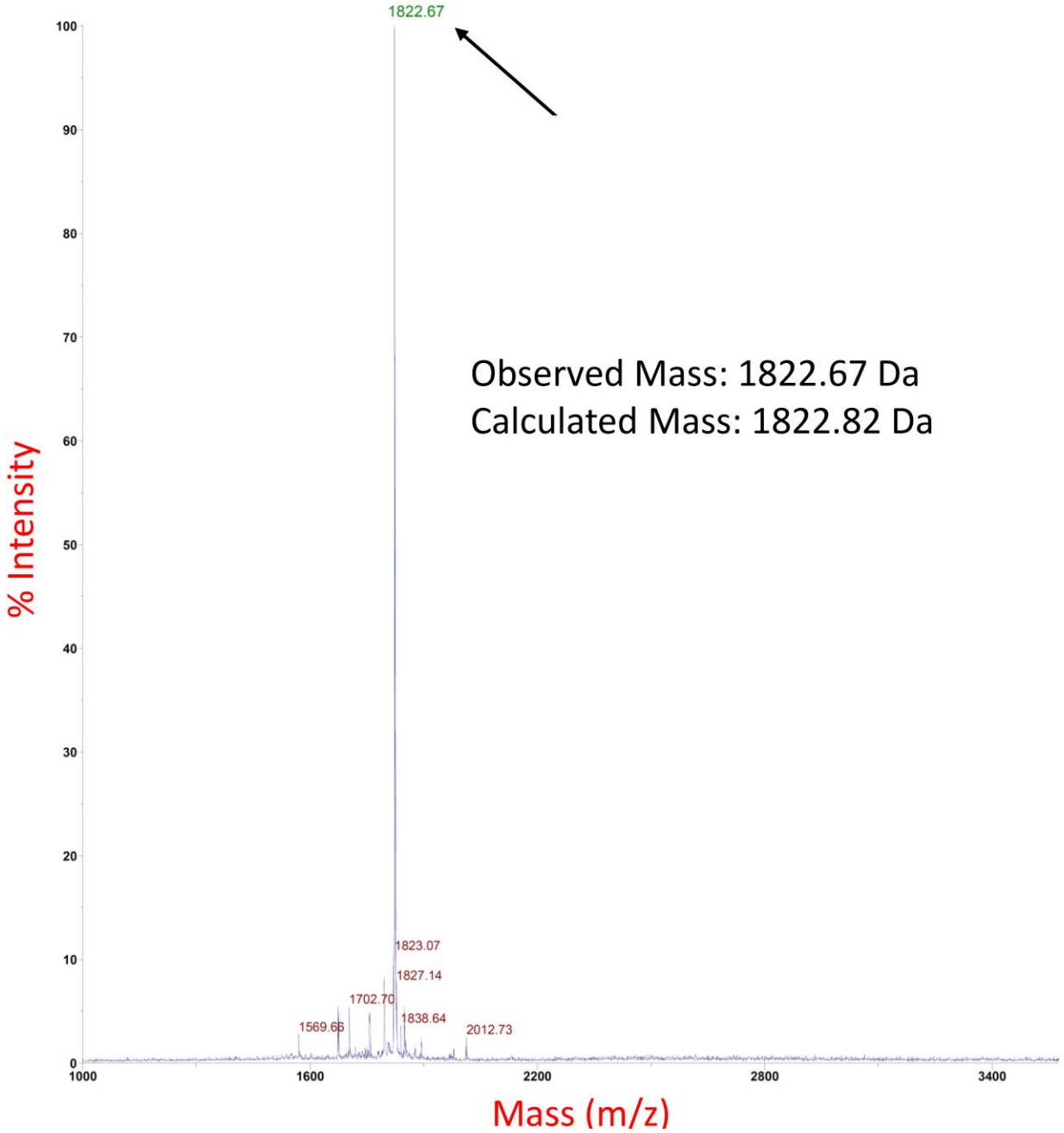

Appendix Figure 9. Peptide 4 Chromatogram

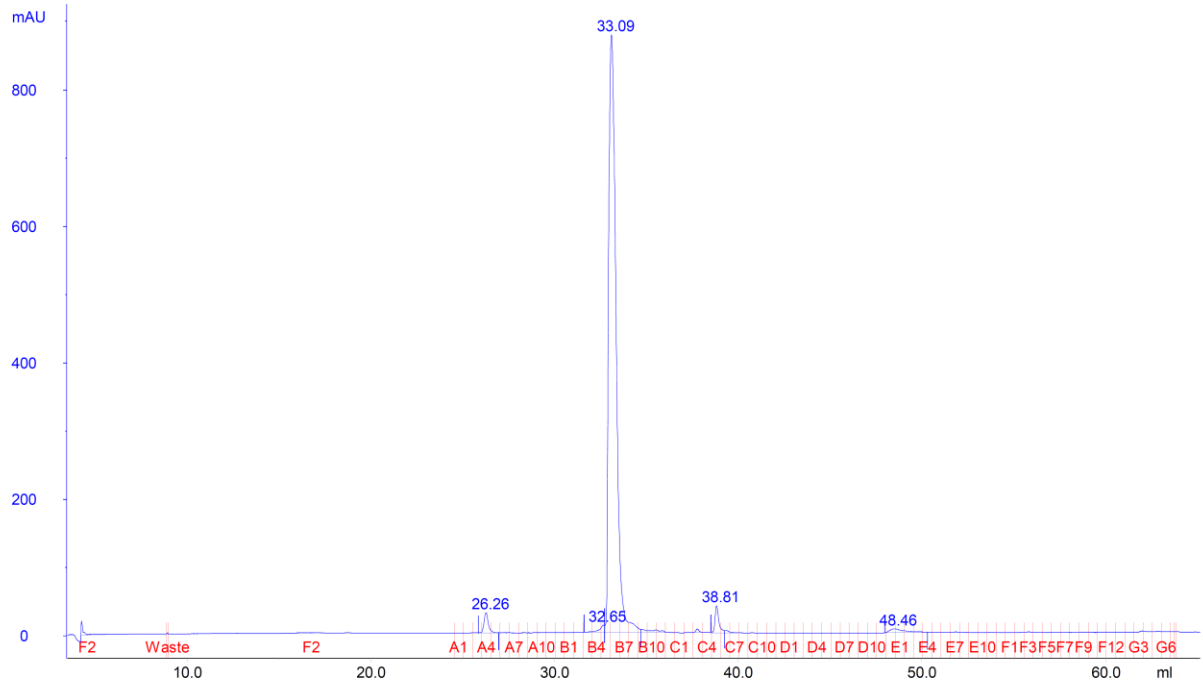

Appendix Figure 10: Peptide 4 Mass Spectrum

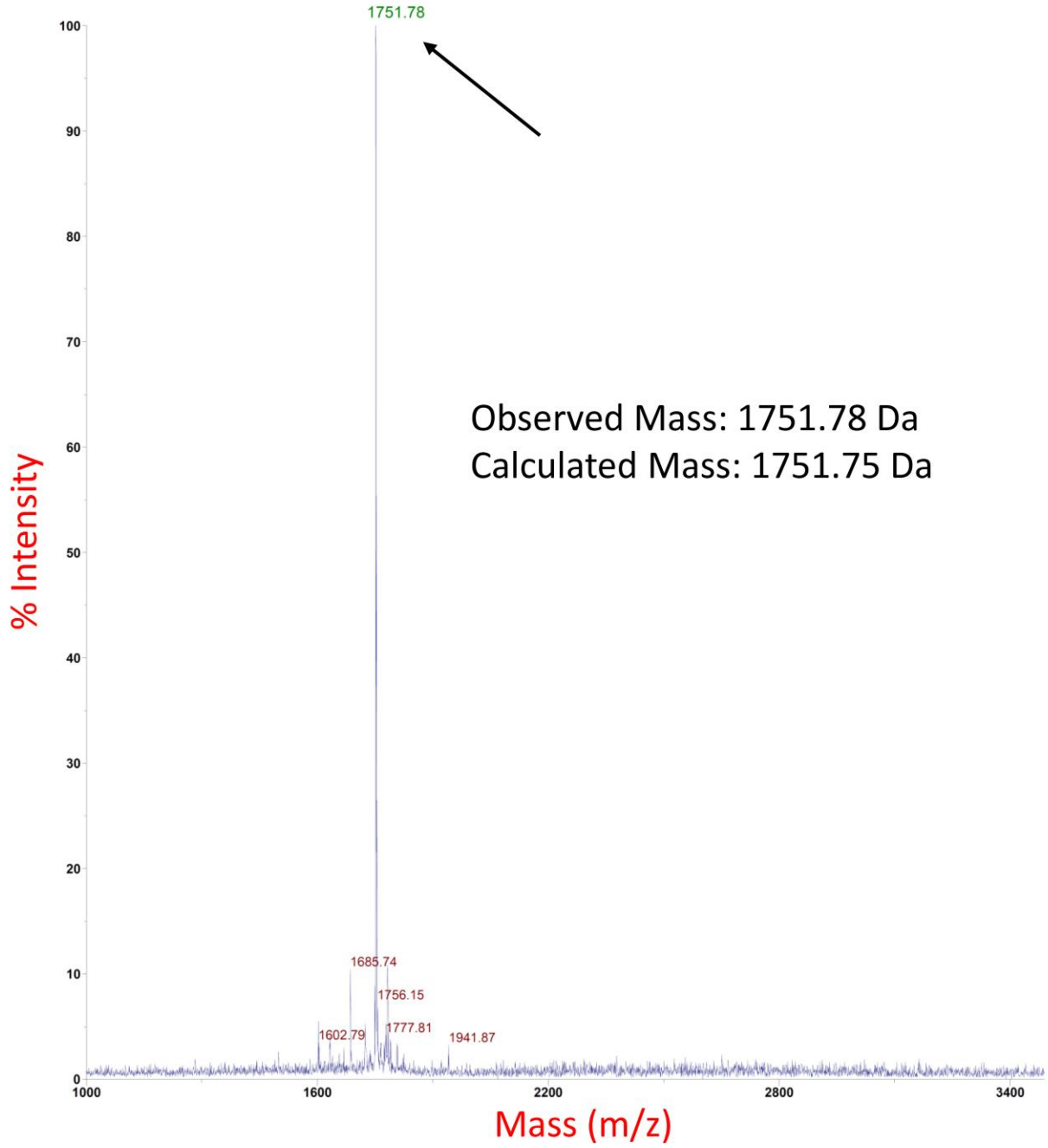

Appendix Figure 11. Peptide 5 Chromatogram

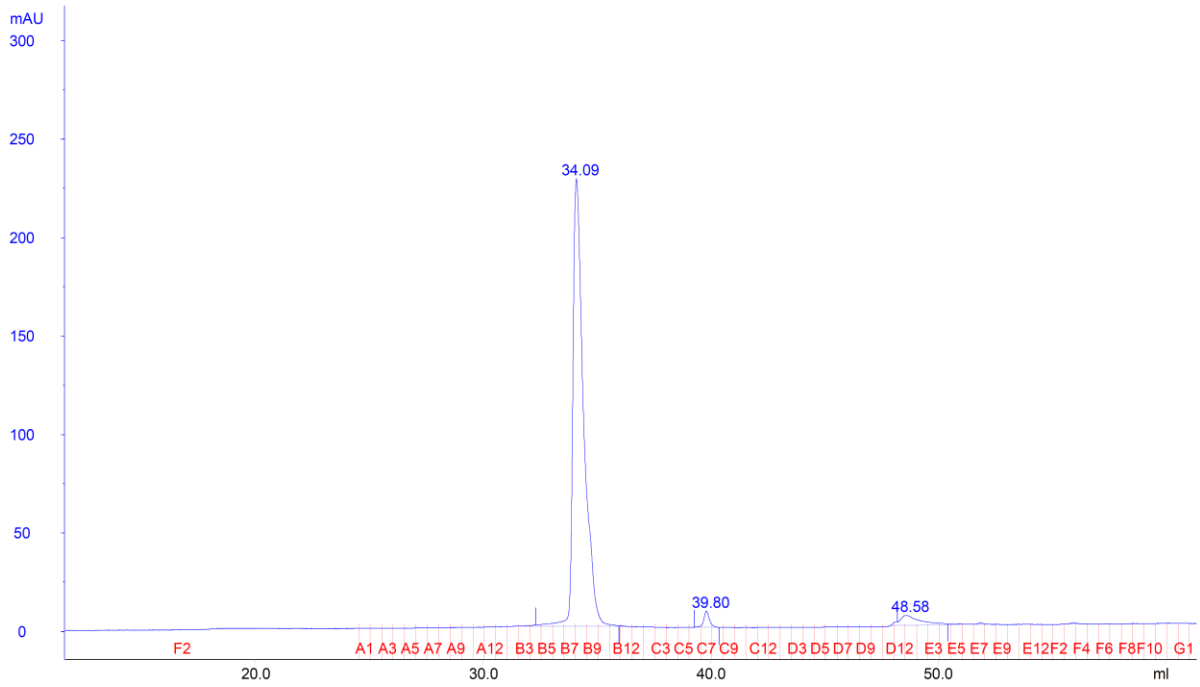

Appendix Figure 12: Peptide 5 Mass Spectrum

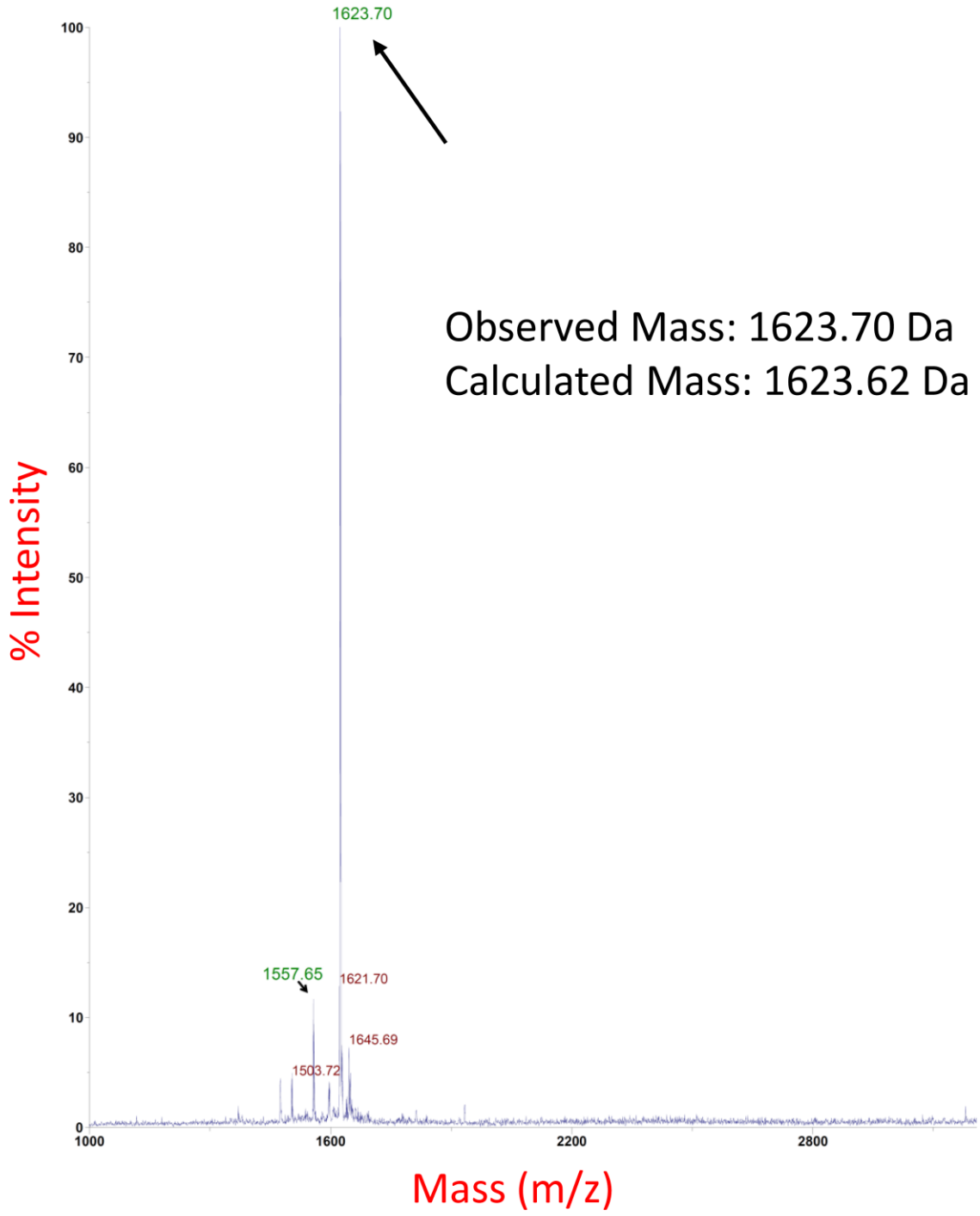

Appendix Figure 13. Peptide 6 Chromatogram

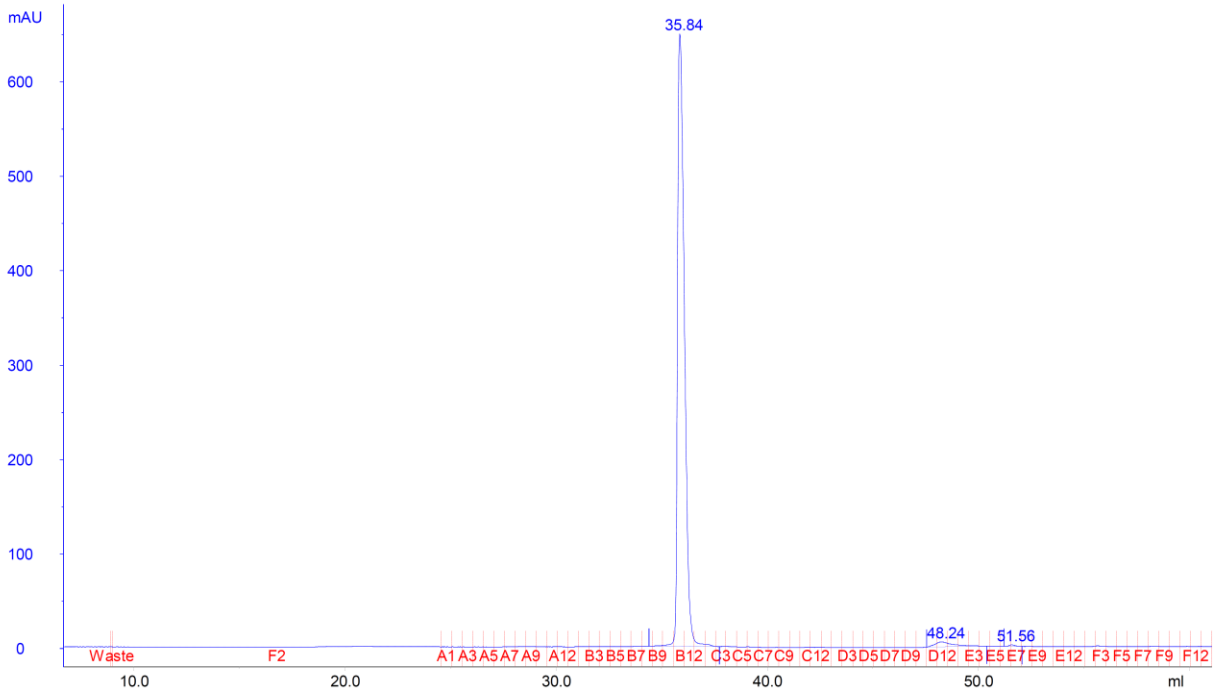

Appendix Figure 14: Peptide 6 Mass Spectrum

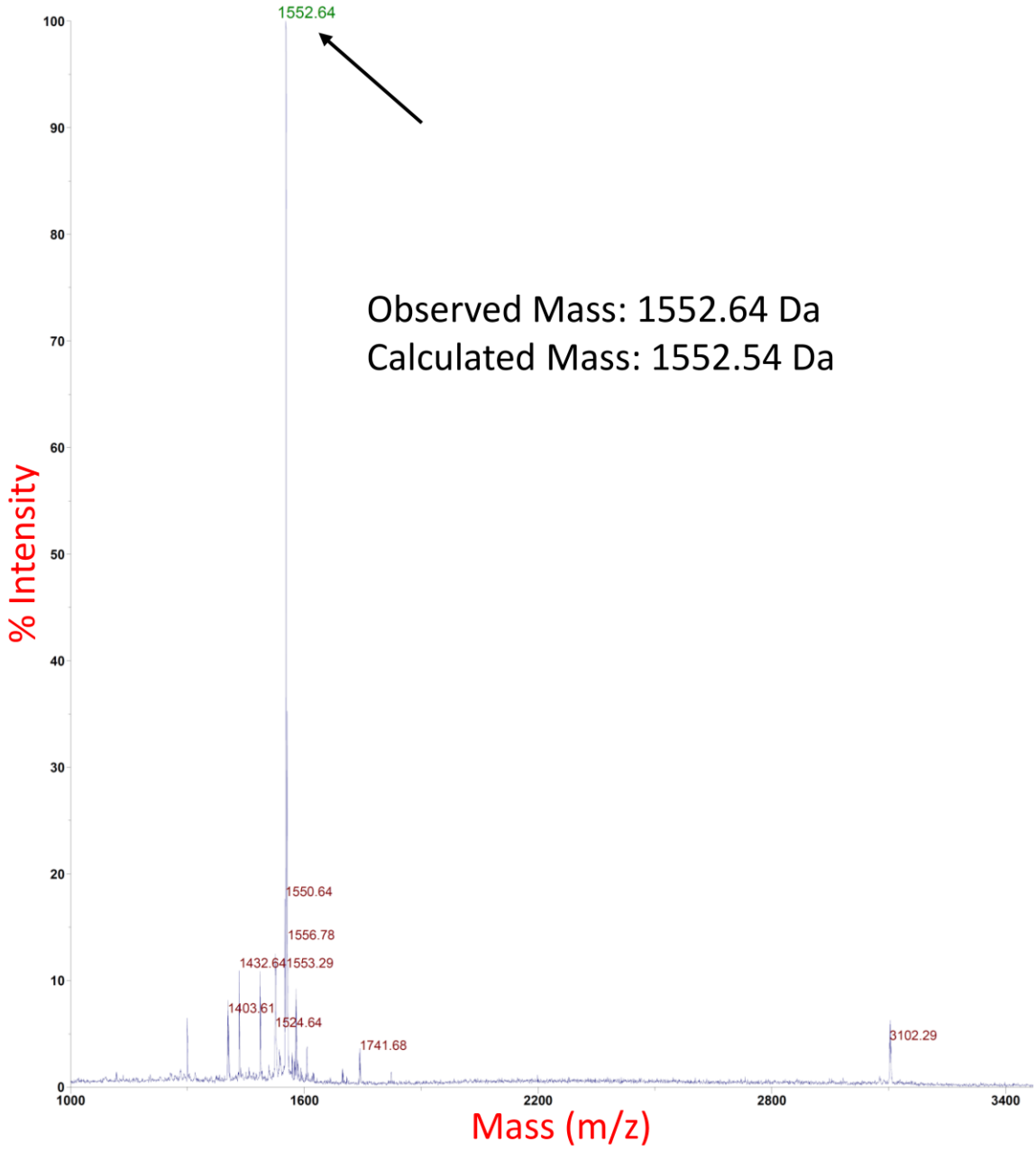

Appendix Figure 15. Peptide 7 Chromatogram

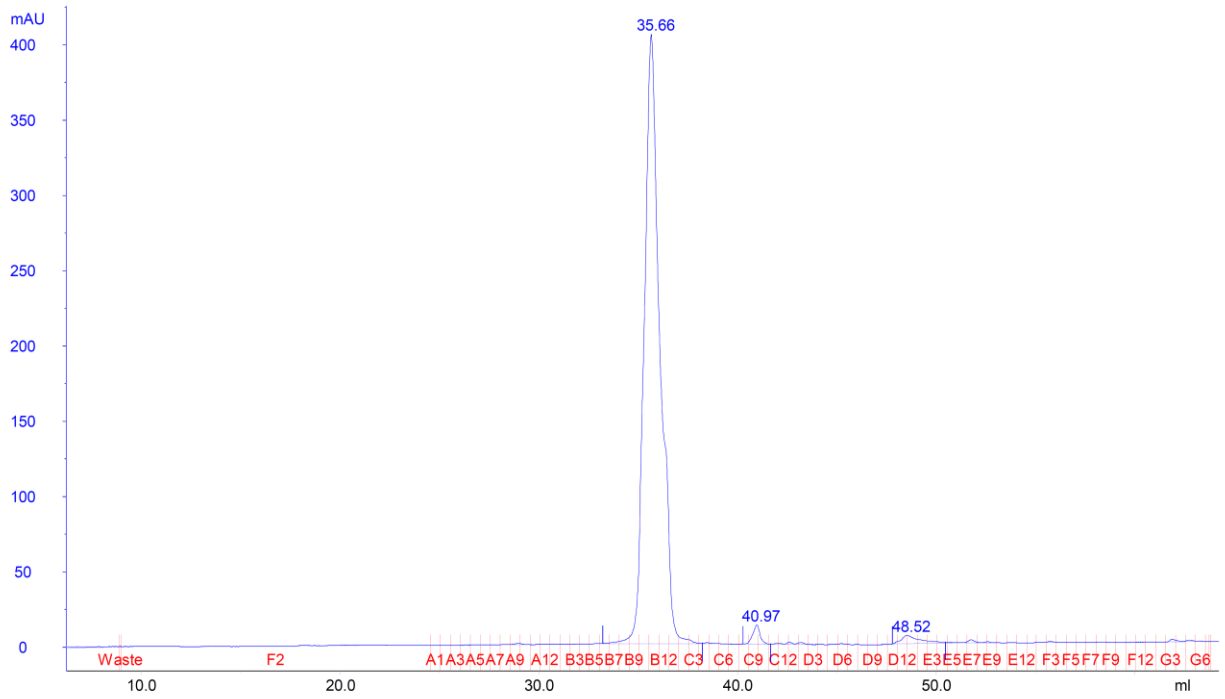

Appendix Figure 16: Peptide 7 Mass Spectrum

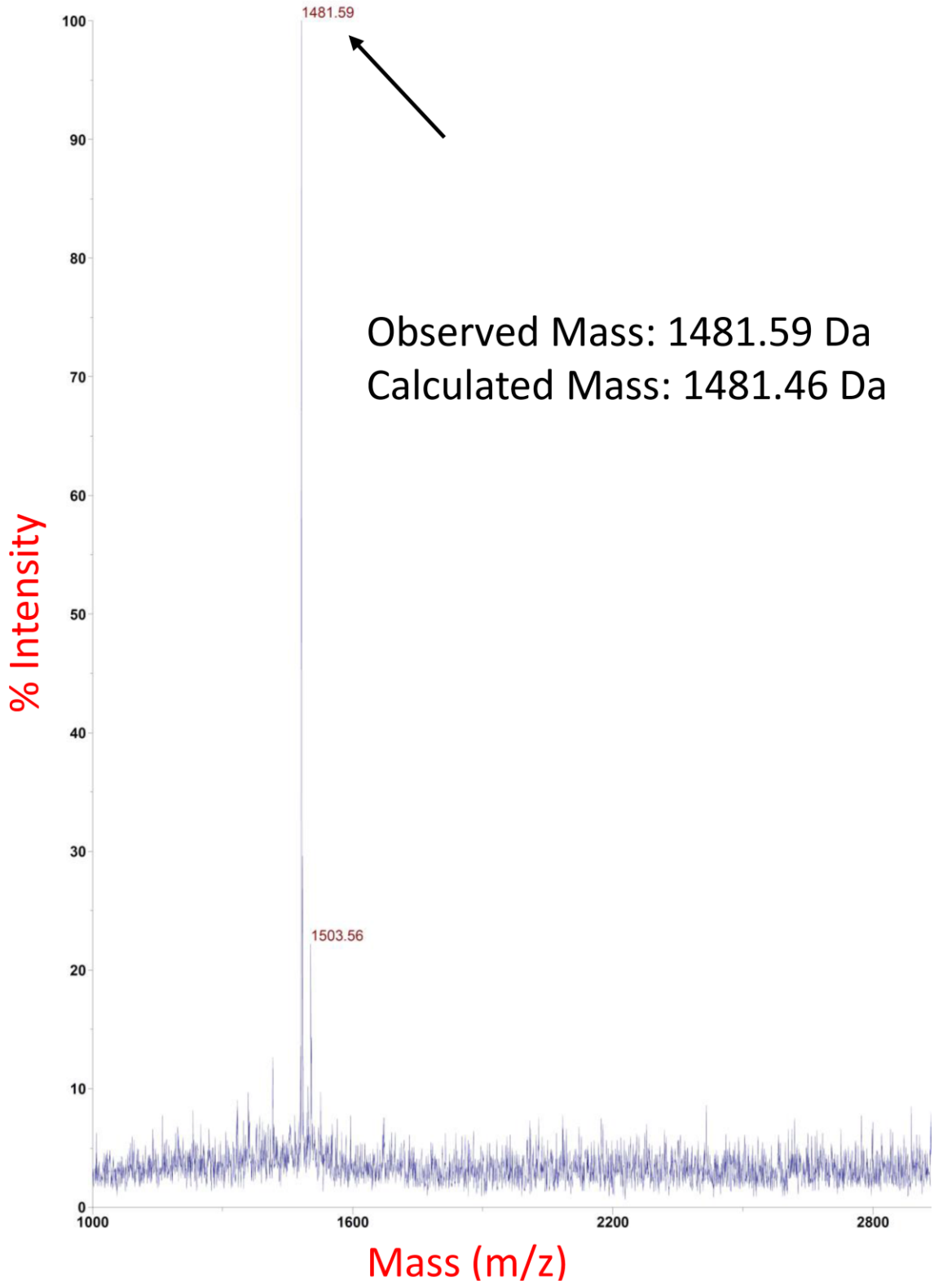

Appendix Figure 17. Peptide 8 Chromatogram

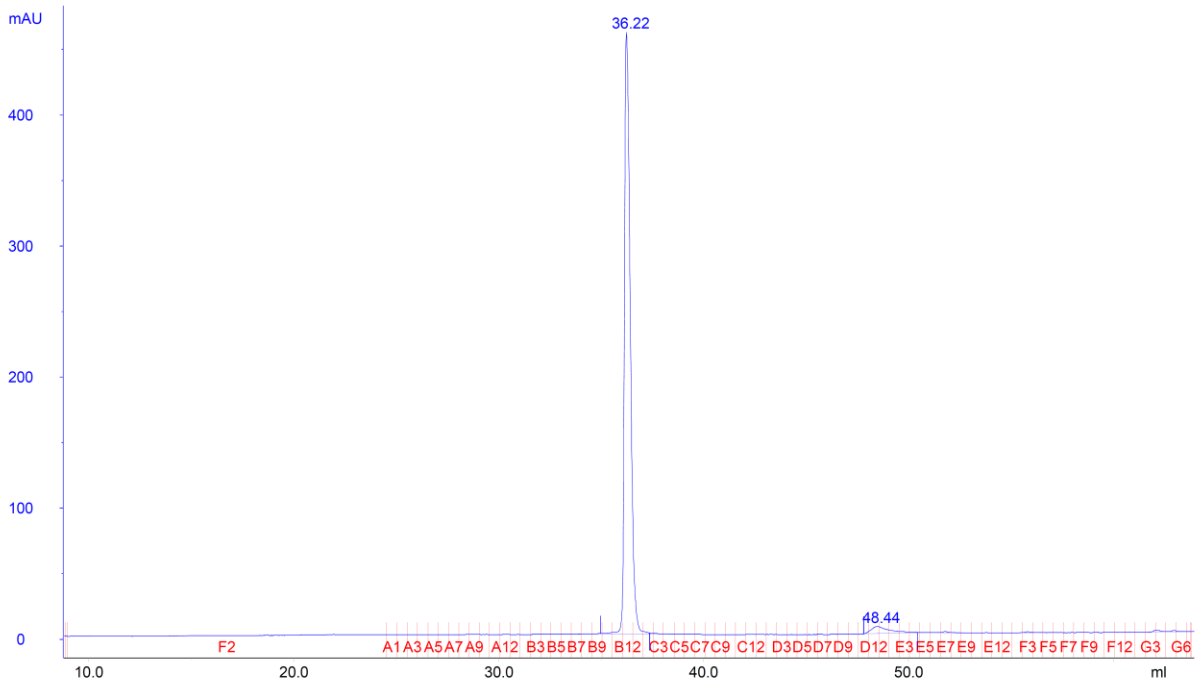

Appendix Figure 18: Peptide 8 Mass Spectrum

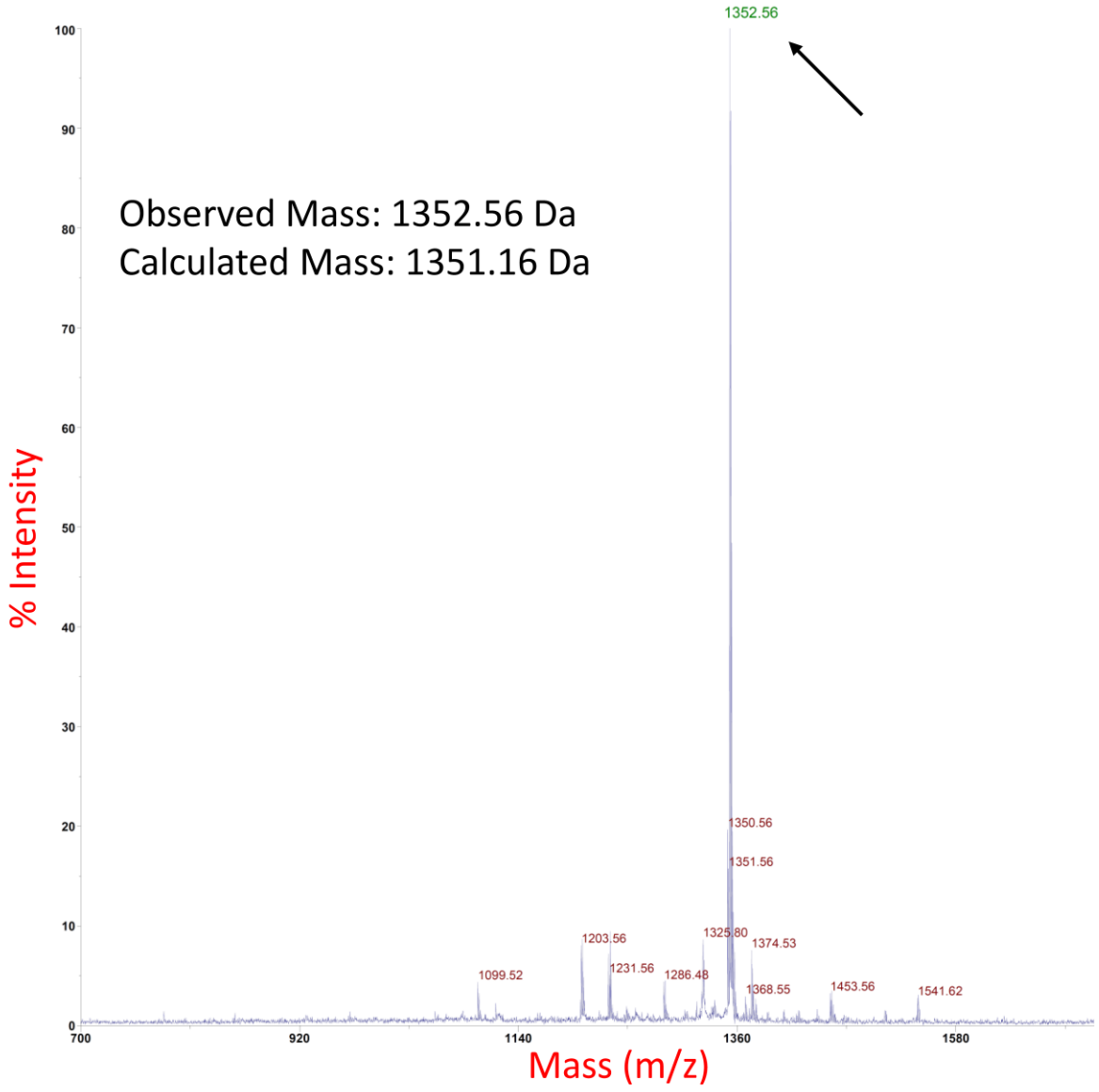

Appendix Figure 19. Peptide 9 Chromatogram

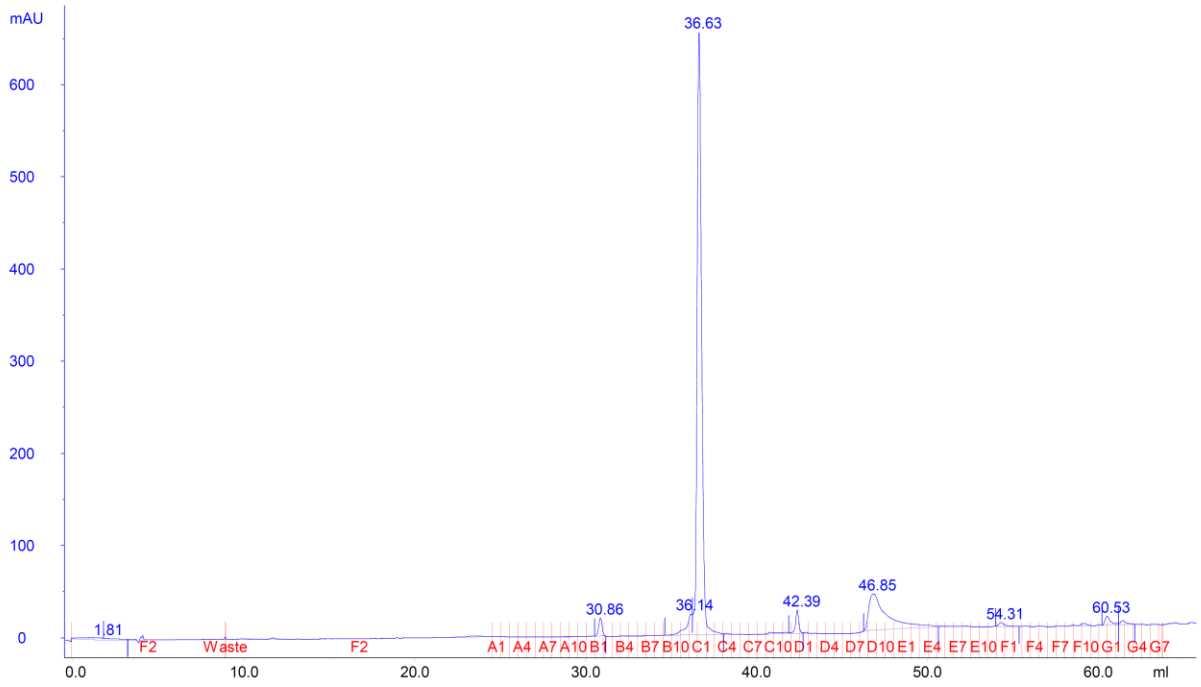

Appendix Figure 20: Peptide 9 Mass Spectrum

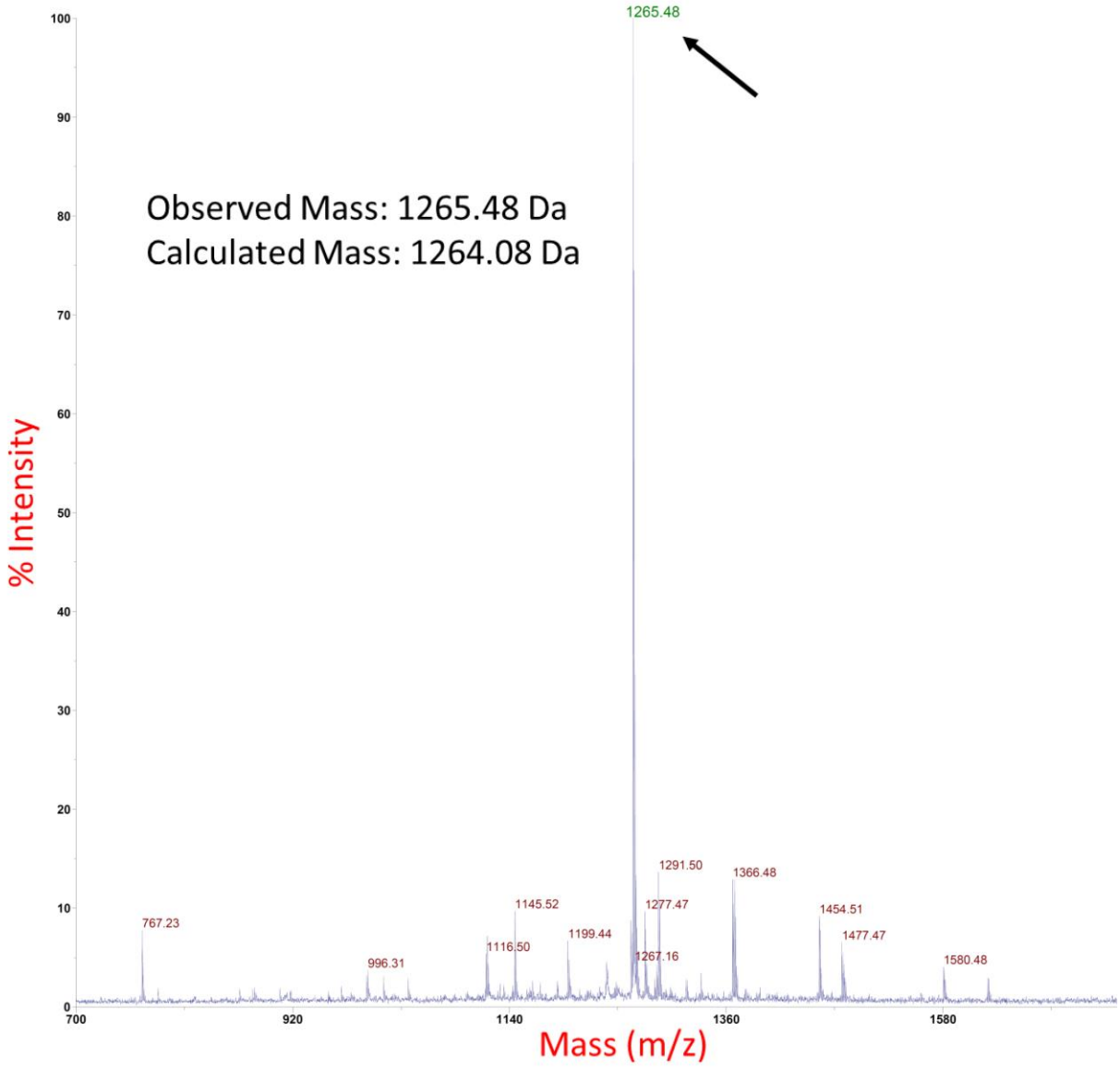

Appendix Figure 21. Peptide 10 Chromatogram

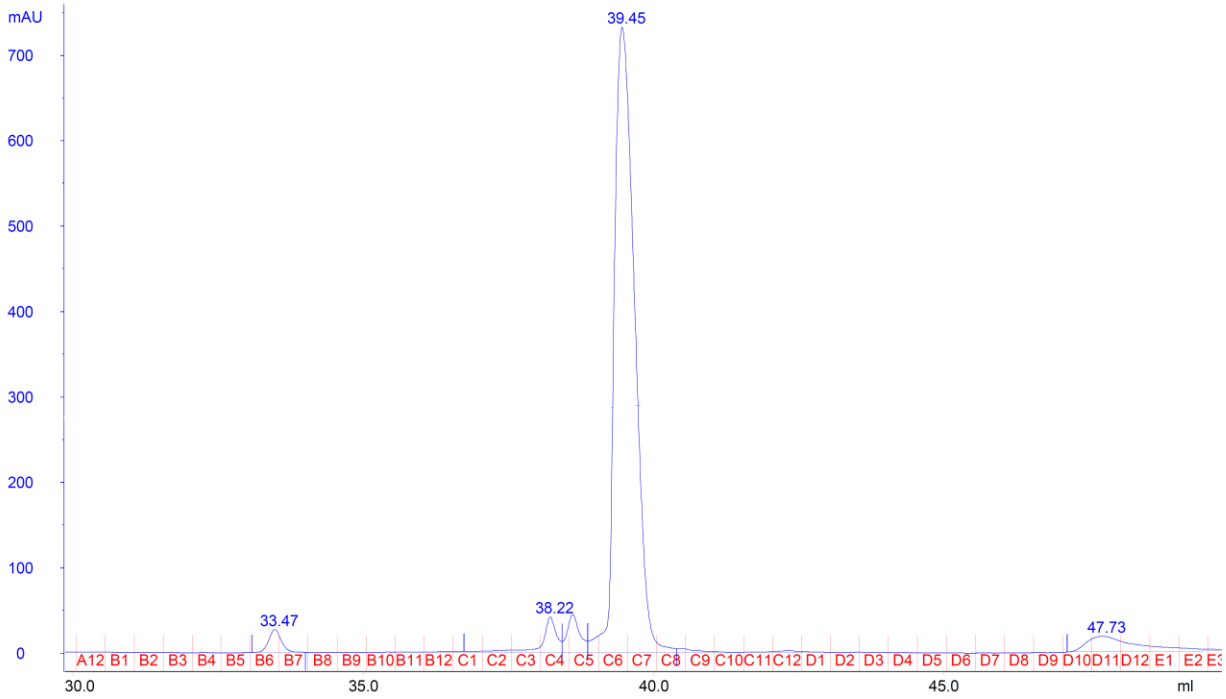

Appendix Figure 22: Peptide 10 Mass Spectrum

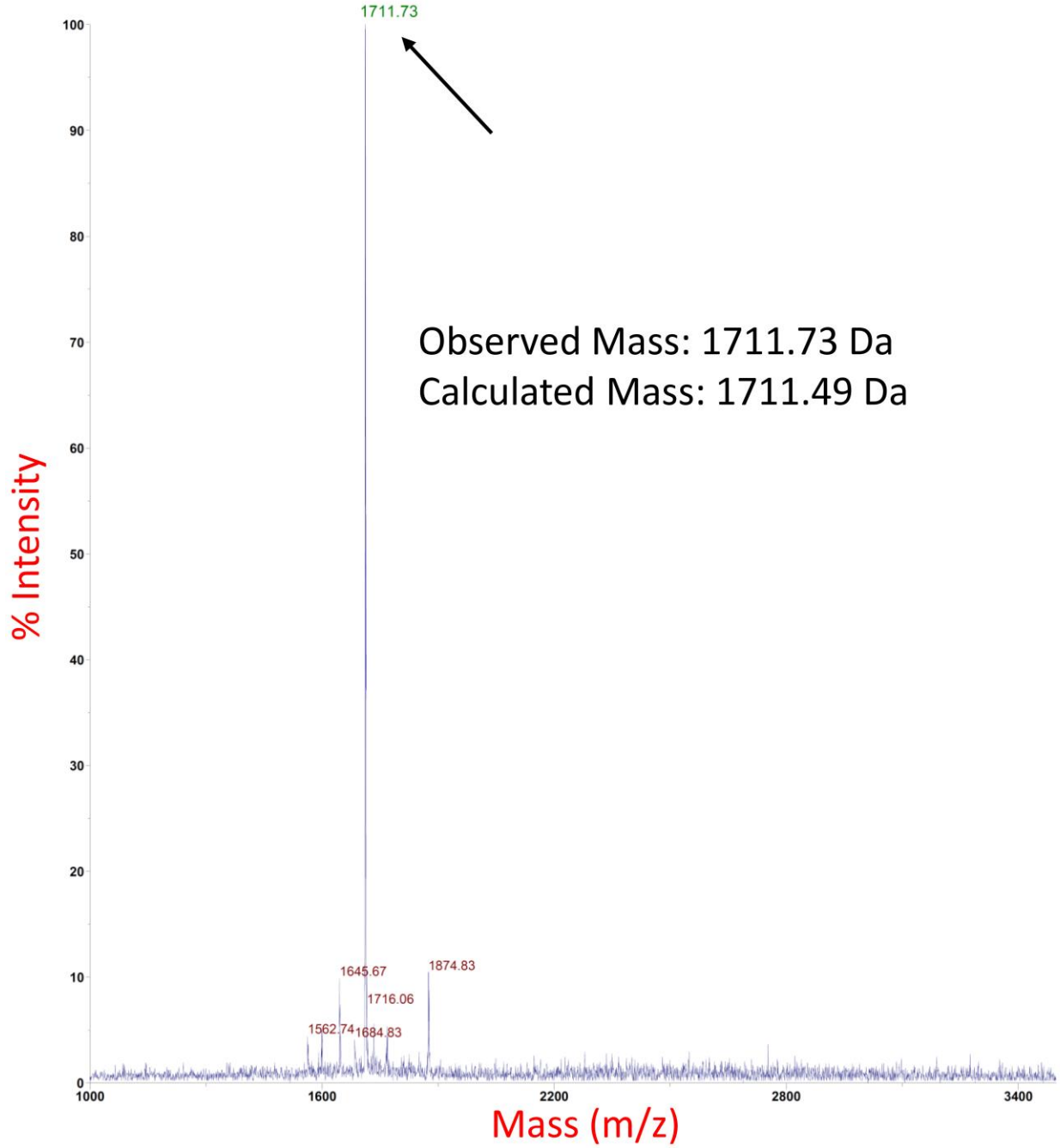

Appendix Figure 23. Peptide 11 Chromatogram

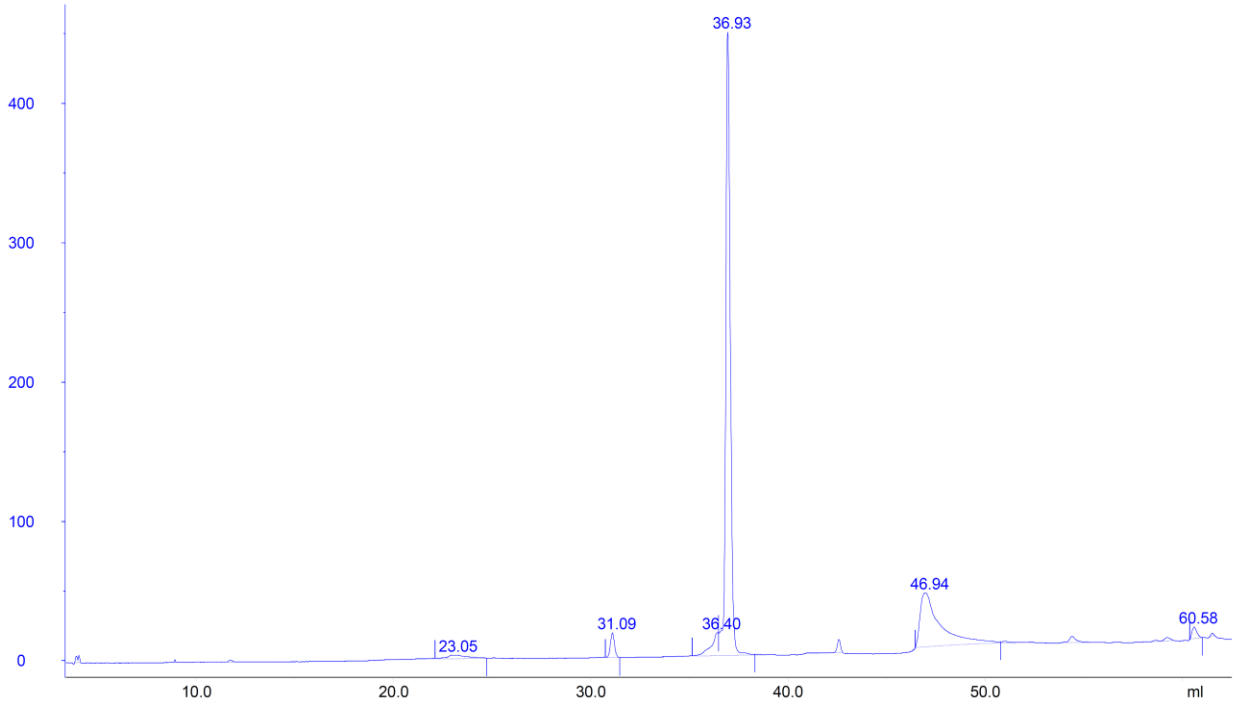

Appendix Figure 24. Peptide 11 Mass Spectrum

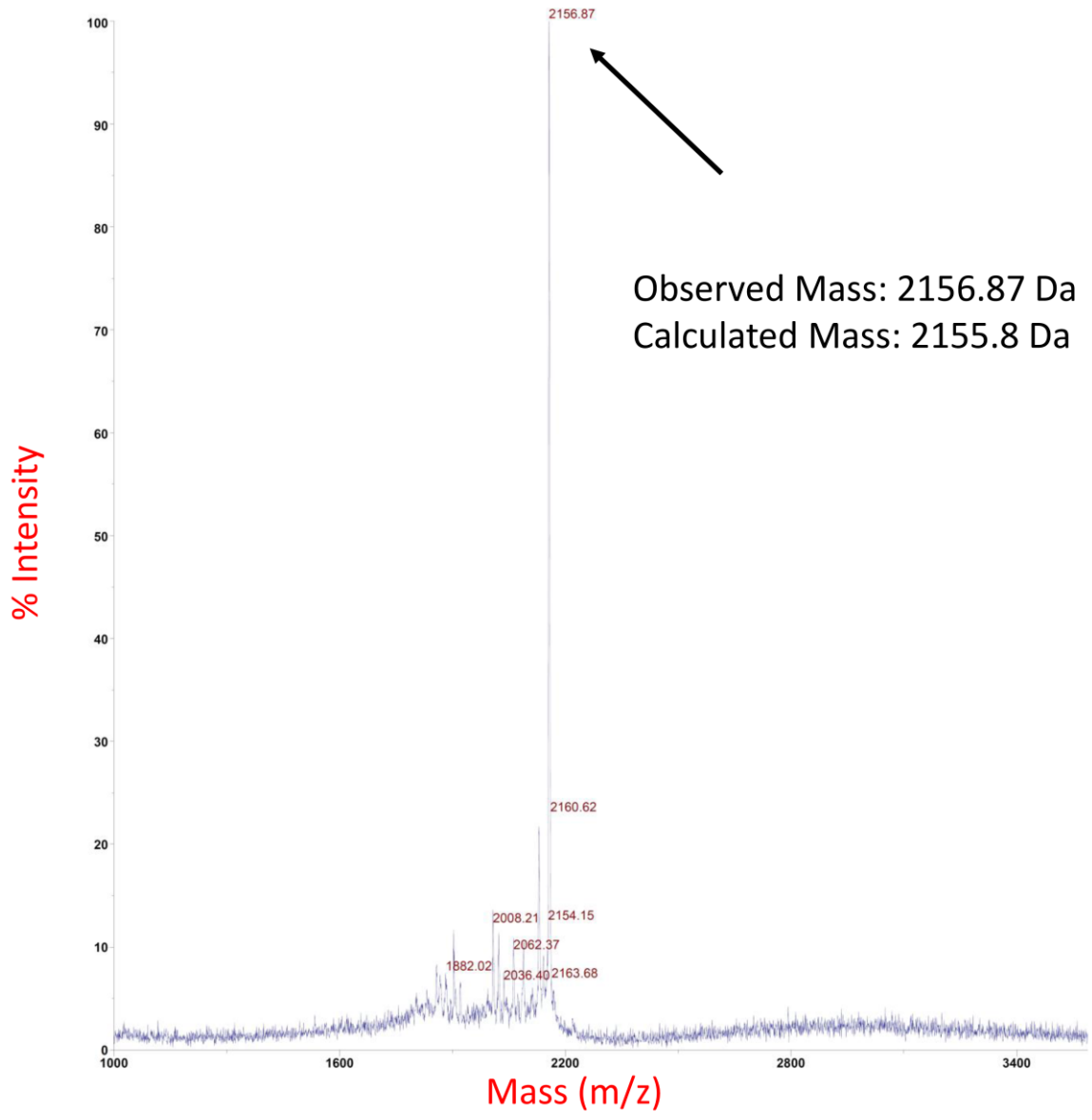

Appendix Figure 25. Peptide 12 Chromatogram

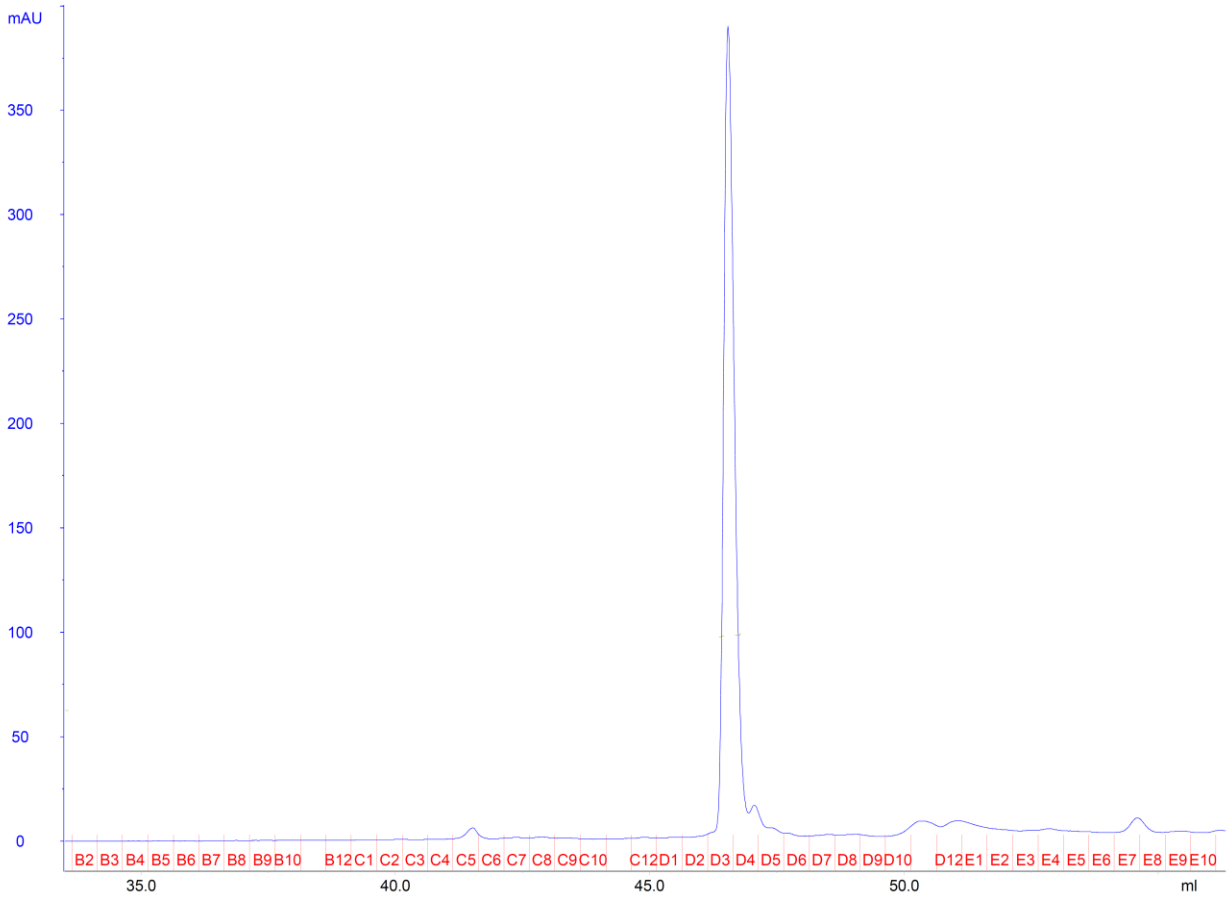

Appendix Figure 26. Peptide 12 Mass Spectrum

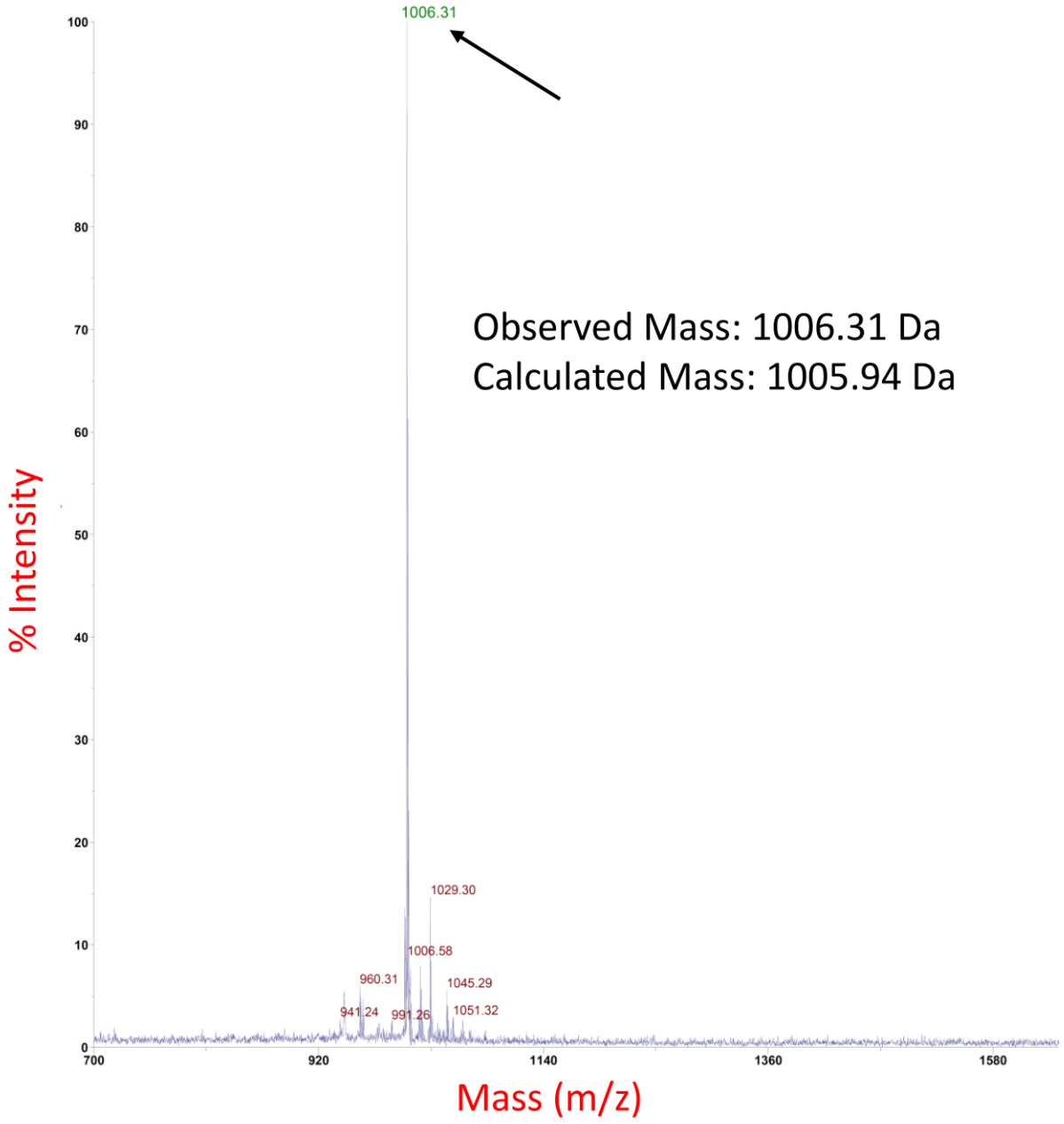

Appendix Figure 27. Bt-KR13 Chromatogram (Prepared by SciLight Peptide)

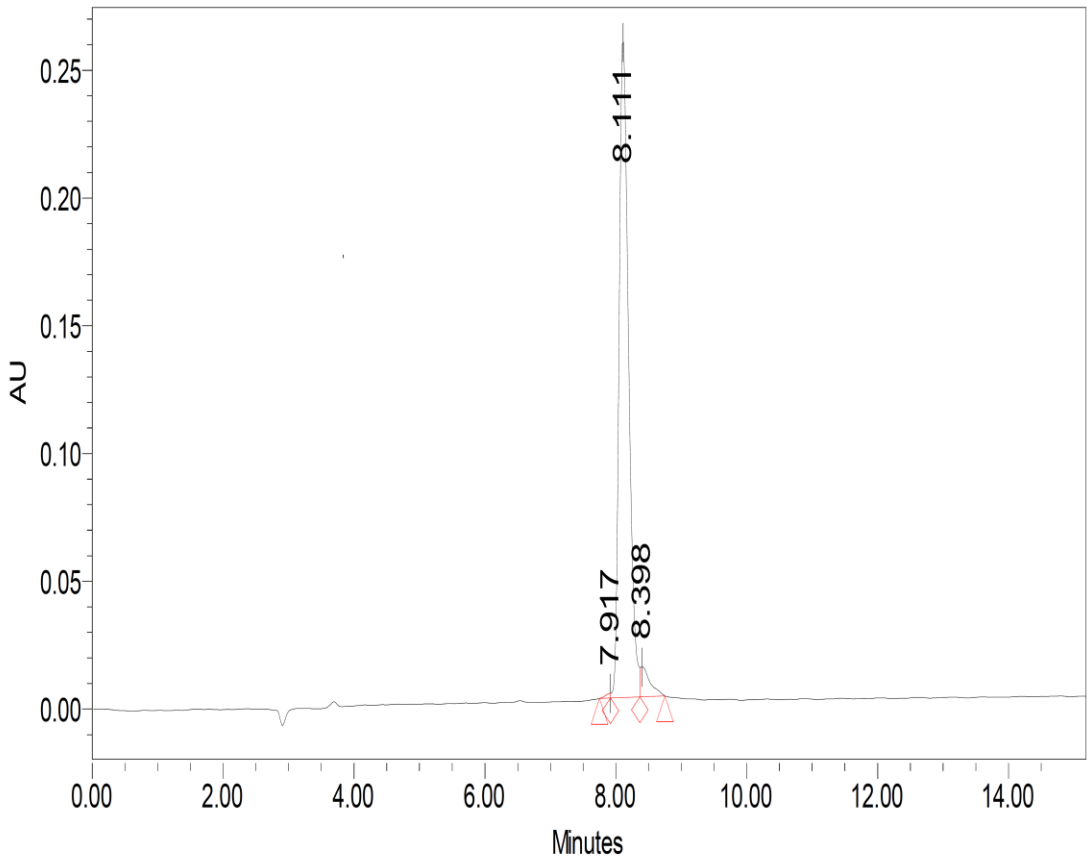

Appendix Figure 28. Bt-KR13 Mass Spectrum (Prepared by SciLight Peptide)

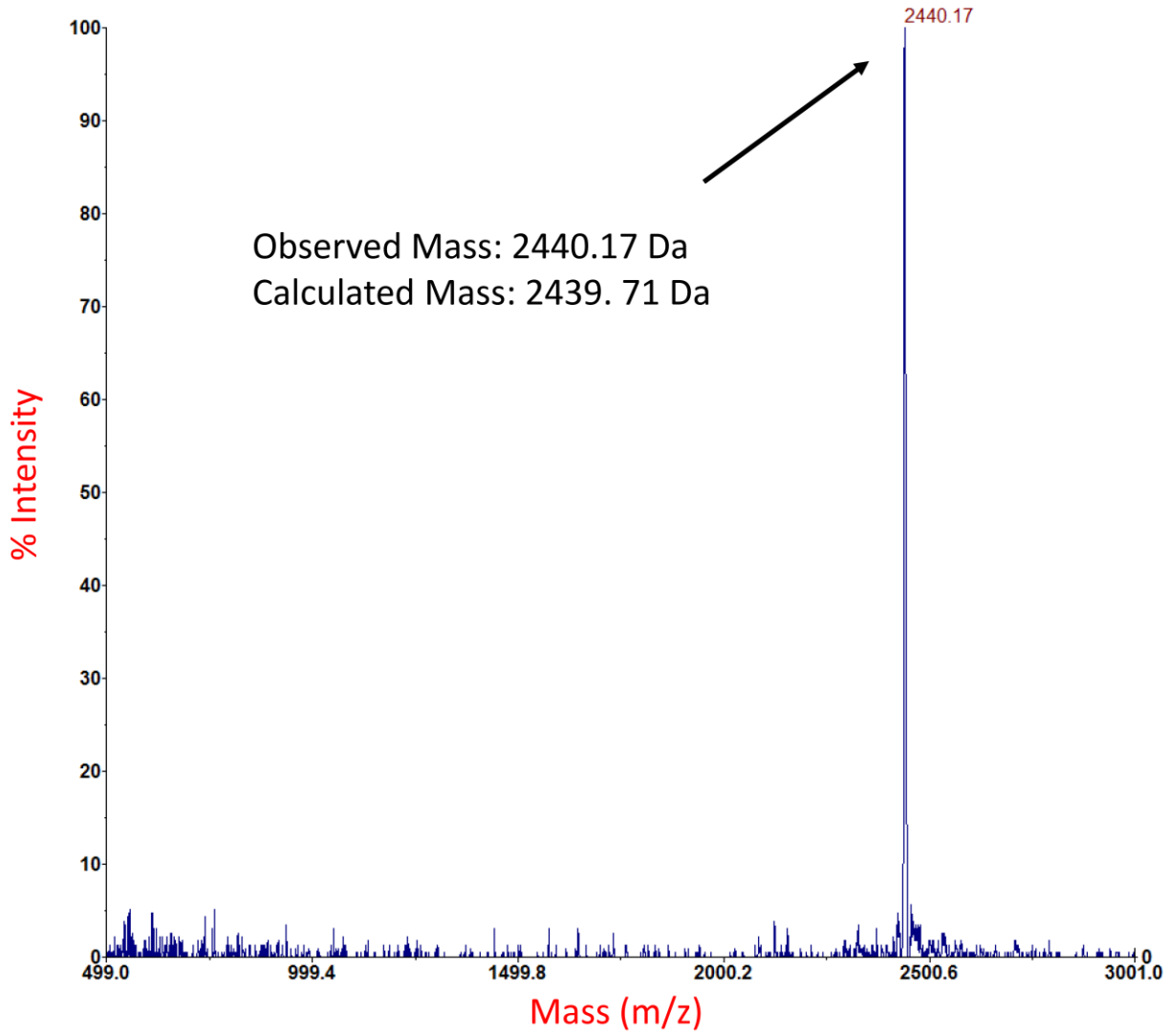

Appendix Figure 29. Bt-KR13b Chromatogram

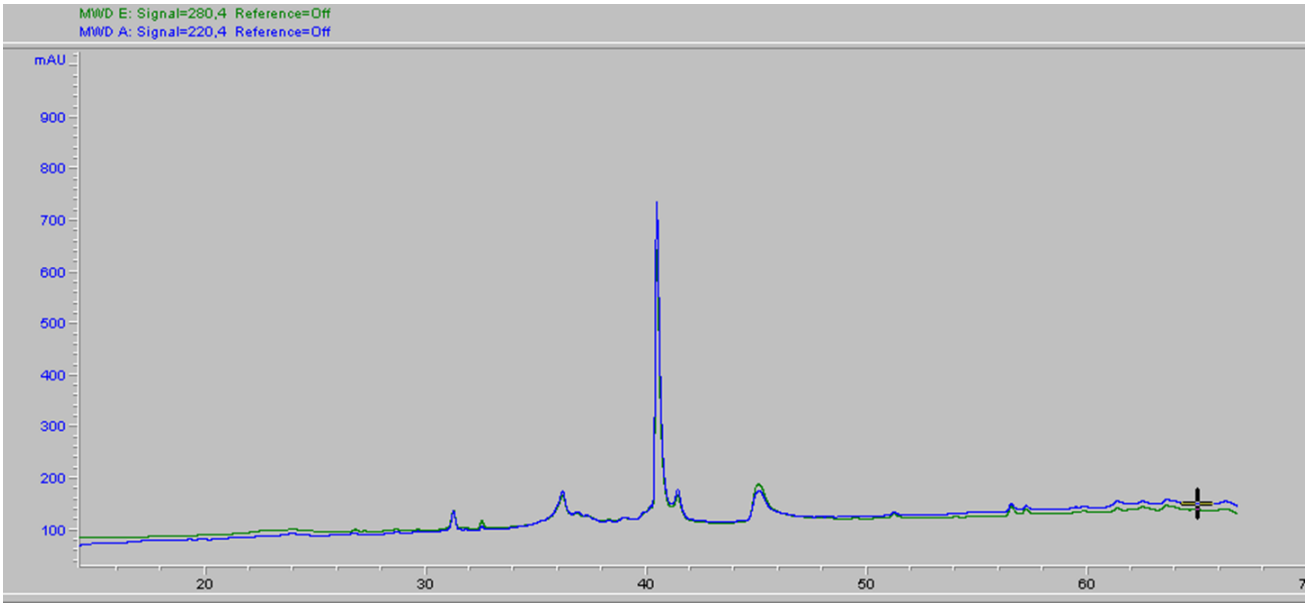

Appendix Figure 30. Bt-KR13b Mass Spectrum

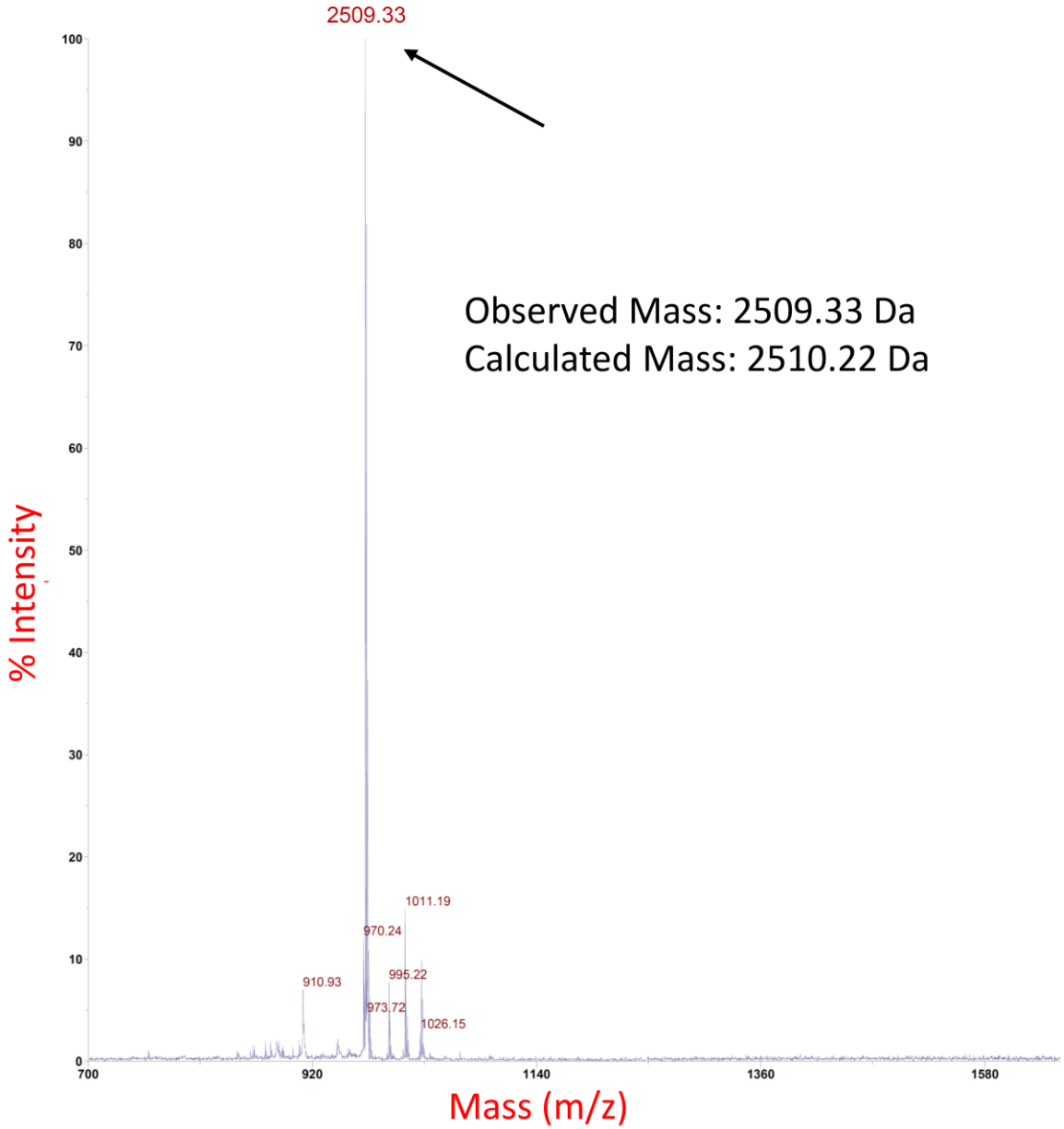

Appendix Figure 31: Effects of sulfhydryl reagents on HIV-1_{BaL} infectivity. (A) DTT treated HIV-1_{BaL} virions were treated with 0.02mM IAAM prior to adding HOS cells to measure infectivity. (B) Infectivity of HIV-1_{BaL} virus pre-treated with 0.02mM IAAm for 60 min. All reagents were removed by centrifugation and PBS washing prior to adding additional reagents or adding to cells.

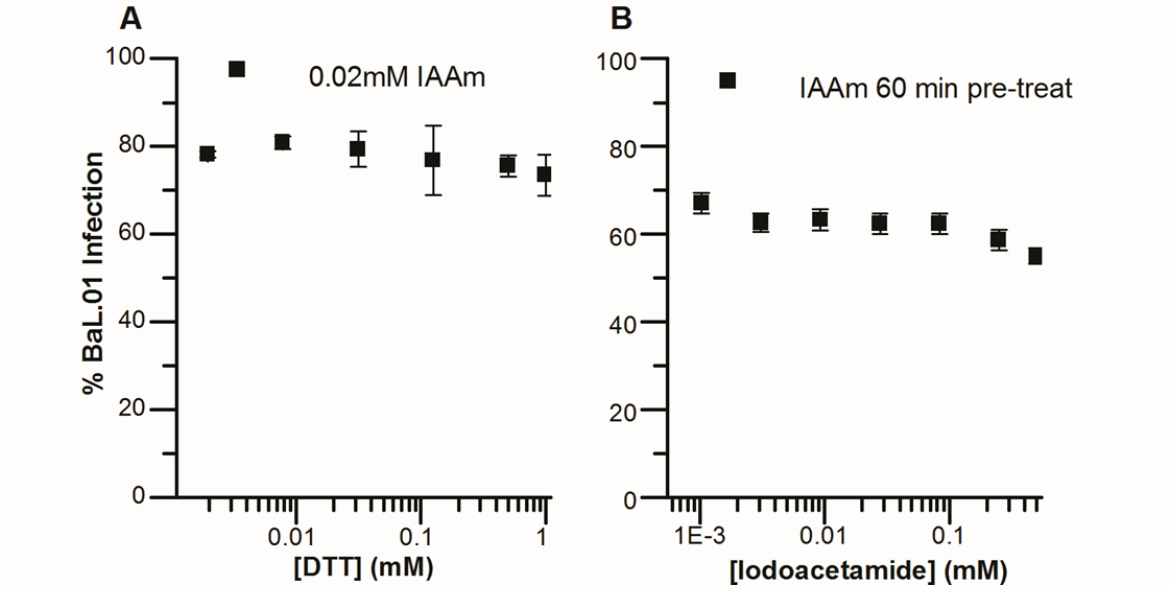

Appendix Figure 32. Lack of inhibition of 6-helix bundle formation by 2G12. Antiviral infection assay performed by adding virus to cells at 4 °C followed by subsequent serial dilutions of 2G12 at 37 °C to allow fusion. Fusion inhibitor, T20, displayed a dose dependent inhibition.

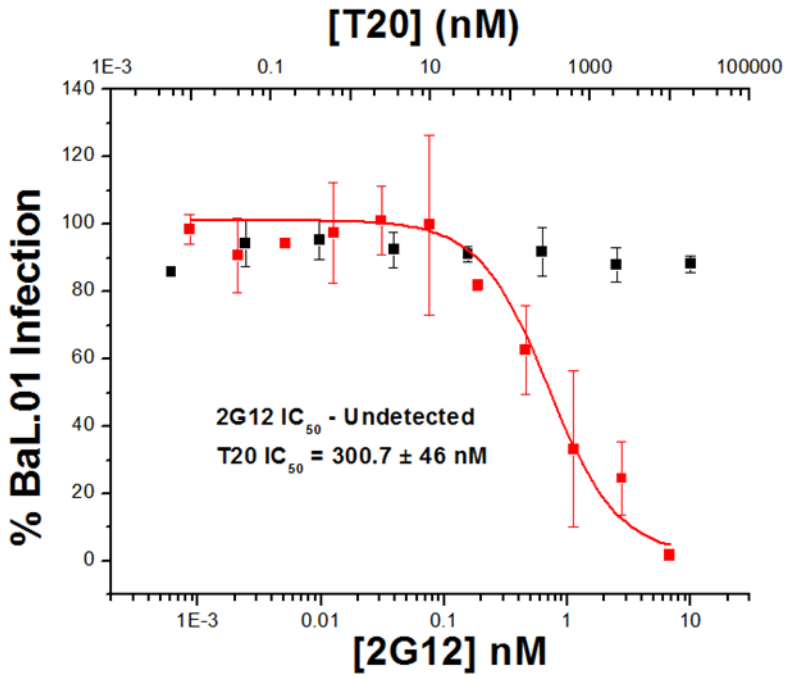

Vita

Laurèn Danielle Bailey was raised in Abington, PA. After completing high school she matriculated at Saint Joseph's University where she earned a Bachelor's of Science degree in Chemistry. After working briefly as an analytical chemist in the pharmaceutical industry she began her PhD research in the Biochemistry department of Drexel University College of Medicine. During her tenure at Drexel, Laurèn received an F31 Ruth L. Kirschstein fellowship from the National Institute of Health to fund her thesis project, "The mechanism of HIV-1 virolytic inactivation by Env-targeting peptide triazoles". While pursuing her PhD, Laurèn also held the position of Co-President of Drexel's Biomedical Graduate Student Association for two years. During her PhD studies, Laurèn participated in student body affairs as Co-President of the Graduate Student Association and received numerous awards and honors, including the American Peptide Symposium Young Investigator Award 2015, Deans' Graduate Student Travel Award 2015, Conference of Retroviruses and Opportunistic Infections (CROI) Young Investigator Award 2014, STD/AIDS Conference Young Scientist Award for Outstanding Oral Presentation 2014, Drexel Graduate Student Association (GSA) Travel Award 2013, and the Student Ambassador of Drexel's Discovery Day. Additionally, her work has resulted in several invited speaking engagements at conferences as well as numerous manuscript publications on studies of peptide triazole thiols.